AD-A073 000 SRI INTERNATIONAL MENLO PARK CA MOLECULAR PHYSICS LAB F/G 7/4
ION PHOTOFRAGMENT SPECTROSCOPY--POTENTIAL SURFACES OF MOLECULAR--ETC(U)
JUL 79 J T MOSELEY, P C COSBY, J R PETERSON F44620-76-C-0095
UNCLASSIFIED SRI-MP-79-49 AFOSR-TR-79-0943 NL

1 OF 2
AD
A073000

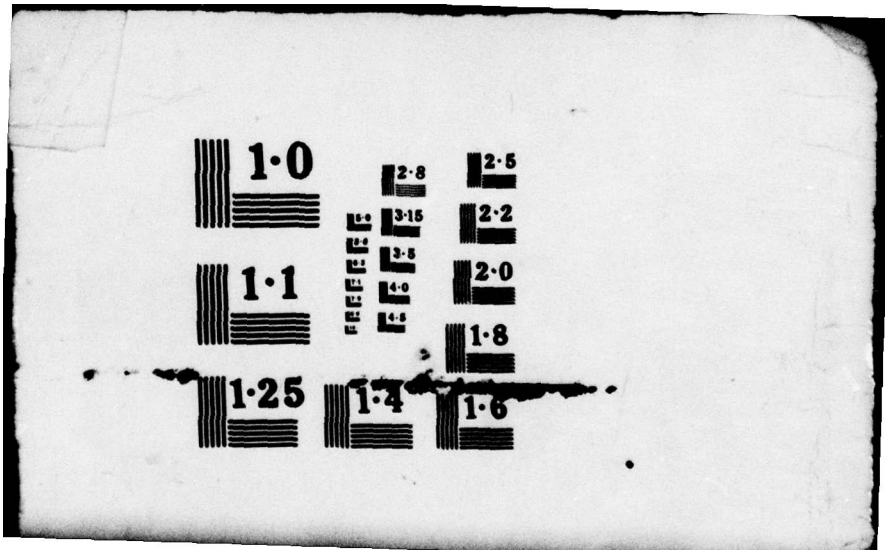
1·0
1·1
1·25
1·4
1·6
1·8
2·0
2·2
2·5
2·8
3·15

SRI International

AFOSR-TR- 79-0943

July 2, 1979

LEVEL II

Final Report
Covering the Period 16 May 1976 to 15 May 1979

ION PHOTOFRAGMENT SPECTROSCOPY-- POTENTIAL SURFACES OF MOLECULAR IONS

By: J. T. Moseley, P. C. Cosby, and J. R. Peterson

SRI International Project No. 5495
AFOSR Contract No. F44620-76-C-0095

Prepared for:

U. S. AIR FORCE OFFICE OF SCIENTIFIC RESEARCH
Bolling Air Force Base
Washington, D. C. 20322

Attention: Captain Russell Armstrong
Directorate of Chemistry

MP 79-49

333 Ravenswood Ave. • Menlo Park, California 94025
(415) 326-6200 • Cable: SRI INTL MPK • TWX: 910-373-1246

UNCLASSIFIED

SECURITY CLASSIFICATION OF THIS PAGE (When Data Entered)

(19) REPORT DOCUMENTATION PAGE

READ INSTRUCTIONS BEFORE COMPLETING FORM

(18) 1. REPORT NUMBER: AFOSR TR-79-0943

2. GOVT ACCESSION NO.

3. RECIPIENT'S CATALOG NUMBER: 0

(6) 4. TITLE (and Subtitle): Ion Photofragment Spectroscopy--Potential Surfaces of Molecular Ions.

5. TYPE OF REPORT & PERIOD COVERED: Final, May 16, 1976 - May 15, 1979

6. PERFORMING ORG. REPORT NUMBER

(10) 7. AUTHOR(s): J. T. Moseley, P. C. Cosby and J. R. Peterson

8. CONTRACT OR GRANT NUMBER(s): F44620-76-C-0095 (15)

9. PERFORMING ORGANIZATION NAME AND ADDRESS: Molecular Physics Laboratory, SRI International, Menlo Park, CA 94025

10. PROGRAM ELEMENT, PROJECT, TASK AREA & WORK UNIT NUMBERS: 61102F (17); (16) 2303 B1

11. CONTROLLING OFFICE NAME AND ADDRESS: U.S. Air Force Office of Scientific Research, Directorate of Chemistry, Bolling Air Force Base, D.C. 20332 (11)

12. REPORT DATE: 2 Jul 1979

13. NUMBER OF PAGES: 97

14. MONITORING AGENCY NAME & ADDRESS(if different from Controlling Office): (12) 97 p.

15. SECURITY CLASS. (of this report): Unclassified

15a. DECLASSIFICATION/DOWNGRADING SCHEDULE

16. DISTRIBUTION STATEMENT (of this Report)

Approved for public release; distribution unlimited.

(14) SRI-MP-79-49

17. DISTRIBUTION STATEMENT (of the abstract entered in Block 20, if different from Report)

Approved for public release. Distribution unlimited.

(9) Final rept. 16 May 76-15 May 79,

18. SUPPLEMENTARY NOTES

19. KEY WORDS (Continue on reverse side if necessary and identify by block number)

photofragment spectroscopy, potential curves, molecular ions, photodissociation, predissociation, molecular structure

20. ABSTRACT (Continue on reverse side if necessary and identify by block number)

(see next page)

DD FORM 1 JAN 73 1473 EDITION OF 1 NOV 65 IS OBSOLETE

UNCLASSIFIED 411 290

ABSTRACT

Techniques of ion photofragment spectroscopy have been used to investigate the structure and dissociations of molecular ions. For this research, a unique laser-ion coaxial beams spectrometer was constructed, allowing substantially improved sensitivity and resolution. The rare gas dimer ions were studied in detail, resulting in the determination of potential curves, absorption and photodissociation cross sections, and photofragment angular distributions for these ions. Effects from spin-orbit coupling were found to be very important. The predissociation of the positive and negative ozone ions were investigated to obtain structural information about these ions. Very high resolution spectroscopy of the quartet states of the positive oxygen ion allowed a substantial improvement in these potential curves, as well as an improved determination of the bond dissociation energy of neutral oxygen. Photofragment spectroscopy of the positive ion of CH led to the observation of two predissociations, one in the singlet and one in the triplet system. Similar measurements on the positive ion of methyl iodide led to the resolution of rotational and fine structure levels in the previously observed predissociation of this ion.

TABLE OF CONTENTS

APPENDICES (Continued)

I INTRODUCTION

In May 1976, we began a research program for the U. S. Air Force Office of Scientific Research, Contract No. F44620-76-C-0095, designed to use newly developed techniques of ion photofragment spectroscopy to study the potential surfaces of molecular ions. At the time this research was started, existing techniques[1,2] of ion photofragment spectroscopy had an energy resolution of about 10 meV, and had been applied only to H_2^+. Through work under this contract,[3-7] related contracts[8-10] at SRI, and our collaborative work[8-13] with researchers in the Laboratoire des Collisions Ioniques in Orsay, France, the techniques have been significantly extended, and a substantial number of important ions have been studied. Now rotational[8] and fine structure[7] levels can be resolved with a precision of 0.003 cm^{-1}, predissociation lifetimes measured[9], molecular bond energies determined[5,10] to within a few wavenumbers, and unique measurements made of photofragment angular distributions. Under this contract, studies have been made on O_2^+ quartet states, the rare gas dimer ions, positive and negative ozone ions, CH_3I^+, and CH^+. These ions are important in various Air Force application areas, including the atmosphere, laser development, and combustion.

In this final report, the results of each research effort supported will be briefly reviewed. The detailed results are included as appendices, which are reprints or preprints of journal articles describing the research.

II RESEARCH ACCOMPLISHMENTS

A. Laser-Ion Coaxial Beams Spectrometer

The major advances in ion photofragment spectroscopy were made possible by the new coaxial beams spectrometer constructed at SRI with the joint support of this contract, the National Science Foundation, the U. S. Army Research Office, and SRI International through its Independent Research and Development Program. This apparatus was constructed to allow laser excitation of ion beams in both coaxial and crossed configurations, and to observe the photofragments produced as a function of their kinetic energy, angle with respect to the laser polarization, and the wavelength of the excitation. In addition to having capabilities not present in the original photofragment spectrometers,[1,2] the SRI apparatus combines substantially increased resolution with a similar increase in sensitivity.

A detailed description of the apparatus and its capabilities is given in Appendix A, a reprint of an article published in the Review of Scientific Instruments. The application of the facility to research sponsored by this contract is described in the remainder of this report.

B. Photofragment Spectroscopy and Potential Curves of Ar_2^+ and Kr_2^+

The rare gases are often used in electron beam and high energy discharge situations, since they can efficiently transfer the electron kinetic energy into electronic excitation. The recently developed rare gas excimer lasers, the oxygen atom laser, and rare gas-halogen lasers all depend on this property of the rare gases. However, under the operating conditions of these lasers, significant quantities of the rare

gas dimer ions, such as Ar_2^+ and Kr_2^+, are formed, and it has been suggested[14] that these ions may be responsible for the gain-inhibiting visible and uv absorption observed in these lasers. Thus, it is important in this application to know precisely the absolute magnitude and the wavelength dependence of the photodissociation cross sections of the rare gas dimer ions.

Photofragment kinetic energy spectra were measured at wavelengths extending from 4579 to 7993 Å for both Ar_2^+ and Kr_2^+. From these measurements and theoretical calculations, accurate potential curves were determined for the ground $1(\frac{1}{2})u$ state and the repulsive $1(\frac{1}{2})g$ and $2(\frac{1}{2})g$ states for both ions. For Ar_2^+, the $1(\frac{3}{2})g$ state was determined as well, and from difference potentials obtained in differential scattering work, the $1(\frac{3}{2})u$ and $2(\frac{1}{2})u$ potential curves were obtained. These potential curves were then used to calculate the photodissociation (absorption) cross section from 2000 to 10,000 Å for ions in the ground vibrational level. For both ions, the effect of spin-orbit coupling was important in determining the magnitude and wavelength dependence of the cross section and the angular distribution of the photofragments.

A reprint of a journal article describing in detail the Ar_2^+ work is given in Appendix B. A similar article on Kr_2^+ is given in Appendix C.

C. Photodissociation Cross Sections of Ne_2^+, Ar_2^+, Kr_2^+, and Xe_2^+

The absorptions in the rare gas dimer ions occur in two bands, as described in Appendices B and C. Previously, under other support, we had measured[15,16] the absolute photodissociation cross sections for the bands centered around 7000 Å, using the drift tube mass spectrometer apparatus. These results were used in the potential curve determinations discussed above. However, no absolute cross section measurements were available for the uv bands, centered around 3000 Å, and thus the absolute

values of the absorption cross sections for this band were dependent on the theoretical calculations. Further, measurements of these cross sections provide an excellent test for the accuracy of the potential curves.

To provide this information on the uv bands, we measured the photodissociation cross sections for Ne_2^+, Ar_2^+, Kr_2^+, and Xe_2^+ over the wavelength range from 3500 to 5400 Å, and compared the results with cross sections calculated using the best available potential curves. The results are given in Appendix D, a preprint of an article accepted for publication in Physical Review A. As a result of this work and the work described above, the potential curves, transition moments, and absorptions of all of the rare gas dimer ions are now very well characterized.

D. Photodissociation and Photofragment Spectroscopy of O_3^-

The photodissociation cross section of O_3^- was measured over the wavelength range from 5000 to 6400 Å, using the drift tube mass spectrometer apparatus. This ion is an important intermediate in the D-region ion chemistry, and also represents a relatively simple system for which detailed calculations of its electron structure are becoming feasible. We observed a structured predissociation that provides new information about the structure of the ion. A detailed description of this work is found in Appendix E, a reprint of an article published in the Journal of Chemical Physics.

The coaxial beams spectrometer was used to measure the kinetic energy distribution of O^- photofragments from O_3^- at seven wavelengths between 4762 and 5905 Å. The angular distribution of the photofragments clearly demonstrates that the transition is parallel, thus identifying the predissociated state as the $^2A_2$. However, in the dissociation, most

of the available energy goes into rotation and vibration of the O_2 photofragment, with very little into kinetic energy. This leads, unfortunately, to poorly resolved kinetic energy spectra. Improvements are being made in the ion source design and the laser cavity configuration so that during a continuation of this work, better resolved spectra can be obtained and additional wavelengths can be studied.

E. The Dissociation Energy of $O_2(X^3\Sigma_g^-)$

By measuring the kinetic energy of dissociation of the N' = 9 level of the $O_2^+(b^4\Sigma_g^-, v=4)$ state with respect to the $O^+(^4S_0) + O(^3P_2)$ dissociation limit, we were able to close a spectroscopic cycle including the ground state of O_2. This allowed the determination of the dissociation energy of $O_2(X)$ with greater precision than the value based entirely on the optical spectroscopy of oxygen. The method by which this was done is discused in Appendix F. Subsequent, more accurate measurements[10] of the O^- photofragment energy allowed a further reduction in this uncertainty by a factor of 3, as well as a similarly precise determination of the bond energies of the $O_2^+(a^4\Pi_u)$ and $O_2^+(b^4\Sigma_g^-)$ states.

F. High Resolution Spectroscopy of $O_2^+(b^4\Sigma_g^-, v'=3,4,5 \rightarrow a^4\Pi_u, v''=3,4,5)$

The laser-ion coaxial beams photofragment spectrometer has been used with a tunable single-mode laser to measure transition energies in the First Negative system of O_2^+; the accuracy of these measurements is an order of magnitude higher than was previously possible in conventional high resolution Doppler-limited emission spectroscopy. The technique depends on observation of photofragment O^+ ions from predissociation of the upper $\underline{b}^4\Sigma_g^-$ state and thus allows study of higher vibrational levels inaccessible to normal emission spectroscopy. A multiply connected set of measurements, involving 400 transitions, was made in the (4,4) and (4,5) bands of the $O_2^+(\underline{b}^4\Sigma_g^- - \underline{a}^4\Pi_u)$ system for n' = 9-23 in the $\underline{b}$ state

to a precision and accuracy of about 0.0035 cm^{-1}. In addition, 5 lines in the (3,3) band, N' = 31 and 33, and 48 lines in the (5,5) band, N' = 5 - 17, were studied. Improved molecular constants for the b state were derived, as well as improved Dunham coefficients. The existing Hamiltonians were shown to be inadequate to describe these states within the precision of the present measurements.

A major article was prepared describing these results, which is now in press in the Journal of Molecular Spectroscopy. The length of this article precludes its reproduction as an appendix here. However, an abstract of the article appears as Appendix G, and a preprint has been submitted to AFOSR.

G. Photofragment Spectroscopy of CH^+

The radical ion CH^+ is well known to be a constituent in flames, and is a basic building block in interstellar molecular formation processes. However, only limited spectroscopic information is available. Kinetic energy distributions for C^+ photofragments were obtained over the wavelength range from 3507 to 6471 Å. In addition to the direct dissociation $X^1\Sigma^+ \rightarrow A^1\Pi$, two sets of predissociations were discovered. The first, leading to near-threshold C^+, has been attributed to predissociated levels of the $A^1\Pi$ and $a^3\Pi$ states. This result is probably of substantial astrophysical importance, and thus an article describing the work has been submitted to The Astrophysical Journal. A preprint appears here as Appendix H.

The second predissociation, which yields photofragments in the range of 1 to 2 eV, is most likely due to the transition $\underline{a}^3\Pi \rightarrow \underline{b}^3\Sigma^-$, with the b state predissociated by the $\underline{c}^3\Sigma^+$ state. Although these data have not yet been analyzed in detail, they should provide important new information about the poorly characterized triplet system of this molecule.

H. Photofragment Spectroscopy of O_3^+

Photofragment kinetic energy spectra of O_3^+ have been obtained at 17 wavelengths between 4579 and 7525 Å. Analysis of these data is only preliminary, since we expect to obtain additional data with improved resolution and at other wavelengths. However, the analysis already made yields a number of interesting, although preliminary, conclusions.

Some of the results are illustrated in Fig. 1. From consideration of all of the spectra, the peak labeled A is most likely due to a transition originating in the (2,0,0) vibrational level of the ground state of O_2^+, and B and D are due to transitions originating in the (1,0,0) and (0,0,0) levels, respectively. From this assignment, the bond energy $D_0(O^+-O_2) = 0.65$ eV, in agreement with photoionization results. The vibrational spacings $\Delta\nu[(1,0,0)-(2,0,0)] = 1450$ cm^{-1} and $\Delta\nu[(1,0,0)-(0,0,0)] = 1700$ cm^{-1} are also obtained. From the dependence of the photofragment kinetic energy of each of these peaks as a function of wavelength, it can be shown that the available energy is partitioned into translation and rotation in approximately the ratio 3/1. Peaks C, E, and F appear approximately 1600 cm^{-1} below peaks A, B, and D, respectively, and are very likely due to transitions that originate in the ground state levels represented by A, B, and D, but for which one quantum of vibration is left in the O_2 photofragment. It should be possible from data such as these to determine energy partitioning into vibration as well as into rotation and translation. We expect to continue research on this ion under a renewal contract, and to prepare a journal article for publication based on these results.

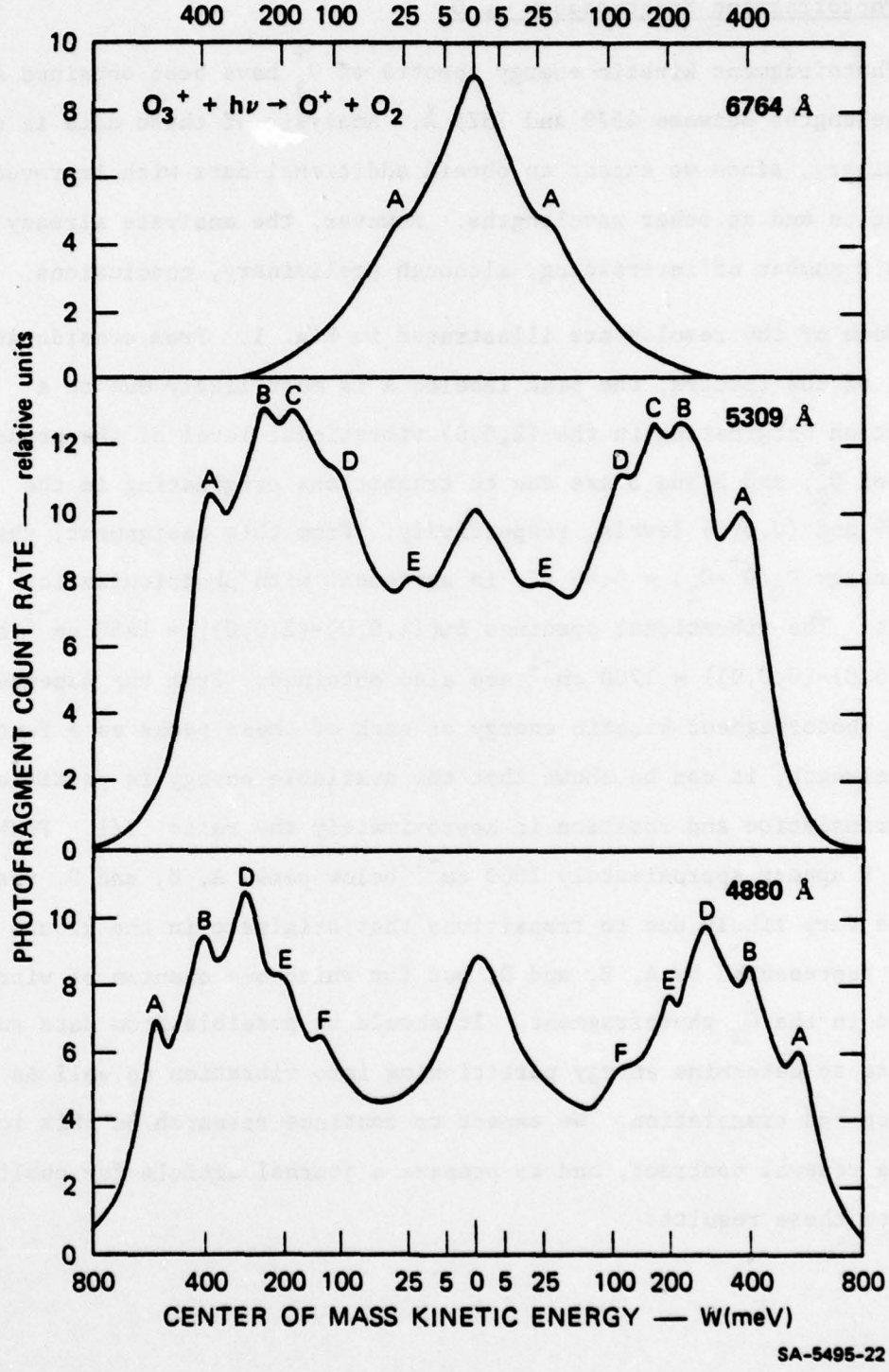

Figure 1 Photofragment kinetic energy spectra for $O_3^+ + h\nu \rightarrow O^+ + O_2$ at three different wavelengths. Peak designations are explained in the text.

I. Photofragment Spectroscopy of CH_3I^+

Photodissociation of CH_3I^+ has been briefly investigated at wavelengths from 6100 to 5750 Å with both moderate (0.5 cm^{-1}) and high (0.002 cm^{-1}) dye laser resolution. In this region the ion predissociates, producing CH_3^+ in seven complex vibrational bands with spacings on the order of 150 cm^{-1}. A moderate-resolution spectrum of these bands is shown in Fig. 2. The kinetic energy of the photofragment CH_3^+ is found to vary regularly from band to band and among the rotational lines within each band. High resolution velocity-tuned spectra of the rotational lines reveal a rich fine structure with line spaces on the order of 0.02 cm^{-1}, as illustrated in Fig. 3.

Current work on CH_3I^+ has been impeded by the rather limited velocity-tuning range of 0.1 cm^{-1}, which is possible with this heavy ion. Because this range is smaller than the mode spacing of the dye laser, continuous high resolution spectra of the bands have not been obtained. We will circumvent this problem in future work by using a continuously tunable ring dye laser. We anticipate that this work will yield the most detailed information to date on the electronic spectroscopy of a symmetric top molecule and will also permit critical testing of current statistical treatments of energy partitioning in the dissociation of polyatomic molecules.

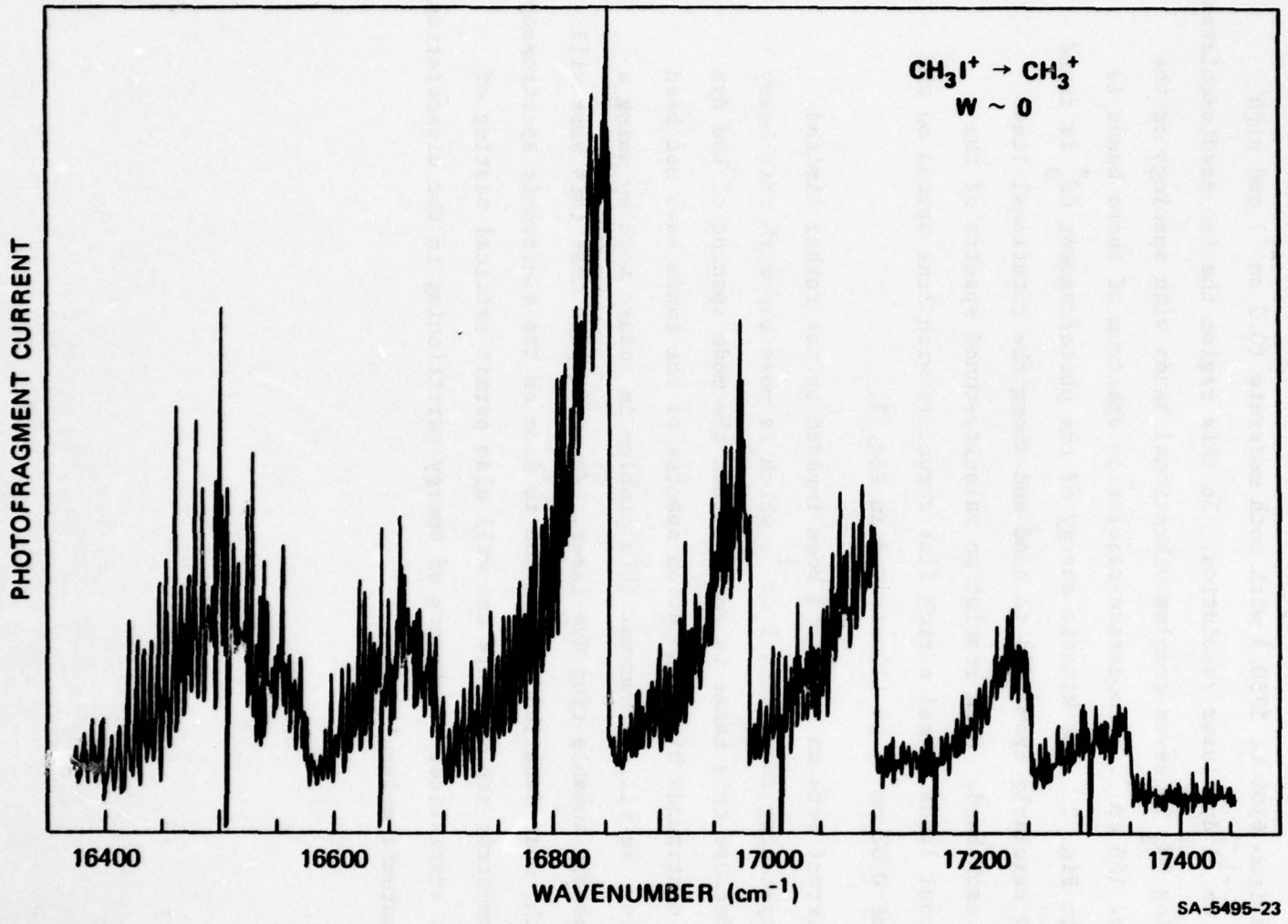

Figure 2 Predissociation photofragment spectrum of CH_3I^+ for CH_3^+ produced with nearly zero kinetic energy in the center-of-mass frame. The resolution of the dye laser was 0.5 cm^{-1}. The six vertical lines extending to the bottom of the figure are markers for the wavelength calibration.

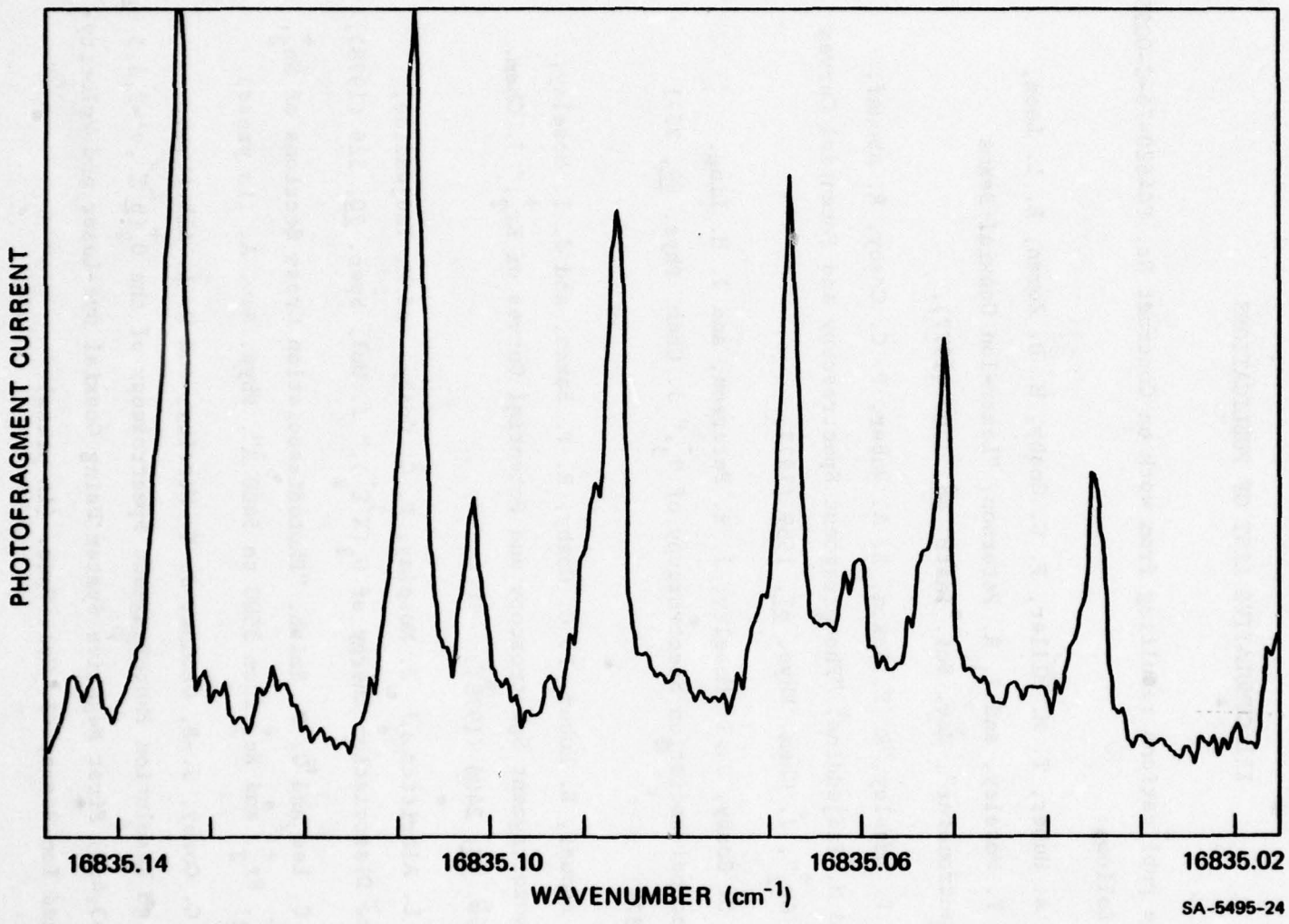

Figure 3 High resolution predissociation photofragment spectrum of CH_3I^+ for CH_3^+ produced with nearly zero kinetic energy in the center-of-mass frame. The 80 Mhz peak widths in the spectrum are due to contributions from jitter in the frequency of the single-mode dye laser and the Doppler width of the ion beam.

III CUMULATIVE LIST OF PUBLICATIONS

The publications resulting from work on Contract No. F44620-76-C-0095 are as follows:

1. B. A. Huber, T. M. Miller, P. C. Cosby, H. D. Zeman, R. L. Leon, J. T. Moseley, and J. R. Peterson, "Laser-Ion Coaxial Beams Spectrometer", Rev. Sci. Instr. 48, 1306 (1977).

2. J. T. Moseley, R. P. Saxon, B. A. Huber, P. C. Cosby, R. Abouaf, and M. Tadjeddine, "Photofragment Spectroscopy and Potential Curves of Ar_2^+", J. Chem. Phys. 67, 1659 (1977).

3. P. C. Cosby, J. T. Moseley, J. R. Peterson, and J. H. Ling, "Photodissociation Spectroscopy of O_3^-," J. Chem. Phys. 69, 2771 (1978).

4. R. Abouaf, B. Huber, P. C. Cosby, R. P. Saxon, and J. T. Moseley, "Photofragment Spectroscopy and Potential Curves of Kr_2^+," J. Chem. Phys. 68, 2406 (1978).

5. D. L. Albritton, J. T. Moseley, P. C. Cosby, and M. Tadjeddine, "The Dissociation Energy of $O_2(X^3\Sigma_g^-)$," J. Mol. Spec. 70, 326 (1978).

6. L. C. Lee and G. P. Smith, "Photodissociation Cross Sections of Ne_2^+, Ar_2^+, Kr_2^+, and Xe_2^+ from 3500 to 5400 Å", Phys. Rev. A. (in press).

7. P. C. Cosby, J.-B. Ozenne, J. T. Moseley, and D. L. Albritton, "High Resolution Photofragment Spectroscopy of the $O_2^+(\underline{b}^4\Sigma^-, v'=3,4,5 \rightarrow \underline{a}^4\Pi_u, v'=3,4,5)$ First Negative System Using Coaxial Dye-Laser and Velocity-Tuned Ion Beams," J. Mol. Spec. (in press).

8. P. C. Cosby. H. Helm and J. T. Moseley, "Observation of Predissociated Levels of CH^+," Astrophys. J. (in press).

IV INVITED TALKS

1. "Ion Photodissociation and Photofragment Spectroscopy", presented at the Tenth International Conference on the Physics of Electronic and Atomic Collisions, Paris, France, 21 July 1977.

2. "Ion Photofragment Spectroscopy", presented at the Division of Electron and Atomic Physics Meeting, Knoxville, Tennessee, 6 December 1977.

3. "Photodissociation and Photofragment Spectroscopy of Molecular Ions," presented at the 1978 Conference on the Dynamics of Molecular Collisions, Asilomar, California, 30 June 1978.

4. "Photofragment Spectroscopy of Molecular Ions Using Fast Ion Beams," presented at the International Conference on Fast Ion Spectroscopy, Lyon, France, 8 September 1978.

5. "Photon Interactions with Negative Ions on the Gas Phase," presented at the Division of Electron and Atomic Physics Meeting, Madison, Wisconsin, 29 November 1978.

6. "Photodissociation and Photofragment Spectroscopy of Molecular Ions," presented at the International Conference on Lasers '78, Orlando, Florida, 12 December 1978.

7. "Ion Molecular Spectroscopy Using Fast Ion Beams", presented at the Western Spectroscopy Association Meeting, Asilomar, California, 25 January 1979.

8. "Ion Photofragment Spectroscopy", presented at the 27th Annual Conference on Mass Spectrometry and Allied Topics, Seattle, Washington, 7 June 1979.

In addition to these invited talks, contributed papers on research supported by this contract were presented at a number of relevant scientific meetings.

V PROFESSIONAL PERSONNEL ASSOCIATED WITH THIS RESEARCH

(1) Principal Investigator and Project Supervisor:
Dr. J. T. Moseley, Program Manager, Photochemistry

(2) Project Leader: Dr. P. C. Cosby, Chemical Physicist

(3) Other SRI Professional Research Personnel:
Dr. R. P. Saxon, Chemical Physicist
Dr. T. M. Miller, Physicist
Dr. L. C. Lee, Physicist
Dr. G. P. Smith, Chemist
Dr. J. R. Peterson, Associate Director, Molecular Physics Laboratory

(4) Visiting Personnel:
Dr. B. Huber
Dr. R. Abouaf
Dr. M. Tadjeddine
Dr. J.-B. Ozenne
Professor J. Durup
Dr. H. Helm

Contributions of the above-mentioned personnel are evidenced by the publications on which they appear as co-authors.

Special mention should be made of the visiting scientists who have participated in this research. Four of these visitors are from the Laboratorie des Collisions Atomiques et Moleculaires of the Université de Paris-Sud in Orsay, France. Each has spent from one month to one year in our laboratory, supported primarily from outside sources. Professor Durup and Dr. Tadjeddine were supported by the Université de Paris, Dr. Abouaf by the Centre National de la Recherche Scientifique

(CNRS), and Dr. Ozenne by an NSF-CNRS Exchange Fellowship and SRI funds, Thus, the accomplishments in the research area covered by the current contract were substantially augmented. Further, these researchers were particularly well suited to our program of ion photofragment spectroscopy, inasmuch as Professor Durup, with the assistance of Dr. Ozenne, was one of the originators of this technique, and continues to be the foremost expert in its application. Dr. Tadjeddine presented a thesis to the Université de Paris in 1978 based primarily on research she performed at SRI.

In addition to these researchers from France, Dr. Bernd Huber from the Ruhruniversität in Bochum, West Germany, was a major participant in the construction of the coaxial beams spectrometer and in the initial research using this apparatus. Dr. Hanspeter Helm, from the Institut fur Atomphysik in Innsbruck, Austria, joined the research group near the end of the final contract year, and will remain at SRI for at least one year. We now have eleven joint publications with contributions from one or more of these visitors, and four other such journal articles have been submitted for publication.

VI REFERENCES

1. J.-B. Ozenne, J. Durup, R. W. Odom, C. Pernot, A. Tabche'-Fouhaille, and M. Tadjeddine, Chem. Phys. 16, 75 (1976).
2. N.P.F.B. van Asselt, J. G. Maas, and J. Los, Chem. Phys. 11, 253, (1975).
3. J. T. Moseley, R. P. Saxon, B. A. Huber, P. C. Cosby, R. Abouaf, and M. Tadjeddine, J. Chem. Phys. 67, 1659 (1977).
4. R. Abouaf, B. A. Huber, P. C. Cosby, R. P. Saxon, and J. T. Moseley, J. Chem. Phys. 68, 2406 (1978).
5. D. L. Albritton, J. T. Moseley, P. C. Cosby, and M. Tadjeddine, J. Mol. Spec. 70, 326 (1978).
6. B. A. Huber, T. M. Miller, P. C. Cosby, H. D. Zeman, R. L. Leon, J. T. Moseley, and J. R. Peterson, Rev. Sci. Instrum. 48, 1306 (1977).
7. P. C. Cosby, J.-B. Ozenne, J. T. Moseley, and D. L. Albritton, J. Mol. Spec. (in press).
8. M. Tadjeddine, R. Abouaf, P. C. Cosby, B. A. Huber, and J. T. Moseley, J. Chem. Phys. 69, 710 (1978).
9. J. T. Moseley, P. C. Cosby, J.-B. Ozenne, and J. Durup, J. Chem. Phys. 70, 1474 (1979).
10. C. Pernot, J. Durup, J.-B. Ozenne, J. A. Beswick, P. C. Cosby, and J. T. Moseley, J. Chem. Phys. (in press).
11. A. Tabché - Fouhaillé, J. Durup, J. T. Moseley, J.-B. Ozenne, C. Pernot, and M. Tadjeddine, Chem. Phys. 17, 81 (1976).
12. J. T. Moseley, M. Tadjeddine, J. Durup, J.-B. Ozenne, C. Pernot, and A. Tabché - Fouhaillé, Phys. Rev. Lett. 37, 891 (1976).
13. J. T. Moseley, P. C. Cosby, J. Durup, and J.-B. Ozenne, Journal de Physique 40, C1-46 (1979).

14. D. L. Huestis and D. C. Lorents, private communication.

15. L. C. Lee, G. P. Smith, T. M. Miller, and P. C. Cosby, Phys. Rev. A 17, 2005 (1978).

16. T. M. Miller, J. H. Ling, R. P. Saxon, and J. T. Moseley, Phys. Rev. A 13, 2171 (1976).

Laser–ion coaxial beams spectrometer

B. A. Huber,[a] T. M. Miller, P. C. Cosby, H. D. Zeman,[b] R. L. Leon, J. T. Moseley, and J. R. Peterson

Molecular Physics Center, SRI International, Menlo Park, California 94025

(Received 7 June 1977; in final form, 30 June 1977)

An apparatus has been constructed to provide laser excitation of ion beams in both coaxial and crossed configurations. The coaxial geometry provides very high sensitivity and nearly Doppler-free wavelength resolution for spectroscopic measurements, and allows the use of the Doppler shift to "tune" the wavelength. A novel transverse quadrupole electric field arrangement is used to deflect the ion beam into and out of the laser beam axis. The ion beam is highly collimated and a high-resolution 180° electrostatic analyzer is used for photofragment energy analysis. The apparatus has demonstrated a resolution of better than 10 meV for normal photofragment spectroscopy and 0.001 meV for coaxial beams photofragment spectroscopy using a single-mode laser. While providing these high resolutions the apparatus has an overall sensitivity several orders of magnitude greater than conventional ones.

I. INTRODUCTION

In recent years, several research efforts have been initiated to study the photodissociation of molecular ions in beams. Von Busch and Dunn[1] first examined the wavelength dependence of H^+ production from H_2^+, using an Xe arc lamp and monochromator, in a crossed-beams arrangement. Subsequently, Ozenne, Pham, and Durup at Orsay,[2] and van Asselt, Maas, and Los in Amsterdam[3] measured the energy spectra of the dissociation fragment ions using fixed-frequency lasers in a crossed-beams geometry. Such photofragment spectroscopy studies yield information on the potential energy curves, on bond energies, on the population of vibrational levels of the parent ions, and on the energy partitioning among the dissociation fragments of polyatomic ions. Recently the group at Orsay[4] showed that a modification of this technique, using tunable dye lasers at wavelengths near the dissociation threshold, can be used to obtain high-resolution spectroscopic data on molecular ions via transitions to predissociating states. In all of these experiments the laser beam intersected the ion beam orthogonally, where there is no Doppler shift (although a Doppler spread exists due to the angular divergence in the ion beam).

Experiments have also made use of Doppler shifts of single-frequency laser lines to excite fast beams. In some cases,[5] laser lines have been shifted by varying the laser-fast beam intersection angle, and in others the Doppler frequencies were "velocity tuned" to the absorption frequency by varying the particle beam energy, with the laser inclined at a small angle[6] or parallel[7–9] to the fast beam. These latter experiments also benefited from a very effective narrowing of the Doppler line profile that can occur in coaxial laser-fast beam arrangements, as is discussed below.

We describe here an apparatus designed to accommodate both laser excitation and dissociation studies of ions in both coaxial (merged beam) and crossed-beams configurations. A novel and efficient ion beam deflection system is used to merge the ion beam with the laser axis in the coaxial case. The apparatus can operate with the ion beam vacuum chamber in the resonant cavity of the laser for increased photon flux in both configurations. The coaxial configuration offers a much longer (10^2–10^3 times) interaction path than the crossed-beams arrangement; thus, the apparatus has a much greater ultimate sensitivity than previous ion photodissociation apparatuses. A high-resolution ($\Delta E/E \approx 3 \times 10^{-3}$) energy analyzer, used for ion photofragment energy measurements, can provide a resolution of 10^{-4} when combined with deceleration of the ions. The apparatus is a versatile and sensitive tool for high-resolution photofragment and optical spectroscopy studies on ion beams.

II. DESCRIPTION OF THE APPARATUS

A. Basic requirements and general description

Because, among other uses, the apparatus is intended for photofragment energy measurements, the ion beams must be well collimated and have low-energy spread and yet must have sufficient intensity to perform the desired experiments. The energy and angular resolution required for photofragment spectroscopy can be estimated as follows.

The velocity diagram in Fig. 1 defines various kinematic parameters in a dissociation event. If a molecule moving with initial kinetic energy E_0 and speed v_0 in the laboratory frame dissociates into two fragments of mass m_1 and m_2, with total center of mass (c.m.) kinetic energy release W, the laboratory energy of m_1, ejected at c.m. angle φ, or laboratory angle θ, with respect to the beam direction is

$$E_1 = \frac{m_1 m_2}{m_2 + m_2}\left[\frac{E_0}{m_2} + 2\left(\frac{E_0 W}{m_1 m_2}\right)^{1/2}\cos\varphi + \frac{W}{m_1}\right].$$

To simplify matters, we consider the case of a homonuclear diatomic molecule ($m_1 = m_2$); then

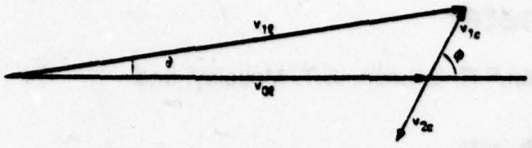

FIG. 1. Velocity diagram for a photodissociation event. θ and φ are the laboratory and center-of-mass angles, respectively, for ejection of a photofragment with respect to the laboratory velocity v_0. The center-of-mass velocities of the two photofragments are v_{1c} and v_{2c}.

$$E_1 = \tfrac{1}{2}E_0[1 + 2(W/E_0)^{1/2}\cos\varphi + W/E_0]. \quad (2)$$

The term W/E_0 is always small ($\sim 10^{-3}$) in our experiments, and we shall neglect it in determining the design parameters of the apparatus. Thus

$$E_1 = \tfrac{1}{2}E_0[1 + 2(W/E_0)^{1/2}\cos\varphi]. \quad (3)$$

Requirements on energy resolution of the apparatus can be estimated by noting that for variations in W only,

$$\Delta E_1 = \frac{\partial E_1}{\partial W}\Delta W = \tfrac{1}{2}\left(\frac{E_0}{W}\right)^{1/2}\cos\varphi\,\Delta W. \quad (4)$$

As a typical example, let $E_0 = 3000$ eV, $W = 1$ eV, and $\varphi = 0$. If the energy difference between the vibrational levels in the parent ion is 400 cm^{-1} (a reasonably small value), then in order to distinguish between ions dissociating from adjacent levels we must resolve $\Delta W = 0.05$ eV. The ions dissociating in the forward direction ($\varphi = 0$) would be separated by a laboratory energy $\Delta E_1 = 1.4$ eV at $E_1 \sim 1555$ eV, and a resolution of $\Delta E/E \sim 10^{-3}$ would be required.

The effective energy resolution is decreased as the range of θ near 0° accepted by the energy analyzer is increased, allowing ions with larger values of φ to be detected. To estimate the required angular collimation, let the laboratory energy of fragment ion A, dissociated at $\varphi = 0$ and $W = W_0$, just equal that of another ion B, at $\varphi = \varphi_{max}$ (the maximum φ allowed by collimation) and $W = W_0 + \Delta W$. From Eq. (3) these conditions establish

$$\varphi_{max} = \cos^{-1}[W/(W + \Delta W)]^{1/2}. \quad (5)$$

The relationship between θ and φ can be seen from Fig. 1 to be

$$\theta = \tan^{-1}[v_{1c}\sin\varphi/(v_{0l} + v_{1c}\cos\varphi)]$$
$$= \tan^{-1}[W^{1/2}\sin\varphi/(E_0^{1/2} + W^{1/2}\cos\varphi)]$$
$$\simeq (W/E_0)^{1/2}\sin\varphi. \quad (6)$$

The approximation in Eq. (6) is made by dropping the second term in the denominator because $W \ll E_0$, and by noting that $\theta \ll 1$. The required collimation, θ_{max}, can be obtained from Eq. (6) by letting $\varphi = \varphi_{max}$ obtained from Eq. (5). Again, for the case $E_0 = 3000$ eV, $W = 1$ eV, and $\Delta W = 0.05$ eV, we find from Eq. (5) that $\varphi_{max} = 0.22$ rad and $\theta_{max} = 4.0 \times 10^{-3}$ rad. In order to permit the actual resolution of vibrational levels separated by 0.5 eV, we estimate the required angular definition by letting $\Delta W' = 0.02$ eV, less than half that of the vibrational spacing. This value sets $\varphi_{max} = 0.14$ rad and $\theta_{max} = 2.5 \times 10^{-3}$ rad. The resolution of the apparatus is actually about 2×10^{-3} rad.

A diagram of the apparatus is shown in Fig. 2. Ions are extracted from an ion source (described below), focused, mass selected, and enter the main collimating drift space which is defined by two 2-mm-diam apertures A2 and A3 separated by 1 m. Sets of vertical and horizontal deflection plates are placed at several appropriate positions along the beam path.

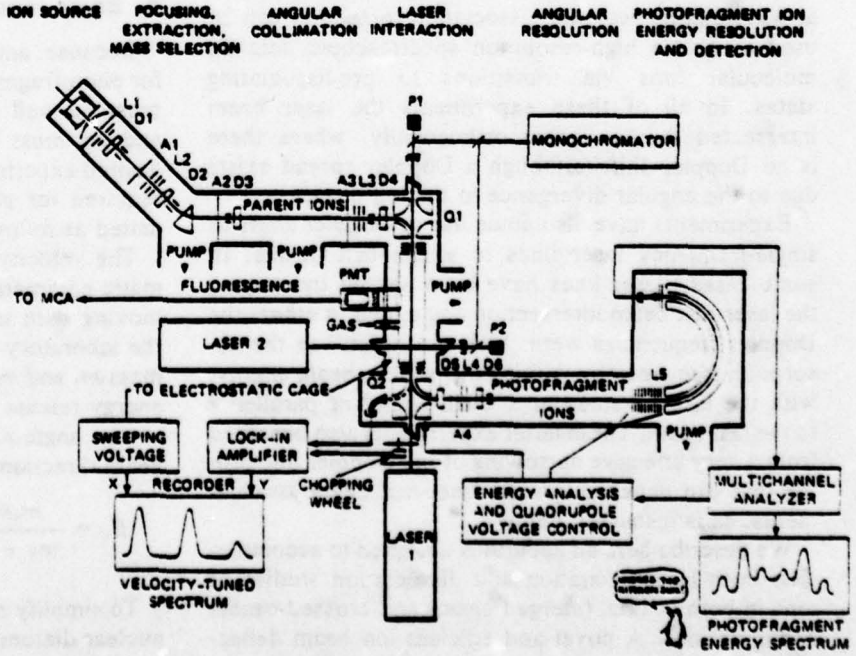

FIG. 2. Schematic of the coaxial beams spectrometer. Ion beam lenses are designated by L, deflectors by D, apertures by A, laser power meters by P, and the quadrupoles by Q.

The collimated ion beam is next deflected 90° and into the laser beam by an electric quadrupole field whose axis is perpendicular to the ion beam. These quadrupole deflectors[10] have exceptionally good ion optical properties as well as a very useful physical configuration for coaxial laser–ion beam experiments. After traversing a 50-cm drift length, the beam (or the desired photofragment sample) is further deflected 90°, parallel to its original direction, by a second electric quadrupole. The potentials on the second deflector are set to direct either the desired fragment ions or the main beam along the final drift path. This path is 1.3 m long and collimation to $\sim 2.5 \times 10^{-3}$ rad is obtained from a 2-mm entrance aperture to the deceleration lens that precedes the energy analyzer.

After energy analysis, the ions are detected by a Channeltron electron multiplier and the resulting pulse signals are counted in a multichannel scaler whose channels are advanced synchronously with the voltage in the energy analyzer so that a spectrum of the dissociation fragment ions is stored in the scaler for eventual readout to a CRT, recorder, or off-line computer.

The laser beam can be placed either coaxially with the ion beam in the interaction region, or at 90°, depending on the polarization requirements, and the interaction chamber can be operated intracavity with the laser. Brewster window ports in the chamber walls minimize the power loss.

B. Ion source

For many of the anticipated photodissociation and spectroscopic studies on molecular ions, it is important to have an ion source capable of operating at relatively high pressures so that ions can be formed from three-body reactions (for complex and rare-gas molecular ions); also it should be possible to form ions that are not too vibrationally or rotationally hot. For these purposes we have chosen a cold-cathode discharge source based on a design of Lange, Huber, and Wiesemann.[11] However, we use a hollow cathode instead of their planar geometry, in order to achieve a quiet discharge and to improve the lifetime of the source. The source operates at pressures between 0.1 and 1 Torr. The cathode–anode spacing can be varied and optimized for maximum output. The ions are extracted from a 0.6-mm aperture in the anode. The anode and extraction lens are shaped to form a planar Pierce system to minimize space charge effects. For ions formed by direct electron impact (Ar^+, O_2^+, O^+, etc.), the extracted ion current behind the extraction lens is in the range of 10^{-6}–10^{-7} A. Ions formed from three-body or secondary reactions such as Ar_2^+ may be 100 times less abundant. The width of the kinetic energy distribution was measured to be as small as 0.6 eV for Ar_2^+ ions, and it was found to depend on source pressure and cathode–anode potential. For O_2^+ formed at low pressure under conditions that maximize $O_2^+(a^4\Pi_u)$ production, the energy spread was found to be ~3 eV.

C. Ion optics

As mentioned above, the experiment requires a mass selected ion beam with an angular divergence of about 2 mrad to obtain adequate energy resolution and a beam diameter close to 2 or 3 mm to maximize overlap with the laser. In order to satisfy these conditions without large losses in beam intensity we deflect the beam through 45° using a magnetic sector with equal entrance and exit angles of 14.38° (between ion beam and the perpendicular to the pole faces). These angles were chosen[12] to achieve equal focusing properties in the bending and in the nonbending planes. Calculations of the ion trajectories, taking into account the effect of the extended fringing field, revealed a distance of 26.88 cm between the focal point and the entrance face of the magnet for point-to-parallel focusing.

In order to obtain a well-collimated ion beam beyond the magnet, the ion optics between the source and the magnet were designed so that the extraction region can be imaged at the focal point of the magnet. The ion optics consist of two einzel lenses separated by a small limiting aperture A1 (Fig. 2). The geometry of the einzel lenses was chosen to minimize aberration effects; the focusing properties were computed using standard matrix methods.[13] The first lens focuses the extracted ion beam onto the aperture and the second lens forms a virtual image at the focal point. The 2-mm apertures A2 and A3 in the drift region following the magnet finally define the ion beam with a maximum angular divergence of 2 mrad. Using the calculated potentials for the einzel lenses (optimized within 10%) we found a 30% loss in ion beam intensity at each of these apertures, resulting in usable ion currents between 1×10^{-6} and 3×10^{-10} A for O_2^+ and Ar_2^+ ions, respectively.

The primary function of the magnet is to provide mass selection for the ion beam. The ions are deflected through an angle of about 45°. From purely geometrical considerations, an angular collimation of 2×10^{-3} in the beam will give a mass resolution $\Delta m/m$ of about 5.6×10^{-3}. This is twice the observed value of about 2.8×10^{-3} FWHM obtained in a Kr_2^+ mass spectrum; thus the effective angular collimation must actually approach 1×10^{-3}.

There is also an energy selectivity associated with the magnetic deflection of a single mass. The relative energy selectivity $\Delta E/E$ should have the same value as the observed $\Delta m/m$, so would be expected to be about 3×10^{-3}. This provides a predicted window of about 9-eV FWHM at 3000 eV, which does not affect the positive ion beams, whose natural energy spreads are much less. For negative ion beams, whose energy widths may exceed 10 eV, a reduction in the size of A1 and A3 can be used to limit the width of the energies transmitted to the interaction region.

For those cases where a higher ion current is needed and the high angular resolution is not necessary, two additional einzel lenses are installed before the first and after the second quadrupole deflector. Thus, a focal

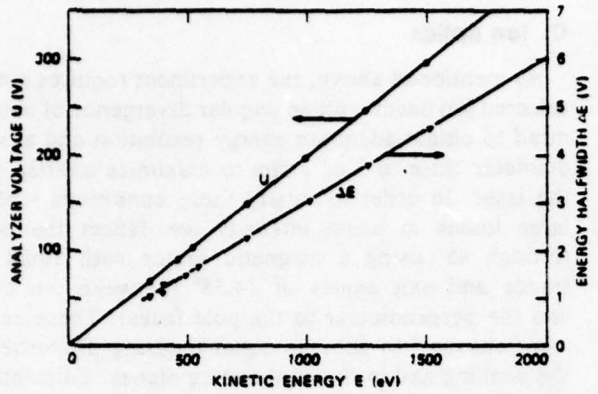

FIG. 3. Energy analyzer test data. Potential U between analyzer plates versus transmitted energy E—dots. Energy width ΔE of analyzer versus E—triangles.

point of the ion beam can be formed in the interaction region between the two bending units.

D. Energy analysis

The relative energy resolution $\Delta E/E$ necessary for photofragment spectroscopy is about $(2-3) \times 10^{-4}$. In the experiment this value is obtained by using a hemispherical 180° electrostatic analyzer combined with a deceleration system. The kinetic energy of the photofragments is first reduced by a factor of 10 without large intensity loss so that the resolution of the analyzer itself has to be only about 2×10^{-3}.

The deceleration system is formed from the first half of a filter lens.[14] It consists of 13 plates with 3-mm apertures, each plate separated by 3 mm. The ion kinetic energy is reduced in a parabolic electric field[14] (achieved with a resistor divider chain) by a factor of 10, accompanied by ion losses of only about 30%–60%. The exit of the deceleration system and the entrance of the energy analyzer are connected by an einzel lens in order to collimate the slightly diverging beam into the entrance aperture of the analyzer.

The 180° hemispherical electrostatic analyzer used for the final energy analysis has a median radius of 150 mm and a gap distance of 15 mm. The width of the two electrodes is 60 mm and the sides of the gap are shielded by two "Matsuda" plates,[15] the potential of which can be adjusted with respect to the center potential. This type of analyzer was chosen rather than a 127° cylindrical analyzer because of the higher energy dispersion and the focusing properties in both planes.

The voltage U between the two electrodes and the kinetic energy E of the ions are related by the following equation[16]:

$$U = 2r_0(r_1 - r_2)E/(r_1r_2) = cE, \qquad (7)$$

where r_1, r_2, and r_0 are the radii of the outer and inner electrodes and the central trajectory, respectively. For a gap distance of 15 mm and $r_0 = 15$ mm, the analyzer constant c was calculated to be 0.2005. This value agrees with an experimental determination from a least-squares fit to the data in Fig. 3, which shows the results of an experimental check of Eq. (7). In order to obtain the same potential for the central trajectory as for the entrance and exit apertures, the potentials of the inner and outer electrodes had to be asymmetric by 5% with respect to central potential. The optical properties of the analyzer, the fringing field effects and the image aberrations, which limit the resolving power, were calculated to second order using the matrices given in Ref. 16. For entrance and exit slits of 1-mm width the calculated[16] resolution of the analyzer was 6.67×10^{-3}. In the experiment we measured the half-width of the primary beam for different kinetic ion energies. The result is also shown in Fig. 3. The linear increase at the energies of these data is due to the finite energy resolution of the analyzer; at lower energies the data would approach a constant value of ΔE of about 0.6 eV, which was previously found to be characteristic of this type of ion source. From the slope of the curve we obtain a resolution of 3.0×10^{-3}. Thus the overall resolution of the detection unit with a factor of 10 deceleration is 3.0×10^{-4}. Better resolution is, of course, possible if the entrance and exit slits are narrower or if greater deceleration is used. However, since the energy half-width of the primary ion beam is about 1 eV, the present geometry is adequate for ion transmission energies of up to 200 eV (after deceleration).

The photofragments exiting the energy analyzer are accelerated again to about 3 keV before entering the Channeltron detector. The pulses are normalized in a preamplifier and accumulated in a multichannel scaler. The photofragment kinetic energy spectrum is obtained by setting the hemispherical analyzer voltages for a fixed ion transmission energy (typically 200–300 eV) and linearly varying the voltage applied to the deceleration lens system over the desired range of photofragment energies. The sweep of the deceleration voltage is generated by a D–A converter/high voltage op-amp combination which is driven by the channel address of the multichannel scaler. Thus, the spectra are obtained with constant transmission energy and energy resolution, and nearly constant transmission efficiency. Since the quadrupole benders are also weakly energy selective (energetic window 40 eV at 1500 eV), the potentials on the second quadrupole must also be changed proportionally to the change in detected photofragment energy. If the einzel lens E5 is used, its voltage must be scanned in a similar manner.

E. Quadrupole beam deflectors

The deflection systems that bend the ion beam into and out of the laser beams are electrostatic quadrupoles oriented perpendicularly to the bending plane, a novel ion optical arrangement,[10] which is very well suited for this use. It permits an ion beam to merge coaxially with a laser beam without either the use of cumbersome magnets or the more conventional types of electrostatic deflection electrodes which would usually require some

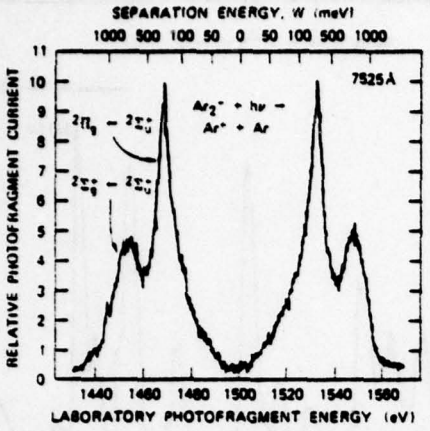

FIG. 4. Photofragment energy spectrum for $Ar_2^+ + h\nu \rightarrow Ar^+ + Ar$ at 7525 Å. The lower energy scale gives the laboratory photofragment energy, which is directly measured; the upper scale gives the total separation energy determined as discussed in the text.

form of opening to be placed in one of the electrodes to afford passage of the laser beam at the expense of field homogeneity. The capability of viewing the ion beam axis before and after deflection greatly eases alignment procedures. Moreover, the quadrupole deflectors are quire achromatic, creating little distortion in the ion beam after it has been bent through 90°. Ions on one side of the beam in the plane of deflection are switched to the opposite side after passage through the quadrupole, but the angular collimation of the beam is essentially unchanged even for a relatively large energy dispersion (10%). Edge effects due to fringing fields at the entrance and exits of the quadrupoles are corrected with shim electrodes as described in Ref. 10. In tests of this apparatus with a 3-keV ion beam whose energy spread was about 1 eV, essentially all of the beam that had passed through the two collimating apertures A2 and A3 (2-mm diam separated by 1 m) also passed through a 3-mm aperture at the end of the 33-cm drift space following the first 90° deflection.

The energy dispersion of a quadrupole deflector is about 85% of that of a conventional 127° energy analyzer of equal angular aberration,[10] and is manifested in a displacement of the ion trajectories in the bending plane, rather than an angular dispersion, so that a long coaxial drift path following the first deflection can be accommodated without loss of overlap of the ion beam with the laser. The absence of angular dispersion due to the benders also permits a high degree of angular resolution without loss of signal at the energy analyzer and permits a much higher resolution of the ion dissociation fragment energy spectra than has been possible in previous experiments.

As the energies of the fragment ions are scanned by the 180° energy analyzer, the potentials on the second quadrupoles are swept so that fragment ions of the proper energy are directed onto the center of the entrance aperture of the energy analyzer. The quadrupole voltage is approximately 0.7 times the kinetic energy (eV) of the transmitted ions.[10]

III. PROPERTIES OF THE APPARATUS

The apparatus can accommodate laser–ion beam studies in both coaxial and 90° crossed-beams geometries. In each case, the ion fragments ejected at angles near $\theta = 0$ or 180° are observed along the beam axis at the lab angle $\theta_1 = 0 \pm 0.001$ ($\Delta\theta \sim 2 \times 10^{-3}$ rad). Proper adjustment of the second quadrupole potentials is required to assure that $\theta = 0$; otherwise the values of W deduced from Eq. (2), with $\theta = 0$ (or π), will be incorrect (and will always be low). This complication is a necessary byproduct of the coaxial geometry which requires deflection of the dissociated ions before they are energy analyzed, and did not exist in earlier experiments. However, this alignment problem is easily solved and has presented no real drawback to the method.

A. Coaxial laser–ion beam configuration

The coaxial configuration permits a large interaction volume; the laser and ion beams are merged over a 33-cm length. Since the laser beam is usually about 2 mm in diameter, the interaction volume is 100–200 times larger than that afforded by the conventional crossed-beams geometry, and the resulting sensitivity of the apparatus is similarly increased. However, since the laser polarization is always at right angles to the ion velocities, this advantage is fully effective only for "perpendicular" transitions, where the fragment ions are ejected primarily perpendicularly to the laser polarization, and thus in the direction of motion of the parent ion beam ($\theta = 0$ or π) for dissociations near the energetic threshold ($W \sim 0$), or for excitations that do not result in dissociation.

A typical spectrum for the reaction $Ar_2^+(^2\Sigma_u^+) + h\nu \rightarrow Ar^+ + Ar$ is shown in Fig. 4 for a 3-keV parent ion beam and coaxial laser at 7525 Å. The spectrum is symmetric since photofragments ejected into c.m. angles 0 and π are detected with nearly equal efficiency. The center of the spectrum is at 1500 eV, as expected for the photodissociation of a homonuclear diatomic. A scale in the photodissociation energy W, as calculated from Eq. (2), is shown at the top of the figure. A detailed study has been made of this photodissociation using both coaxial and crossed laser beams at 14 wavelengths between 4579 and 7993 Å. This work[17] was used to determine the $^2\Sigma_u^+$, $^2\Sigma_g^-$, and $^2\Pi_g$ potential curves of Ar_2^+ to substantially higher accuracy than had been previously possible. The identification of the peaks shown in Fig. 4 was based on this work.

We note that individual vibrational levels are not resolved here, as they have been for H_2^+ [2,3] and O_2^+.[18] This is not surprising since the spacing of the Ar_2^+ vibrational levels is only about 30 meV, and the rotational spread at our ion source temperature (~400 K) is of this order. When this rotational spread is combined with the finite energy resolution of the apparatus, it is clearly difficult to resolve the individual vibrational levels in Ar_2^+. An example will be shown later where vibrational levels

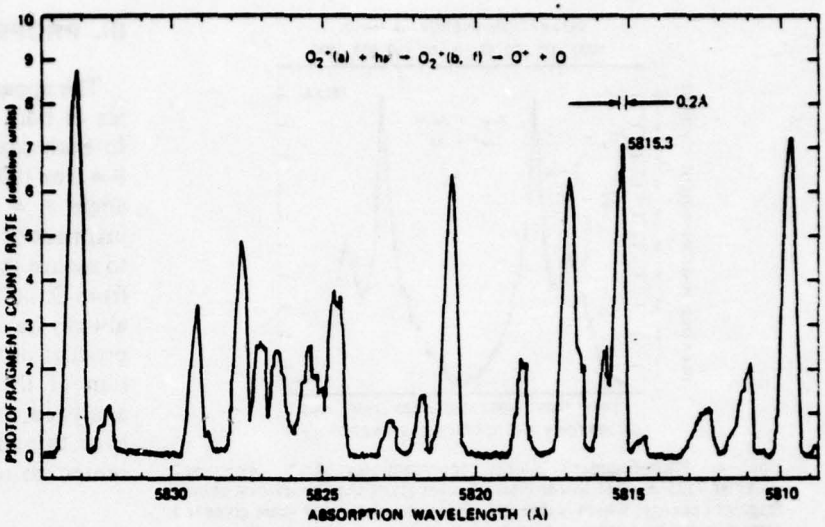

FIG. 5. Spectrum of photofragments observed near $W = 0$ as a function of wavelength for the transition indicated on the figure.

of O_2^+ are well resolved, and the energy resolution of the apparatus is demonstrated to be about 5×10^{-4}.

The angular dependence of the photodissociation fragment ions has been treated by Zare and Hershbach[19] for cases of zero and infinite dissociation (or predissociation) times and by Ling[20] for varying lifetimes of the intermediate state. In the zero-lifetime case[19] the distributions behave as $P(\beta) \propto [1 + \beta/2(3\cos^2\beta - 1)]$, where β is the angle between the laser polarization vector and the c.m. fragment ion velocity, and $-1 \leq \beta \leq 2$.

The angular distribution can thus vary from isotropic to $\cos^2\beta$ or $\sin^2\beta$. Inclusion of varying lifetimes[20] and the effects of spin-orbit coupling[17] significantly complicate this picture, but all basically tend to make the angular distribution more nearly isotropic. Thus fragment ion spectra can often be observed even for basically parallel transitions ($\Delta\Lambda = 0$), with coaxial beams where $P(\beta) \propto \sin^2\beta$ in the limiting case. An example of this is the $^2\Sigma_g^+ \leftarrow {}^2\Sigma_u^+$ transition shown in Fig. 4.

The coaxial beams arrangement is also well suited to the threshold (or, perhaps better, "predissociation") photofragment spectroscopy.[4] With this technique, a tunable laser is used to investigate photodissociations as a function of laser wavelength, near the threshold, which result in near-zero-energy photofragments. These photodissociations can result from transitions to a repulsive potential, to quasibound levels near the dissociation limit (as in rotational predissociation), or to a predissociating bound state. For predissociations such as are observed in O_2^+, the resolution depends primarily on the lifetime of the predissociating level, the energy spread in the ion beam, and the linewidth of the laser. The characteristics of the photofragment spectra observed as a function of both kinetic energy and wavelength allow the dissociating state to be identified, and levels of both initial and final states to be determined. A typical wavelength spectrum of the dissociation cross section obtained in this way for the transition $O_2^+(a^4\Pi_u, v = 4) + h\nu \rightarrow O^+ + O$ is shown in Fig. 5. Here the observed energy resolution is 0.1 meV, as compared with about 30 meV for normal photofragment spectroscopy.[2,3,17,18] The peaks shown in this figure correspond to transitions between specific rotational and fine structure levels of the $a^4\Pi_u$ state and the $b^4\Sigma_g^-$ and $f^4\Pi_g$ states. Work is currently underway to interpret results such as those shown in Fig. 6 in terms of the energy levels of these states. In order to avoid the complication of the two Doppler-shifted frequencies, $\nu_0(1 \pm v/c)$, seen by the beam in the intracavity operation, these data are obtained using the extracavity laser beam.

Another advantage of the coaxial configuration is that the ions in fast beams can have a very narrow Doppler width for absorption of the laser photons. This effect was recognized early in the planning of our apparatus and has since been discussed[21] and exploited[6-9] by others. The energy spreads of a few eV or less in the laboratory frame of reference that characterize

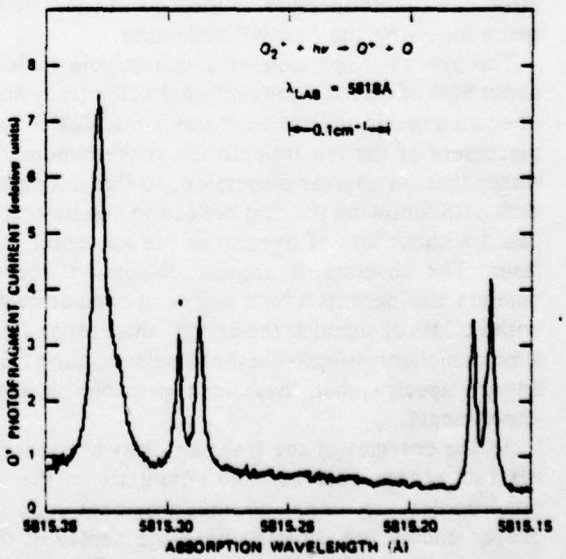

FIG. 6. Velocity-tuned spectrum of O^+ photofragments covering the 0.2-Å wavelength range near 5815 Å indicated in Fig. 5 (laser was operated single mode).

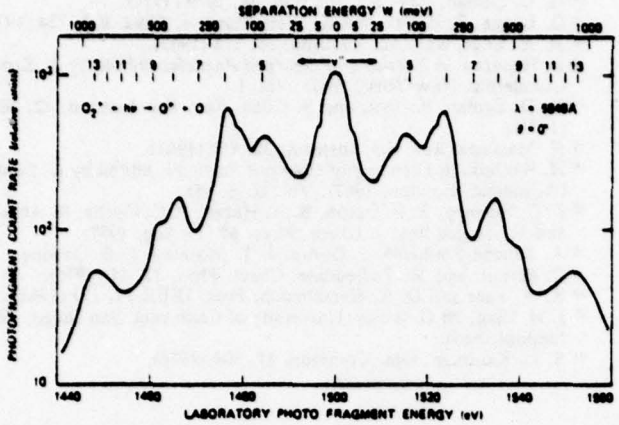

FIG. 7. Photofragment energy spectrum for $O_2^+(a^4\Pi_u) + h\nu \rightarrow O^+ + O$ obtained at 5846 Å using crossed beams.

beams from many ion sources are unchanged when the ions are accelerated through electrostatic fields and the c.m. distribution of velocity components along the beam axis becomes very narrow, with equivalent kinetic temperatures, as seen by the laser, of a few kelvins. The increased absorption strength at line center and narrowness of optical transition lines can be very useful in high-resolution spectroscopic studies and photoexcitation of ions, or using fast neutral beams produced by charge transfer from ion beams. To achieve optimum resolution, single-frequency lasers must be used. Fine "tuning" of the absorption wavelengths can be achieved at a fixed laser frequency by varying the ion beam energy and Doppler-shifting the absorption lines through the laser frequency. The electrostatic cage shown in Fig. 2 is used to vary the beam energy and obtain such a "velocity-tuned" spectrum. Thus by use of a relatively simple voltage sweep one can effectively use fixed frequency, multiline lasers such as CO and CO_2 lasers as though they were continuously tunable, and can "tune" single-frequency dye lasers in the visible over several angstroms.

An example of a velocity-tuned spectrum is shown in Fig. 6. To obtain this spectrum, the beam energy was swept from 3180 to 3600 eV, while the laser was operating single-frequency near 5818 Å. While the absolute wavelength is uncertain by ±1 Å, the relative wavelength is precise to within ±0.0005 Å (50 MHz) and the laser linewidth was only 0.0001 Å. The five distinct peaks and the shoulder all lie within the band of 0.2 Å indicated in Fig. 6, and together make up the peak labeled 5815.3 in that figure. The peak widths in this spectrum vary from 170 MHz (0.7×10^{-6} eV) to 700 MHz (2.9×10^{-6} eV), reflecting the lifetime of the predissociating states. The 3-eV energy spread of the ion beam causes a Doppler width of 120 MHz which is folded into the observed widths. This technique should yield measurements of transition energies that are an order of magnitude more precise than existing spectrographic measurements.

Obviously, the velocity-tuned spectroscopy described above can also be applied using a collisional detection scheme[7,9] for both vibrational and electronic transitions. This technique has the advantage of not requiring that the transition lead to predissociation, but requires the use of phase-sensitive detection since a small change in the primary ion current must be observed.

Finally, although this capability has not yet been demonstrated, calculations show that it should not be difficult to observe laser-induced fluorescence from the beam. A photomultiplier and filter for this type of observation are indicated in Fig. 2. In some cases, it should be possible to use a monochromator to observe the fluorescence and determine not only the absorbing states but also the fluorescence channels.

B. Crossed-beam configuration

When "parallel" transitions ($\Delta\Lambda = 0$) in photodissociation yield angular distributions with near-zero fragment ion intensities along the axis in the coaxial arrangement, the laser polarization vector can be oriented along the beam axis by directing the laser at 90° to the ion beam axis in the more traditional arrangement. An example is shown in Fig. 7, which shows the photofragment energy spectra of the photofragments following the $a^4\Pi_u \rightarrow f^4\Pi_g$ transition in O_2^+, as was observed by Tabché-Fouhaillé *et al.*[18] (as compared to the wavelength dependence of the cross section near threshold as shown in Fig. 5). Here the vibrational spacings of the $a^4\Pi_u$ initial state are sufficiently large to be well resolved by the energy analyzer, and the structure seen in Fig. 7 shows the high-energy resolution obtainable in this apparatus.

These data were obtained at 5846 Å, and are directly comparable to the same results shown in Fig. 5 of Ref. 18. The apparent differences are the larger peak at $W = 0$ and the additional structure in our data. The main vibrational levels observed here ($v'' = 5$, 6, and 8) agree with those in Ref. 18 within the combined experimental uncertainties (±20 meV), and with the locations expected from optical and photoelectron spectroscopy (see Ref. 18). Dissociation from levels $v'' = 9$ and 13, not observed in Ref. 18, is clearly present here as are shoulders on the $v'' = 5$ and 6 peaks and on the central peak. The $v'' = 5$ and 6 shoulders probably arise from dissociation via the $O(^3P_1)$ state.[18] The fact that the $W = 0$ peak is larger in the present data can be due to a very slight difference in wavelength in the two experiments, since the photofragment signal near 5846 Å varies rapidly with wavelength, as in the data of Fig. 5.

ACKNOWLEDGMENT

This work was supported by the National Science Foundation, Army Research Office, Air Force Office of Scientific Research, and SRI International through its Independent Research and Development Program.

[a] Present address: Ruhruniversität Bochum, 4630 Bochum, West Germany.

[b] Present address: High Energy Physics Laboratory, Stanford University, Stanford, CA.

[1] G. von Busch and G. H. Dunn, Phys. Rev. A 5, 1726 (1972).

[2] J.-B. Ozenne, D. Pham, and J. Durup, Chem. Phys. Lett. 17, 422 (1972).
[3] N. P. F. B. van Asselt, J. G. Maas, and J. Los, Chem. Phys. Lett. 24, 555 (1974).
[4] J. T. Moseley, M. Tajeddine, J. Durup, J.-B. Ozenne, C. Pernot, and A. Tabché-Fouhaillé, Phys. Rev. Lett. 37, 851 (1976).
[5] H. J. Andrä, A. Gaupp, and W. Wittmann, Phys. Rev. Lett. 31, 501 (1973), and subsequent publications. An extreme example of this method is given by H. C. Bryant *et al.*, Phys. Rev. Lett. 38, 228 (1977).
[6] W. H. Wing, G. A. Ruff, W. E. Lamb, Jr., and J. J. Spezeski, Phys. Rev. Lett. 36, 1488 (1976).
[7] P. M. Koch, L. D. Gardner, and J. E. Bayfield, *Proc. Fourth Int. Conf. on Beam Foil Spectroscopy*, edited by I. Sellin and D. Pegg (Plenum, New York, 1976).
[8] M. Dufay, M. Carré, M. L. Gaillard, G. Neunier, H. Winter, and A. Zgainski, Phys. Rev. Lett. 37, 1678 (1976).
[9] A. Carrington and P. J. Sarre, Mol. Phys. 33, 1495 (1977).
[10] H. D. Zeman, Rev. Sci. Instrum. 48, 1079 (1977).
[11] G. Lange, B. Huber, and K. Weisemann, J. Phys. E 9, 734 (1976).
[12] H. A. Enge, Rev. Sci. Instrum. 35, 278 (1963).
[13] L. Hanszen, in *Focusing of Charged Particles*, edited by A. Septier (Academic, New York, 1967), Vol. I.
[14] H. D. Zeman, K. Jost, and S. Gilad, Rev. Sci. Instrum. 42, 485 (1971).
[15] H. Matsuda, Rev. Sci. Instrum. 32, 850 (1961).
[16] H. Wollnik, in *Focusing of Charged Particles*, edited by A. Septier (Academic, London, 1967), Vol. II, p. 163.
[17] J. T. Moseley, R. P. Saxon, B. A. Huber, P. C. Cosby, R. Abouaf, and M. Tadjeddine, J. Chem. Phys. 67 (15 Aug. 1977).
[18] A. Tabché-Fouhaillé, J. Durup, J. T. Moseley, J.-B. Ozenne, C. Pernot, and M. Tadjeddine, Chem. Phys. 17, 81 (1976).
[19] R. N. Zare and D. R. Herschbach, Proc. IEEE 51, 173 (1963).
[20] J. H. Ling, Ph.D. thesis (University of California, San Diego, 1975) (unpublished).
[21] S. L. Kaufman, Opt. Commun. 17, 309 (1976).

Photofragment spectroscopy and potential curves of Ar_2^+ [a]

J. T. Moseley, R. P. Saxon, B. A. Huber,[b] P. C. Cosby, R. Abouaf,[c] and M. Tadjeddine[d]

Molecular Physics Center, Stanford Research Institute, Menlo Park, California 94025
(Received 5 May 1977)

Photofragment energy distributions have been measured for the process $Ar_2^+(^2\Sigma_u^+)+h\nu \rightarrow Ar^+ + Ar$ using a 3 keV ion beam and cw lasers both coaxial and crossed with the ion beam, polarized, respectively, perpendicular and parallel to the ion beam direction. Measurements were made at 14 wavelengths between 4579 and 7993 Å. Transitions to the dissociative states $^2\Pi_g$ and $^2\Sigma_g^+$ are observed, as are the effects of the spin–orbit interaction in Ar_2^+. The experimental results are used along with theoretical calculations to determine the $^2\Sigma_u^+$, $^2\Sigma_g^+$, and $^2\Pi_g$ potentials. The effects of the spin–orbit interaction on the potential curves, the magnitude and wavelength dependence of the photodissociation cross section, and the angular distributions of the photofragments are considered.

I. INTRODUCTION

The potentials of Ar_2^+ have been extensively investigated using techniques of collision spectroscopy. Early measurements[1–6] established the effects of the $^2\Pi_g$ and $^2\Pi_u$ states in producing the dominant interference pattern observed in differential scattering measurements. More recent measurements of this type[4–6] were used to determine the $^2\Pi_g$–$^2\Pi_u$ difference potential and the $^2\Sigma_u^+$ well depth, and, through comparison with theoretical calculations such as those of Mulliken[7] and of Gilbert and Wahl,[8] to construct these three Ar_2^+ potentials. Other *ab initio* calculations of these Ar_2^+ potentials have been made by Sidis, Barat, and Dhuicq[9] and by Stevens, Gardner, and Karo.[10]

Figure 1 shows the four Ar_2^+ potentials relevant to this work, in the absence of spin–orbit splitting. The potentials shown here are drawn to represent those determined from the measurements reported in this paper. They are introduced at this point to show qualitatively the expected positions of the potentials in order to facilitate discussion. All of the above-mentioned Ar_2^+ potentials are within ± 0.2 eV of the potentials illustrated in Fig. 1.

The absolute photodissociation cross section for the reaction

$$Ar_2^+(^2\Sigma_u^+)+h\nu \rightarrow Ar^+ + Ar \qquad (1)$$

taking place via the $^2\Pi_g$ potential has been measured over the wavelength range from 5650 to 6950 Å by Miller, Ling, Saxon, and Moseley.[11] This cross section was compared with the cross section which would result from the potentials of Mittmann and Weise[6] and Gilbert and Wahl,[8] and it was concluded that neither of these potentials could result in the measured photodissociation cross sections. However, shifts of these potentials on the order of 0.1 eV (in opposite directions) could produce agreement with the data, and 0.1 eV is certainly within the expected uncertainty in these potentials. The more recent calculations of Stevens *et al.*[10] produce much better agreement for the wavelength dependence of the photodissociation. In this work the transition matrix element which is needed to calculate the absolute value of the cross section was also determined. This yielded[10] a cross section about three times smaller than was experimentally observed.

The photodissociation of Ar_2^+ has also been observed by Vestal and Mauclaire,[12] and by Carrington, Milverton, and Sarre,[13] but neither of these observations were sufficiently detailed to allow conclusions to be drawn concerning the Ar_2^+ potentials.

We report here the measurement and interpretation of photofragment energy spectra for Reaction (1), for dissociation via both the $^2\Pi_g$ and $^2\Sigma_g^+$ potentials, at 14 wavelengths between 4579 and 7993 Å. There are a number of motivations for this study. It was clear from our previous work[11] that the existing Ar_2^+ potentials are inadequate to quantitatively predict important features of the molecule, such as its photodissociation (and ab-

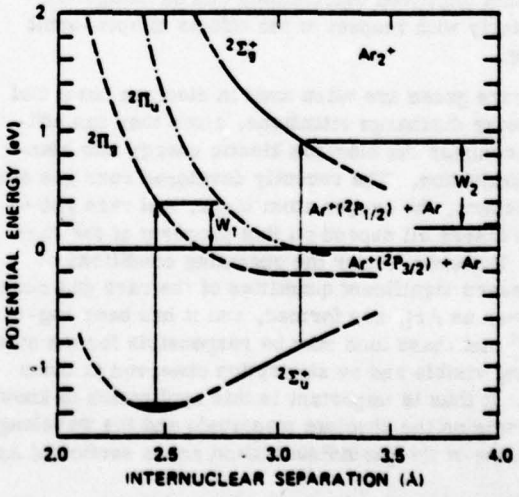

FIG. 1. Potential curves of Ar_2^+. The solid line portions of the curves were investigated in the work reported here. The dashed line portions are extrapolations based on the potentials of Ref. 10. The dot–dash potential was determined using the $^2\Pi_g$–$^2\Pi_u$ difference potential of Ref. 5. The indicated transitions correspond to 7525 Å.

[a] Supported by the National Science Foundation under Grant No. CHE-7510085 and the U. S. Air Force Office of Scientific Research.

[b] Permanent address: Ruhruniversität, Institut für Experimental-Physik II, Bochum, West Germany.

[c] Permanent address: Laboratoire des Collisions Electroniques, Université de Paris-Sud, 91405 Orsay, France.

[d] Permanent address: Laboratoire des Collisions Ioniques, Université de Paris-Sud, 91405 Orsay, France.

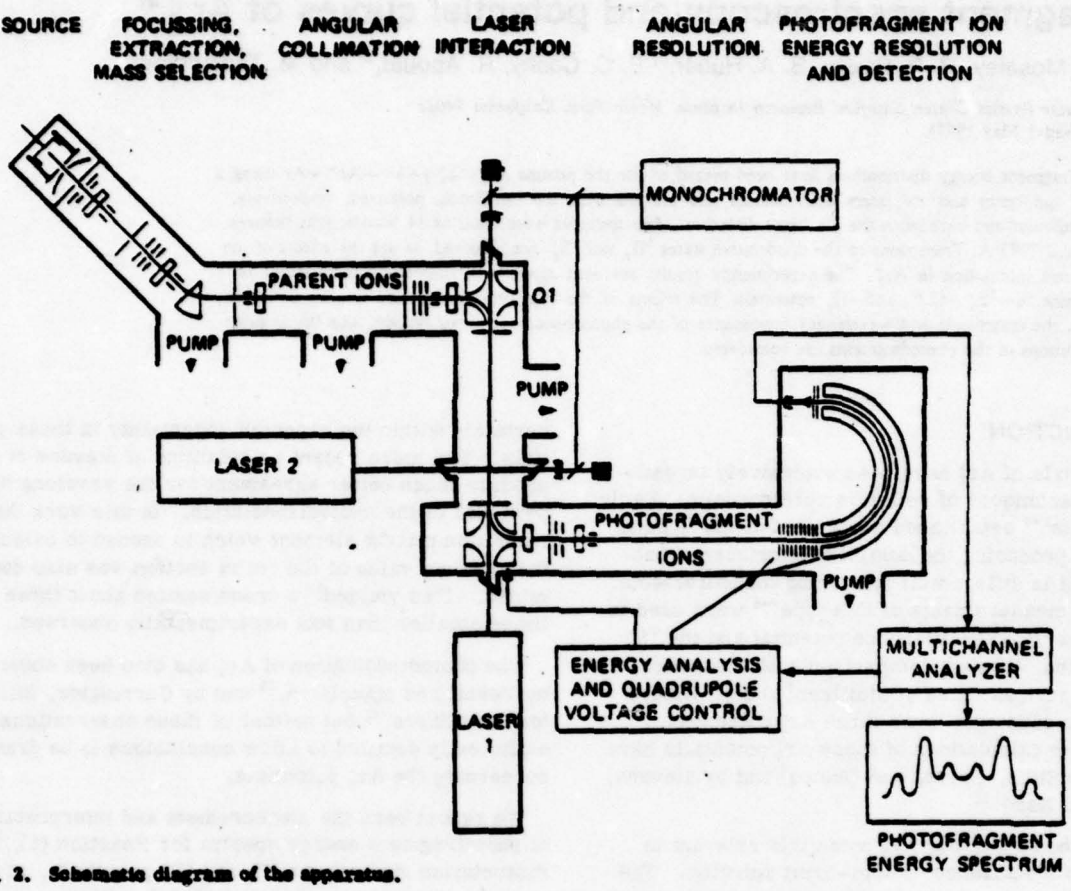

FIG. 2. Schematic diagram of the apparatus.

sorption) cross section. As has been pointed out,[9] spin–orbit effects are also likely to be important in this molecule. It is therefore useful both to determine more accurate Ar_2^+ potentials based on spectroscopic measurements and to provide detailed experimental information with which improved calculations can be compared, particularly with respect to the effects of spin–orbit coupling.

The rare gases are often used in electron beam and high energy discharge situations, since they can efficiently transfer the electron kinetic energy into electronic excitation. The recently developed rare gas excimer lasers, the oxygen atom laser, and rare gas–halogen lasers all depend on this property of the rare gases. However, under the operating conditions of these lasers significant quantities of the rare gas dimer ions, such as Ar_2^+, are formed, and it has been suggested[14] that these ions may be responsible for the gain-inhibiting visible and uv absorption observed in these lasers. It thus is important in this application to know with precision the absolute magnitude and the wavelength dependence of the photodissociation cross section of Ar_2^+.

II. EXPERIMENTAL PROCEDURES

The measurements reported here were made on a new ion photofragment spectrometer which is described in detail elsewhere.[15] A schematic of the apparatus is shown in Fig. 2. The Ar_2^+ ions are formed by the associative ionization reaction

$$Ar^* + Ar \rightarrow Ar_2^+ + e \qquad (2)$$

in a hollow-cathode discharge source,[16] with an energy spread of less than 0.6 eV full width at half-maximum. The Ar_2^+, along with a much larger current of Ar^+ and some impurity ions, are accelerated to typically 3 keV and focussed into a 45° sector magnet. The Ar_2^+ ions of interest are selected by the magnetic analyzer, collimated to 2 mrad, and directed into a transverse quadrupole field[17] which bends the ion beam through 90° without disturbing the high degree of collimation.

The ions exit from this first quadrupole into the laser interaction region. Here the intracavity photons from an argon ion laser or a krypton ion laser can be made either coaxial with the ion beam for a distance of 33 cm, or crossed with it. Good alignment is assured for the coaxial beams since both the ions and the intracavity photons of the laser must pass through 3 mm apertures at each end of the interaction region. Similar apertures define the intersection of the crossed beams. In the coaxial beams configuration the laser polarization is necessarily always perpendicular to the ion beam direction. In the crossed beams configuration the laser polarization can, in principle, be made to have any direction with respect to the beam, but for the work reported here it was always parallel to the ion beam direction.

Following the laser interaction region the ions enter a second quadrupole bender whose potentials are adjusted to pass the Ar^+ photofragments, which have ap-

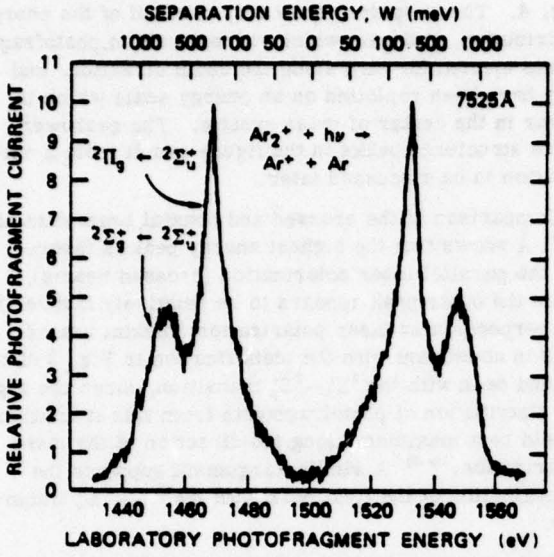

FIG. 3. Experimental photofragment energy spectrum for $Ar_2^+ + h\nu \rightarrow Ar^+ + Ar$ at 7525 Å, obtained with coaxial beams.

proximately half the Ar_2^+ beam energy of 3000 eV. After this quadrupole the Ar^+ ions pass through a second set of apertures, which yield an angular resolution in the lab system of 2 mrad for the photofragments. The ions are then decelerated by approximately 1200 eV and enter a hemispherical energy analyzer set to pass ions of a fixed energy near 300 eV. The resolution $\Delta E/E$ of the energy analyzer is 3×10^{-3} with respect to the energy with which the ions traverse the analyzer. For typical conditions used here changes in the laboratory energy of 1 eV could be easily resolved. This corresponds to a resolution of 7×10^{-4} with respect to the nominal 1500 eV photofragment energy. Ions which are passed by the energy analyzer are detected individually by a continuous-dynode electron multiplier and the resulting counts directed into a multichannel analyzer.

Typical photofragment energies in the laboratory frame in these experiments were 1500 ± 70 eV. In order to obtain a spectrum of photofragment energies the deceleration voltage is stepped proportionately with the channel advance of the multichannel analyzer, while the voltage on the hemispherical analyzer remains fixed. Since the quadrupoles are also energy analyzers, the potentials on the second quadrupole are also stepped in proportion to the change in the deceleration voltage, so that this quadrupole is always set to optimally transmit photofragment ions of the energy being passed by the energy analyzer.

A typical spectrum obtained in this way at 7525 Å is shown in Fig. 3. The spectrum is symmetric since photofragments ejected with kinetic energy either forward or backward along the beam direction are detected with nearly equal efficiency. The center of the spectrum is at 1500 eV, as expected for the photodissociation of a homonuclear diatomic of energy 3000 eV. As has been discussed in detail by Durup and co-workers,[18] and by van Asselt, Maas, and Los[19] for a homonuclear diatomic, a photofragment from a dissociative transition such as those indicated in Fig. 1 will appear at 0° in the laboratory with an energy T given by

$$T = \tfrac{1}{2}T_0 \pm (WT_0)^{1/2} + \frac{W}{2}, \tag{3}$$

where T_0 is the parent ion energy and W is the total kinetic energy of separation in the center of mass frame (see Fig. 1). In fact, when one includes the finite angular resolution of the apparatus there is a small shift[19] of the peak of the photofragment energy spectrum to lower a value of W. However, due to the high angular resolution of this apparatus (2 mrad), and the relatively large center of mass photofragment energies involved here (250 to 1500 meV), this shift is within the uncertainty of the laboratory photofragment energy measurement, and is neglected. Equation (3) is thus used to convert the laboratory energy scale to separation energy W. Such a W scale is shown at the top of Fig. 3.

It is important to note the amplification of center of mass energies when measured in the laboratory frame, For example, a kinetic energy release of 300 meV in the center of mass appears as 30 eV when measured in the laboratory frame. Our resolution of 1 eV in the laboratory frame corresponds to an uncertainty of ± 10 meV in this 300 meV peak. In practice, it is not difficult to locate peaks repeatedly to within ± 5 meV, and an uncertainty of ± 10 meV is believed to be conservative for the location of peaks with center of mass energies less than 600 meV. This uncertainty increases slowly with increasing center of mass energy, reaching ± 20 meV for a 1400 meV peak.

By comparison of the energies of the peaks with the potentials of Fig. 1 it is possible to determine to which transitions the peaks correspond, assuming these potentials are approximately correct. The vertical arrows in Fig. 1 are drawn to correspond to a wavelength of 7525 Å, and it is assumed that the transition to the $^2\Sigma_g^+$ state leads to dissociation with respect to the $Ar^+(^2P_{1/2}) + Ar$ limit since this state correlates asymptotically with this limit and does not cross any states originating from the $Ar^+(^2P_{3/2}) + Ar$ limit. Transitions to the $^2\Pi_u$ state are not expected, since they are dipole forbidden. We thus make a tentative identification of the transitions resulting in the peaks shown in Fig. 3, as indicated on the figure.

We note that individual vibrational levels do not appear to be resolved here, as they have been for H_2^+[18,19] and O_2^+.[20] This is not surprising since the vibrational spacing for Ar_2^+ is expected to be only about 30 meV, and the rotational spread at our ion source temperature of near 400 °K has a half-width of about 50 meV. When this rotational spread is combined with the finite energy resolution of the apparatus it will clearly be difficult to resolve the individual vibrational levels in Ar_2^+.

It it is possible to show that a series of peaks at different wavelengths correspond to transitions arising from the same vibrational level, a relative photodissociation cross section for this vibrational level can be obtained simply by appropriately normalizing the observed photofragment current for photon flux, parent ion beam intensity, and angular and energy resolution.

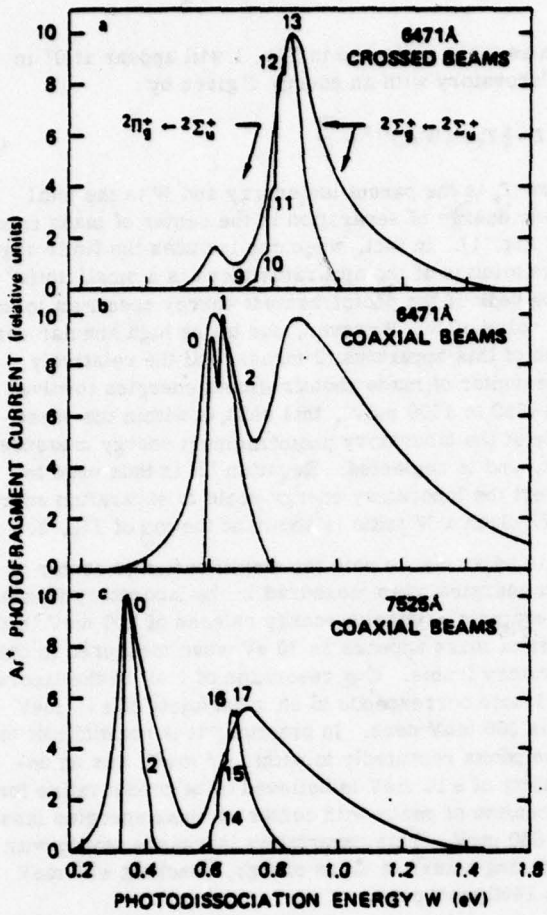

FIG. 4. Experimental and calculated photofragment energy spectra. The calculated spectra are discussed in Sec. IV and include rotational broadening, but do not include broadening due to the ion beam energy spread and the finite energy and angular resolution of the apparatus. The numbers refer to the structure in the calculated spectra, and correspond to the vibrational levels of the ground state.

It should be noted that the stated wavelengths are the wavelengths in air. No correction was made for the fact that in the vacuum the wavelength is slightly different since this difference (in energy) is more than an order of magnitude smaller than the uncertainty of ± 10 meV in the center of mass kinetic energy measurements. Additionally, in the intracavity coaxial beams measurements the 3 keV Ar_2^+ actually interacts with two wavelengths Doppler shifted by about ± 2–3 Å from the laboratory wavelength. The uncertainty introduced by this is also much smaller than the uncertainty in the kinetic energy measurements, and is neglected.

III. EXPERIMENTAL RESULTS

Photofragment energy spectra such as the one illustrated in Fig. 3 were obtained at 14 wavelengths between 4579 and 7993 Å. At most of these wavelengths spectra were obtained both in the coaxial beams configuration with the laser polarization perpendicular to the ion beam direction and in the crossed beams configuration with the laser polarization parallel to the ion beam direction. Three such spectra are illustrated in Fig. 4. These spectra show only one half of the energy distribution, that part which corresponds to photofragments ejected forward along the beam direction, and they have been replotted on an energy scale which is linear in the center of mass system. The narrower, more structured peaks in the figure result from a calculation to be discussed later.

Comparison of the crossed and coaxial beam data at 6471 Å shows that the highest energy peak is favored for the parallel laser polarization (crossed beams), while the other peak appears to be relatively favored for the perpendicular laser polarization (coaxial beams). This is consistent with the identification in Fig. 3 of the second peak with the $^2\Sigma_g^+ - {}^2\Sigma_u^+$ transition, since the angular distribution of photofragments from this transition should be a maximum along the direction of the laser polarization.[18–21] A similar argument supports the identification of the first peak with the $^2\Pi_g - {}^2\Sigma_u^+$ transition.

Table I summarizes the results of measurements on the first peak at four wavelengths. The first striking feature is that the values of the photon energy $h\nu$ minus the separation energy W are equal to within the ± 10 meV uncertainty in the determination of the peak location. This means that all of these photodissociations originate in the same ground state vibrational level. The wide wavelength range over which this single level is dominant argues strongly for its identification as $v = 0$. Relative cross section measurements determined from the peak intensities indicate a single maximum, as would be expected from $v = 0$. The location of this maximum is between 6764 and 7525 Å, probably 7200 ± 200 Å, consistent with the recent calculations of Stevens *et al.*[10] The ratio of the cross section at 6764 to that at 6471 Å is in excellent agreement with our measurements[11] of the absolute values of the photodissociation cross section for Ar_2^+ ions in a thermal vibrational distribution at 300 °K (i.e., primarily in $v = 0$). We thus identify these transitions as $^2\Pi_g - {}^2\Sigma_u^+(v = 0)$.

The average value of 1.31 eV for $(h\nu - W)$ is then nearly equal to the dissociation energy with respect to the first vibrational level $D_0(Ar_2^+)$. It must only be corrected by the average rotational energy of the ions. At the assumed source temperature of 400 °K this is 17 meV. Thus, we determine $D_0(Ar_2^+) = 1.33 \pm 0.02$ eV. The uncertainty in the source temperature of ± 50 °C contrib-

TABLE I. Summary of results for the transition $^2\Pi_g - {}^2\Sigma_u^+$. All experimental results are for coaxial beams.

λ (Å)	W_{exp} (eV)	$h\nu - W_{exp}$ (eV)	σ (relative units)	W_{calc} (eV)	R^a (Å)
7993	0.248	1.303	4.3	0.241	2.51
7525	0.337	1.311	12.6	0.340	2.47
6764	0.525	1.308	7.2	0.520	2.41
6471	0.603	1.313	5.1	0.607	2.38

[a]Internuclear distance corresponding to the transition determined using the $^2\Sigma_u^+$ potential discussed in Sec. IV.

TABLE II. Summary of results for the transition $^2\Sigma_g^+ - {}^2\Sigma_u^+$.

λ (Å)	W_{exp} (eV) Crossed	Coaxial	$h\nu - W_{exp}$ (eV)	W_{calc} (eV)	R^b (Å)	Vibrational level at peak
7993		0.629				16–18
7525	0.666	0.710	0.962	0.670	3.11	15–17
6764	0.790	0.910	1.043	0.790	3.05	12–14
6471	0.828	0.970	1.088	0.845	2.99	12–13
5682	1.00	1.06	1.18	1.020	2.91	9–10
5309	1.12	1.17	1.22	1.120	2.87	7–9
5145	1.17	1.19	1.24	1.185	2.85	6–8
4965	1.22	1.24	1.28	1.220	2.82	5–7
4880	1.25	1.29	1.29	1.260	2.80	5–7
4825		1.33				
4765	1.30		1.30	1.315	2.78	5–6
4763		1.36				
4680	1.33		1.32	1.340	2.76	4–6
4579		1.38				

[a]Calculated relative to the crossed-beams results only.
[b]Internuclear distance corresponding to the transition determined using the $^2\Sigma_u^+$ potential discussed in Sec. IV.

utes only 5 meV to the uncertainty in D_0. This value for D_0 is in good agreement with the values obtained by Lorents, Olson, and Conklin[4] (1.25 eV), Mittman and Weise[6] (1.34 eV), Gilbert and Wahl[8] (1.25 eV), and Stevens, Gardner, and Karo[10] (1.20 eV), when it is considered that the estimated uncertainty in each of these determinations is ± 0.1 eV.

A bond energy of 1.33 ± 0.02 eV is, however, in slight disagreement with the recently reported value[22] of 1.23 ± 0.02 eV of Ng, Trevor, Mahan, and Lee, obtained from the photoionization spectrum of Ar_2. The value of Ng *et al.* was determined from the observed onset of photoionization at 852.7 Å. The threshold in this region is not at all sharp (see Fig. 2 of Ref. 22), and the photoionization cross section is very small due to unfavorable Franck–Condon factors. Our determination of the bond energy, which does not depend on the observation of a weak photoionization signal near threshold, implies that the true ionization potential of Ar_2 is 858.6 Å. We do not believe a significant systematic error is present in our experiments, due to the agreement we have obtained on our spectrometer with earlier work in another laboratory[20] on O_2^+, and to the fact that the bond energy we determine for Kr_2^+ of 1.14 ± 0.03 eV[23] is in excellent agreement with the 1.15 ± 0.02 eV determined by Ng *et al.* For Kr_2^+ the Franck–Condon factors are more favorable, and the photoionization threshold is well-defined (see Fig. 2 of Ref. 22).

Note from the two coaxial beams spectra in Fig. 4 that the two peaks are coming closer together at shorter wavelength, and the $\Sigma - \Sigma$ peak is becoming relatively more intense. Qualitatively, this movement of the peaks is to be expected from the potential curves. Assuming a one-to-one correspondence between internuclear separation and wavelength, as we go from 7525 Å toward shorter wavelength, the two Σ curves are changing in opposite directions, thus retarding the increase of W with $h\nu$. Therefore, the two peaks would be expected to merge, and then at some shorter wavelength the peak corresponding to the $\Pi - \Sigma$ transition should appear at higher photon energy than that corresponding to the $\Sigma - \Sigma$. In fact, at the next available wavelength 5682 Å only one peak is visible, corresponding to the $\Sigma - \Sigma$ transition, although there is a shoulder on the low energy side corresponding to the $\Pi - \Sigma$. Over the remainder of the wavelength range studied no clear features emerged which could be definitely assigned to the $\Pi - \Sigma$ transition.

Table II shows a summary of results for the $\Sigma - \Sigma$ transition. Since this is a parallel transition, results from the crossed-beams configuration are the most definitive for determining the potentials, and only these results are used to calculate $(h\nu - W_{exp})$. The $\Sigma - \Sigma$ peaks are substantially broader than the $\Pi - \Sigma$ peaks, indicating that a number of vibrational levels are participating in the photodissociation. These individual vibrational levels are not resolved since the rotational broadening of individual levels is approximately equal to the vibrational spacings, and to the effective resolution of the apparatus.

It is qualitatively apparent that these levels are quite high, probably $v > 10$ for the 6471 and 7525 Å transitions illustrated in Fig. 4. This will be better quantified by calculations to be discussed later. The fact that at 6471 Å with coaxial beams the $\Sigma - \Sigma$ peak is as intense as the $\Pi - \Sigma$ indicates that the $\Sigma - \Sigma$ transition is much stronger than the $\Pi - \Sigma$. Under these conditions everything else seems to favor the $\Pi - \Sigma$—it originates at $v = 0$, and the polarization is correct for maximum collection of ions from such a perpendicular transition, while strongly discriminating against parallel transitions such as the $\Sigma - \Sigma$. This observation is consistent with the calculations of Stevens *et al.*,[10] which predicts that the $\Sigma - \Sigma$ photodissociation cross section should be about three orders of magnitude larger than that for the $\Pi - \Sigma$.

It is in fact surprising that the $\Pi - \Sigma$ transition is visible at all in the crossed beams spectra at 6471 Å. It is easy to calculate,[24] assuming no rotation before dissociation and pure parallel and perpendicular transitions for the $\Sigma - \Sigma$ and $\Pi - \Sigma$, respectively, that the detection efficiency in our apparatus in coaxial beams is 200 times better for the $\Pi - \Sigma$ than for the $\Sigma - \Sigma$, while almost exactly the opposite is true in crossed beams. Thus, since the two peak heights are equal at 6471 Å in coaxial beams, where the $\Pi - \Sigma$ is favored, the relative peak heights in crossed beams should differ by a factor of $(200) \times (200) = 4 \times 10^4$ in favor of the $\Sigma - \Sigma$ transition. In fact, the observed difference is only a factor of 6! Inclusion of rotation[24] cannot reduce this by more than a factor of 4, and may be negligible since the dissociations are occurring via a purely repulsive curve at separation energies substantially larger than the rotation energies involved. The effect of spin–orbit coupling is in the right direction—it will give some parallel ($\Sigma - \Sigma$) character to the perpendicular ($\Pi - \Sigma$) transition, and vice versa. We will return to this observation in the following sections.

It is noted that the $\Sigma - \Sigma$ peaks obtained with coaxial beams consistently peak at slightly higher W values (typically 30 meV—see Table II), and the peaks are significantly broader than the peaks obtained with

crossed beams. These effects are not understood, but are probably associated with the rotation of the molecule during dissociation. Similar effects were observed[18] for H_2^+, where the transition is purely parallel. In any case, for a parallel transition the data obtained with crossed beams and the laser polarization parallel to the beam direction should be used for the determination of potential curves.

IV. ANALYSIS

Two different types of experimental information have been determined in this work: separation energy (W) spectra as a function of wavelength and the relative photodissociation cross section as a function of photon wavelength. Potential curves for the states participating in the photoabsorption process in this experiment $^2\Sigma_u^+$, $^2\Pi_g$, and $^2\Sigma_g^+$ were determined by adjusting the potentials until the W spectra and cross sections calculated from them matched the experimental results. The analysis in this section will ignore the effects of spin–orbit coupling, which is discussed in the following section.

For a bound–free transition the absorption cross section as a function of photon frequency ν is given by[10,25]

$$\sigma_\nu = \frac{k_\nu}{N^a} = \frac{8\pi^3\nu}{3hc} \sum_{vJ} \int_{J'} d\epsilon\, S_{JJ'}\, \delta \times \left(\nu - \frac{\Delta E}{hc}\right) |\langle avJ \mid \mu \mid bJ'\epsilon\rangle|^2 \frac{N^a_{vJ}}{g_a(2J+1)}, \quad (4)$$

where avJ denotes the vibration–rotation quantum numbers of the initial bound electronic state a, and $bJ'\epsilon$ denotes the rotation quantum number and continuum energy of the final electronic state b. The quantity ΔE is the energy difference between the initial and final states, μ is the electronic transition moment, g_a and g_b are the electronic degeneracies of the initial and final states, respectively, and N^a_{vJ} is the fraction of the total number of state a molecules N^a in the vJ level. The absorption coefficient (customarily expressed in cm^{-1}) is denoted by k_ν. $S_{JJ'}$ is the Hönl–London factor. Assuming a Boltzmann distribution of initial levels

$$N^a_{vJ} = Q^{-1}(2J+1)\exp(-E_{vJ}/kT), \quad (5)$$

and

$$Q = \sum_{vJ} (2J+1)\exp(-E_{vJ}/kT), \quad (6)$$

where E_{vJ} is the binding energy of the vJ level. Using the sum rule for the Hönl–London factors $\sum_{J'} S_{JJ'} = 2J+1$ and the assumption that the matrix element $\langle avJ \mid \mu \mid bJ'\epsilon\rangle$ is largely independent of J', Eq. (4) may be written

$$\sigma_\nu = \frac{8\pi^3\nu}{3hc} \sum_{vJ} \int d\epsilon\, \delta\left(\nu - \frac{\Delta E}{hc}\right) \times |\langle avJ \mid \mu \mid bJ\epsilon\rangle|^2 \frac{g_b}{g_a} \frac{(2J+1)\exp(-E_{vJ}/kT)}{Q}. \quad (7)$$

To each initial state vJ and photon frequency ν there corresponds a unique value of separation energy W, which is equivalent to ϵ in Eqs. (4) and (7). The absorption cross section for photodissociation with energy W by a photon of wavelength $\lambda = c\nu^{-1}$ is given by

$$\sigma_\lambda(W) = \frac{8\pi^3\nu}{3hc} |\langle avJ \mid \mu \mid bJW\rangle|^2 \frac{g_b}{g_a} \frac{(2J+1)\exp(-E_{vJ}/kT)}{Q}, \quad (8)$$

where $\nu hc = \Delta E = E_{vJ} + W$.

The calculations evaluating Eqs. (7) and (8) used the computer program of K. Sando.

Since the calculation of Stevens *et al.*[10] provides the most detailed information for Ar_2^+, we have used it as a basis for construction of potentials which are consistent with our experimental results. We first modified the bound state $^2\Sigma_u^+$ potential curve by translating it downward by 0.141 eV to bring the dissociation energy into agreement with the D_0 value of 1.33 eV determined from the data. The potential was made to correlate to the appropriate $Ar^+(^2P_{3/2})$+Ar limit by exponentially decreasing the size of the translation with internuclear separation R, for $R > 3.7$ Å. This has no effect on the transitions observed in these experiments.

Using this $^2\Sigma_u^+$ potential curve the $^2\Pi_g$ potential curve given by Stevens *et al.* was then translated until the peak in W of the calculated cross section $\sigma_\lambda(W)$ agreed with experiment for the four wavelengths reported in Table I. Only coaxial beams data, where the perpendicular laser polarization is appropriate for this $^2\Pi_g - {}^2\Sigma_u^+$ transition, were considered. The transition moment μ calculated by Stevens *et al.* was used in Eq. (8). For this $\Pi - \Sigma$ transition the appropriate operator for μ is $(x+iy)/\sqrt{2}$, the Π state degeneracy g_b is 2, and g_a is 1. The relative photodissociation cross section as a function of wavelength, discussed above, indicates the peak of the cross section lies between 6764 and 7525 Å. Assuming the peak is at 7200 Å and that it corresponds to the center of the Franck–Condon region for $v=0$ gives an initial estimate for the appropriate translation. Agreement with the peaks in W was found by lowering the $^2\Pi_g$ potential curve by 0.178 eV. The potential was made to correlate to the $Ar^+(^2P_{3/2})$ +Ar limit in the same manner as for the $^2\Sigma_u^+$ state. Numerical values for the $^2\Sigma_u^+$ and $^2\Pi_g$ potential curves are given in Table III. As shown in Table I, the largest discrepancy between the observed and calculated peaks in W is 7 meV. Also given in Table I is the internuclear distance R corresponding to the $(^2\Pi_g - {}^2\Sigma_u^+)$ potential difference for the observed transition. From this quantity it is clear that the $^2\Pi_g$ potential curve has been determined between 2.38 and 2.51 Å.

The theoretical W spectra for the $\Pi - \Sigma$ transition at 6471 and 7525 Å are also shown in Fig. 4, where the cross section is expressed in relative units. The cross section displayed is the sum of that due to absorption out of individual vibrational levels. The W spectrum corresponding to absorption by all the rotational levels of a given vibrational level shows a single peak reflecting mainly the assumed Boltzmann distribution of rotational levels. (See Fig. 6 for a more detailed representation of the $^2\Sigma_g^+ - {}^2\Sigma_u^+$ transition at 6471 Å, discussed below.) For the four wavelengths studied in the coaxial beams configuration only vibrational levels 0, 1, and 2 were found to contribute to the $\Pi - \Sigma$ transition. Neglecting the variation of the transition moment with R

TABLE III. Ar_2^+ potential curves used in this work.

R (Å)	$^2\Sigma_u^+$ (eV)	$^2\Pi_g$ (eV)	$^2\Sigma_g^+$ (eV) ($^2P_{1/2}$ asymptote)
2.000	0.4513	3.3920	8.3636
2.100	−0.5955	2.5181	6.8974
2.200	−1.0552	1.6671	5.4602
2.300	−1.2333	1.0068	4.2638
2.400	−1.3328	0.5796	3.3716
2.500	−1.3368	0.2807	2.6661
2.600	−1.2986	0.0798	2.1138
2.700	−1.2119	−0.0513	1.6810
2.800	−1.1180	−0.1356	1.3591
2.900	−1.0172	−0.1872	1.1319
3.000	−0.9186	−0.2191	0.9439
3.100	−0.9252	−0.2370	0.7895
3.200	−0.7378	−0.2441	0.6644
3.300	−0.6573	−0.2437	0.5635
3.400	−0.5845	−0.2392	0.4811
3.500	−0.5203	−0.2337	0.4113
3.600	−0.4648	−0.2286	0.3526
3.700	−0.4177	−0.2239	0.3066
3.800	−0.3596	−0.2071	0.2875
3.900	−0.3104	−0.1911	0.2779
4.000	−0.2696	−0.1762	0.2741
4.100	−0.2359	−0.1624	0.2731
4.200	−0.2078	−0.1496	0.2716
4.300	−0.1841	−0.1378	0.2665
4.400	−0.1640	−0.1270	0.2575
4.500	−0.1467	−0.1169	0.2461
4.600	−0.1316	−0.1076	0.2336
4.700	−0.1180	−0.0991	0.2215
4.800	−0.1055	−0.0913	0.2111
4.900	−0.0937	−0.0841	0.2030
5.000	−0.0824	−0.0775	0.1970
5.100	−0.0719	−0.0714	0.1927
5.200	−0.0620	−0.0658	0.1896
5.300	−0.0529	−0.0608	0.1875
5.400	−0.0446	−0.0561	0.1858
5.500	−0.0371	−0.0519	0.1846
5.600	−0.0305	−0.0480	0.1836
5.700	−0.0248	−0.0445	0.1828
5.800	−0.0202	−0.0412	0.1821
5.900	−0.0166	−0.0383	0.1814
6.000	−0.0139	−0.0356	0.1806

the relative contributions depend on the Franck–Condon overlap and the assumed Boltzmann distribution. At 6471 Å absorption out of $v=1$ has a strong influence on the W spectrum, while at 7525 Å there is no contribution from $v=1$. The theoretical value entered in Table I for 6471 Å is the peak for $v=0$ since the experimental evidence indicates that the observed peaks in W correspond to the same vibrational level for all four wavelengths in Table I. Since the Franck–Condon factor depends sensitively on the shape of the bound state potential curve, a slight alteration would most likely be sufficient to reduce the calculated influence of absorption from $v=1$. The difference in width between the theoretical and experimental photofragment spectra gives an indication of the experimental broadening. Note that the $\Pi-\Sigma$ peak at 6471 Å is significantly broader than at 7525 Å, indicating that the contribution of $v=1$ is important at 6471 Å, although apparently not important enough to shift the peak location significantly.

The $^2\Sigma_u^+$ and $^2\Pi_g$ potential curves which have been adjusted to give agreement with the coaxial beams photofragment data should also predict the photoabsorption cross section as a function of wavelength in agreement with experiment. In Fig. 5 the cross section from Eq. (7) calculated using our adjusted potentials and the transition moment of Stevens *et al.* multiplied by 1.7 (see below) is compared with the relative cross sections of Table I and the absolute cross section measurements of Miller *et al.*[11] With the exception of the single point at 7525 Å the relative agreement is good. It is not known whether this point is in error experimentally; however, efforts are currently under way to measure the absolute cross section between 7000 and 8000 Å using the techniques of Miller *et al.* It was necessary to multiply the transition moment of Stevens *et al.* by 1.7 in order to bring the calculated cross section into absolute agreement with the measurements of Miller *et al.* However, it will be shown later that inclusion of spin–orbit effects substantially increases the magnitude of the calculated cross section.

The $^2\Sigma_g^+$ potential may be deduced from the data summarized in Table II. As stated before, for this parallel transition the crossed-beams data is the most definitive. As for the Π case, taking the adjusted $^2\Sigma_u^+$ potential curve as given, the upper state potential curve was modified until the W peaks were in agreement with experiment.

An initial approximation for the potential can be constructed by assuming the transition takes place at the classical outer turning point. Then at each wavelength, from the given $^2\Sigma_u^+$ curve, the binding energy $(h\nu - W_{exp})$ determines the internuclear distance R at which the transition occurs and W_{exp} gives the final state potential at that R value. Although spin–orbit effects have been neglected so far, we are assuming here that the $^2\Sigma_g^+$ curve dissociates to the correct limit $Ar^+(^2P_{1/2})+Ar$.

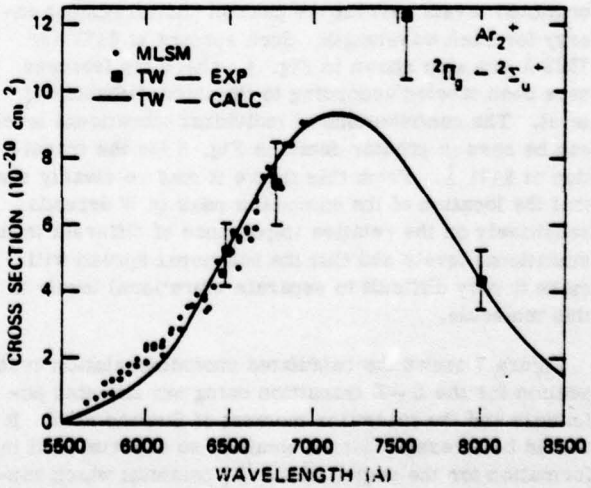

FIG. 5. Photodissociation cross section for $Ar_2^+(^2\Sigma_u^+, v=0) + h\nu \rightarrow Ar_2^+(^2\Pi_g) \rightarrow Ar^+ + Ar$. The dots are the absolute cross section measurements of Ref. 11, the squares are the relative cross section measurements of this work, and the solid curve is calculated from the potential curves determined here and the transition moment of Ref. 10 multiplied by 1.7 (see text).

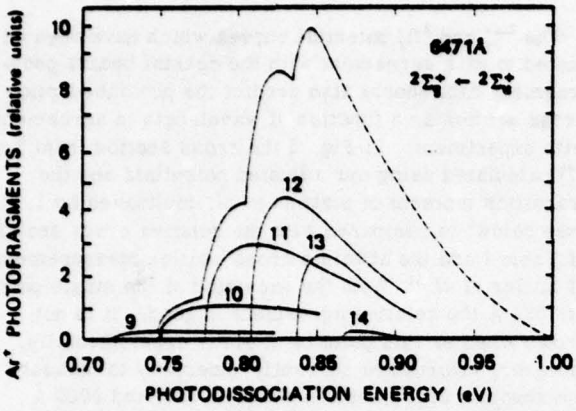

FIG. 6. Calculated photofragment energy spectrum showing the vibrational levels involved in this $\Sigma - \Sigma$ transition, and the effect of rotational broadening on the spectrum. Experimental broadening effects are not included. The dashed portion is an extrapolation since the calculation extended only to the 79th rotational level.

In order to bring the W peaks into agreement it was necessary to lower this initial potential by about 80 meV.

The modified $^2\Sigma_g^+$ potential curve is listed in Table III and may be expressed in terms of the $^2\Sigma_g^+$ curve of Stevens *et al.*,[10] which has been placed at the $^2P_{1/2}$ asymptote, 0.178 eV above the $^2P_{3/2}$ asymptote, and then decreased by a varying amount which equals 0.244 eV at 2.76 Å and 0.124 eV at 3.11 Å. The calculated peaks in photofragment energy for 12 wavelengths are listed in Table II, where the maximum discrepancy with experiment is seen to be 17 meV. The photofragment spectra were calculated from Eq. (8) using the adjusted potentials and the transition moment of Stevens *et al.* In this case $g_b = g_a = 1$. Many initial vibrational levels contributed at each wavelength. The theoretical peak entered in Table II is the peak in the sum over the initial vibrational levels. Also entered in Table II are the vibrational levels nearest the peak in photofragment energy for each wavelength. Such spectra at 6471 and 7525 Å are also shown in Fig. 4, where the features have been labeled according to the initial vibrational level. The contributions of individual vibrational levels can be seen in greater detail in Fig. 6 for the transition at 6471 Å. From this figure it may be clearly seen that the location of the composite peak in W depends sensitively on the relative importance of different initial vibrational levels and that the rotational spread will make it very difficult to separate vibrational levels in this molecule.

Figure 7 shows the calculated photodissociation cross section for the $\Sigma - \Sigma$ transition using our adjusted potentials and the transition moment of Stevens *et al.* It should be stressed that we obtained *no* experimental information for the region of the $^2\Sigma_g^+$ potential which contributes to this cross section. The shortest wavelength used was 4579 Å. However, the extrapolation of our potential curve to shorter wavelengths should provide a better approximation to reality than the previously existing $^2\Sigma_g^+$ potentials.

V. SPIN–ORBIT EFFECTS

The analysis in the previous section ignored the existence of spin–orbit coupling except for taking the correct $Ar^+(^2P_{1/2})$ states as the dissociation limit for the $^2\Sigma_g^+$ state. There are, however, two points that cannot be understood without an analysis of spin–orbit effects. The first is the observation of the $\Pi - \Sigma$ transition in crossed beam where the laser polarization is not appropriate for a perpendicular transition. In the previous section the shape of the relative photodissociation cross section as a function of wavelength was found to be in reasonable agreement with experiment, but its magnitude cannot be reliably determined without considering spin–orbit effects.

Our spin–orbit analysis is based on the discussion of Cohen and Schneider[26] for the analogous system Ne_2^+, which follows the treatment of Condon and Shortly.[27] Treating the spin–orbit coupling as a perturbation the energies of the spin–orbit states for the angular momentum projection $\Omega = \frac{1}{2}$ are given by the eigenvalues of the matrix

$$\begin{pmatrix} E(^2\Pi) - \alpha & \sqrt{2}\,\alpha \\ \sqrt{2}\alpha & E(^2\Sigma) \end{pmatrix}, \tag{9}$$

where α is $\frac{1}{3}$ of the $Ar^+(^2P_{3/2} - {}^2P_{1/2})$ splitting $= -0.059$ eV, the sign being negative for this case, where the $^2P_{3/2}$ is lower in energy than the $^2P_{1/2}$. The quantity $E(^2\Pi)$ is the energy of the $^2\Pi_g$ or $^2\Pi_u$ state. The matrix is diagonalized separately for g and u states at each value of R. For $\Omega = \frac{1}{2}$ states the energy considering spin–orbit is given by $E(^2\Pi) + \alpha$.

The structure of the states, including spin–orbit coupling, is indicated in Fig. 8, where they are labeled by their Ω quantum number. (Although this figure is drawn approximately to scale, it is meant to be schematic only.) There are four states correlating to the $Ar^+(^2P_{3/2})$ + Ar limit: the $1(\frac{1}{2})_u$ which is similar to the $^2\Sigma_u^+$ without spin–orbit coupling, the $1(\frac{1}{2})_g$ and $1(\frac{1}{2})_g$ which are similar to the $^2\Pi_g$, and the $1(\frac{1}{2})_u$ which is similar to the $^2\Pi_u$.

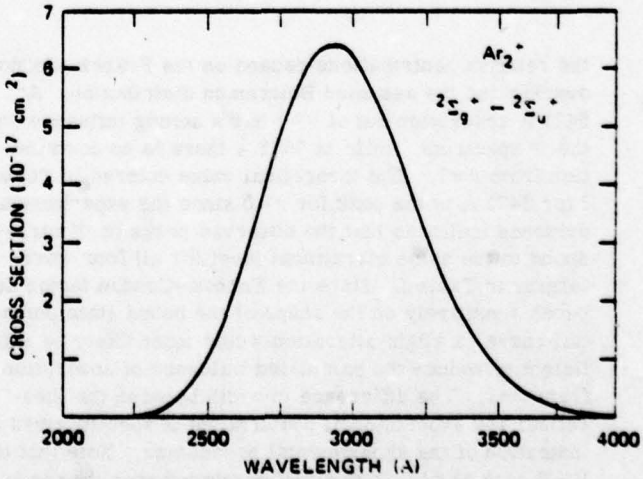

FIG. 7. Photodissociation cross section for $Ar_2^+(^2\Sigma_u^+, v=0) + h\nu \rightarrow Ar_2^+(^2\Sigma_g^+) \rightarrow Ar^+ + Ar$ calculated from the potential curves determined here and the transition moment of Ref. 10.

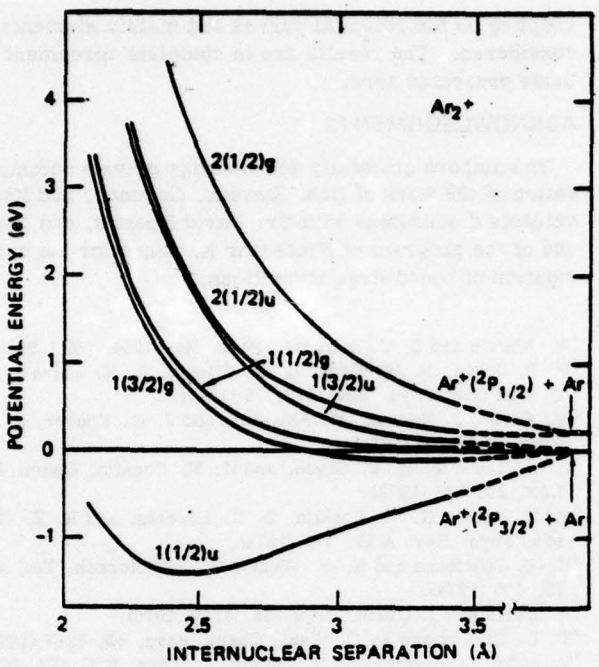

FIG. 8. Schematic potential curves for Ar_2^+ including spin–orbit coupling.

Correlating to the $Ar^+(^2P_{1/2})+Ar$ limit are the $2(\frac{1}{2})_u$ similar to the $^2\Pi_u$ and the $2(\frac{1}{2})_g$ similar to the $^2\Sigma_g^+$. The $1(\frac{1}{2})_g$ and $1(\frac{1}{2})_g$ states are separated by approximately 2α, the $1(\frac{1}{2})_g$ being lower than the original $^2\Pi_g$ by precisely α (see the previous paragraph, recalling that α is negative) and the $1(\frac{1}{2})_g$ being higher than the $^2\Pi_g$ by an amount approximately equal to α. From the $1(\frac{1}{2})_u$ state perpendicular transitions may be made to the $1(\frac{1}{2})_g$, and both perpendicular and parallel transitions may be made to the two $(\frac{1}{2})_g$ states.

For the $\Omega=\frac{1}{2}$ states the appropriate wavefunctions may be expressed as linear combinations of the Σ and Π wavefunctions with coefficients given by the eigenvectors of the matrix of Eq. (9). Using these linear combination wavefunctions transition moments for all possible transitions are given as linear combinations of the transition moments for the $^2\Sigma_g^+-{}^2\Sigma_u^+$, $^2\Pi_g-{}^2\Sigma_u^+$ and $^2\Pi_g-{}^2\Pi_u$ transitions.

Potential curves including spin–orbit coupling were calculated from the potentials curves of Stevens *et al.*[10] using Eq. (9). At internuclear distances near the equilibrium separation the coefficient of the Π state in the wavefunction for the bound $1(\frac{1}{2})_u$ state is -0.03, as is the coefficient of the Σ state in the $1(\frac{1}{2})_g$ wavefunction. Electronic transition moments between the spin–orbit states were calculated from the transition moments given by Stevens *et al.* For the perpendicular transitions $1(\frac{1}{2})_g-1(\frac{1}{2})_u$ and $1(\frac{1}{2})_g-1(\frac{1}{2})_u$ the transition moment is essentially equal to that for the $^2\Pi_g-{}^2\Sigma_u^+$ transition. For the parallel transition $2(\frac{1}{2})_g-1(\frac{1}{2})_u$ the transition moment is essentially that of the $^2\Sigma_g^+-{}^2\Sigma_u^+$ transition. Of the two transitions not predicted without spin–orbit coupling, the transition moment for the perpendicular transition $2(\frac{1}{2})_g-1(\frac{1}{2})_u$ is smaller by an order of magnitude than any other and may be neglected, but the parallel transition $1(\frac{1}{2})_g-1(\frac{1}{2})_u$ has a substantial transition moment on the order of a few percent of the strong $^2\Sigma_g^+-{}^2\Sigma_u^+$ transition in the Franck–Condon region. It is larger by a factor of 2–3 than the $^2\Pi_g-{}^2\Sigma_u^+$ transition moment in this region. The prediction of a significant transition moment for the parallel transition $1(\frac{1}{2})_g-1(\frac{1}{2})_u$ explains the observation in crossed beams, which favors parallel transitions, of a photofragment peak at a W appropriate for the $\Pi-\Sigma$ transition [see Fig. 4(a)].

In order to attempt to quantitatively describe the photoabsorption cross section the adjusted potentials of the previous section further modified by consideration of spin–orbit must be used together with the appropriate spin–orbit matrix element. The $^2\Sigma_u^+$ and $^2\Sigma_g^+$ determined previously are actually the $1(\frac{1}{2})_u$ and $2(\frac{1}{2})_g$ states, respectively. Since both the $1(\frac{1}{2})_g-1(\frac{1}{2})_u$ and $1(\frac{1}{2})_g-1(\frac{1}{2})_u$ transitions occur, the $^2\Pi_g$ state determined previously is a combination (nearly the average) of the $1(\frac{1}{2})_g$ and $1(\frac{1}{2})_g$ states. A reasonable description of these states is provided by shifting the $^2\Pi_g$ by the same shift found for the Stevens *et al.* potentials. For the $1(\frac{1}{2})_g$ this amounts to lowering the $^2\Pi_g$ by $-\alpha=+0.059$ eV and for the $1(\frac{1}{2})_g$, raising the adjusted $^2\Pi_g$ state by 0.055 eV. Cross sections are again calculated from Eq. (7), where for all transitions $g_e=g_b=1$. In the coaxial beam experiment the perpendicular transitions $1(\frac{1}{2})_g-1(\frac{1}{2})_u$ and $1(\frac{1}{2})_g-1(\frac{1}{2})_u$ are preferentially observed, and the measured cross section is the sum of these two, as shown in the upper part of Fig. 9. In the drift tube experiment the effect of the parallel $1(\frac{1}{2})_g-1(\frac{1}{2})_u$ transition is seen as well, and in fact dominates the total cross section.

The sum of these three transitions is shown in the lower part of Fig. 9. While the total cross section is predicted to be an order of magnitude larger than that of the cross section due to the perpendicular transitions only, in both experiments the peak is predicted at essentially the same wavelength 7160 Å. This may seem unexpected since the total cross section is dominated by the parallel transition to the $1(\frac{1}{2})_g$ potential curve, while the coaxial beam measurements are sensitive to essentially the average of the $1(\frac{1}{2})_g$ and $1(\frac{1}{2})_g$ potential curves. In this system, however, the different variations of the respective transitions moments with internuclear distance approximately compensates for this difference.

It is now clear that the total photodissociation cross sections as measured by Miller *et al.*[11] should be substantially larger than cross sections calculated without inclusion of spin–orbit effects, but should have approximately the same wavelength dependence, thus explaining the observations shown in Fig. 5. The fact that the calculated cross sections including spin–orbit coupling (Fig. 9) are now about a factor of 3 larger than the experimental cross sections (Fig. 5) is not yet understood.

VI. SUMMARY AND CONCLUSIONS

From the photofragment kinetic energy spectra measured in this work at 14 wavelengths potential curves for the $^2\Sigma_u^+$, $^2\Pi_g$, and $^2\Sigma_g^+$ states of Ar_2^+ have been deduced. The potential curves calculated by Stevens *et al.*[10] were adjusted to give agreement with the pres-

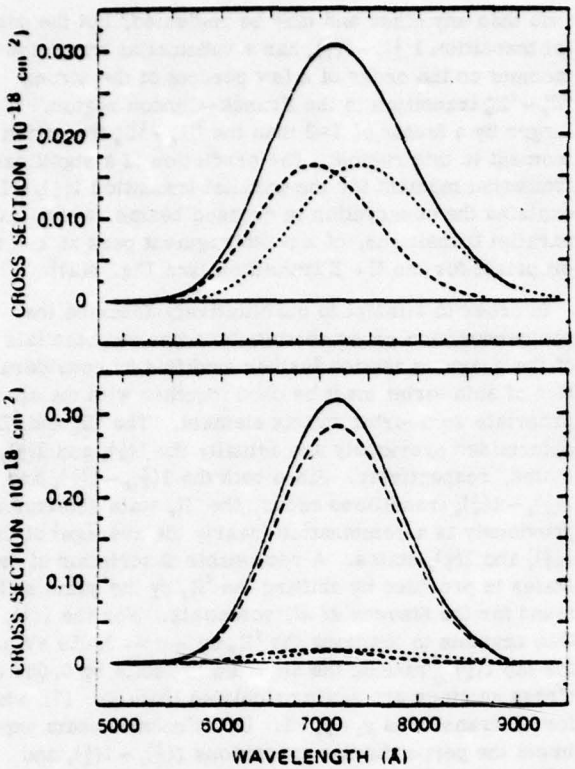

FIG. 9. *Calculated photodissociation cross sections including spin–orbit coupling for the* $\Pi - \Sigma$ *transition.* (upper) Long dash—$1(\frac{1}{2})_g - 1(\frac{1}{2})_u$ perpendicular transition; short dash—$1(\frac{3}{2})_g - 1(\frac{1}{2})_u$ perpendicular transition; solid curve—sum of these two transitions. (Lower) Two lower curves—same as in upper figure; long dashed curve—$1(\frac{1}{2})_g - 1(\frac{1}{2})_u$ parallel transition; solid curve—sum of these three transitions.

ent data. For the $^2\Sigma_u^+$ state their curve was translated downward by 0.141 eV to give agreement with the experimental D_0 value of 1.33 ± 0.020 eV. The $^2\Pi_g$ and $^2\Sigma_g^+$ were determined relative to this $^2\Sigma_u^+$ potential curve with an additional uncertainty of less than 20 meV. No direct information was gained on the $^2\Pi_u$ state, which is not dipole connected to the $^2\Sigma_u^+$ ground state. However, its location can be determined from the $^2\Pi_g$–$^2\Pi_u$ difference potential given by Jones *et al.*[5] The $^2\Pi_u$ shown in Fig. 1 was determined in this way.

Considering the effects of spin–orbit coupling, the $^2\Sigma_u^+$ and $^2\Sigma_g^+$ states determined above are actually the $1(\frac{1}{2})_u$ and $2(\frac{1}{2})_g$ spin–orbit states, while the $^2\Pi_g$ state is essentially an average of the $1(\frac{3}{2})_g$ and $1(\frac{1}{2})_g$ states. Spin–orbit states are needed to explain the observation of a strong parallel transition at an energy corresponding to the $^2\Pi_g - {}^2\Sigma_u^+$ transition, which has only a perpendicular transition in the absence of spin–orbit coupling. Additionally, all transitions allowed by spin–orbit coupling must be considered to explain the magnitude of the cross section for this transition.

Note added in proof: The calculations of Ref. 10 will appear in W. J. Stevens, M. Gardner, A. Karo, and P. Julienne, "Theoretical determination of bound-free absorption cross sections in Ar_2^+," J. Chem. Phys. (to be published). In that paper, the effects of spin–orbit coupling on the potential curves and matrix elements is considered. The results are in complete agreement with those presented here.

ACKNOWLEDGMENTS

The authors gratefully acknowledge private communication of the work of Drs. Stevens, Gardner, and Karo, valuable discussions with Dr. David Huestis, and the use of the program of Professor K. Sando for the calculation of bound–free transitions.

[1] W. Aberth and D. C. Lorents, Phys. Rev. 144, 109 (1966).
[2] P. R. Jones, N. W. Eddy, H. P. Gilman, A. K. Jhaveri, and G. Van Dyk, Phys. Rev. 147, 76 (1966).
[3] M. Barat, J. Baudon, M. Abignoli, and J. C. Houver, J. Phys. B 3, 230 (1970).
[4] D. C. Lorents, R. E. Olson, and G. M. Conklin, Chem. Phys. Lett. 20, 589 (1973).
[5] P. R. Jones, G. M. Conklin, D. C. Lorents, and R. E. Olson, Phys. Rev. A 10, 102 (1974).
[6] H.-U. Mittmann and H.-P. Weise, Z. Naturforsch. Teil A 29, 400 (1974).
[7] R. Mulliken, J. Chem. Phys. 52, 5170 (1970).
[8] T. L. Gilbert and A. C. Wahl, Chem. Phys. 55, 5247 (1971).
[9] V. Sidis, M. Barat, and D. Dhuicq, J. Phys. B 8, 474 (1975).
[10] W. J. Stevens, M. Gardner, and A. Karo (private communication).
[11] T. M. Miller, J. H. Ling, R. P. Saxon, and J. T. Moseley, Phys. Rev. A 13, 2171 (1976).
[12] M. L. Vestal and G. H. Mauclaire, Chem. Phys. Lett. 43, 499 (1976).
[13] A. Carrington, D. R. J. Milverton, and P. J. Sarre, Mol. Phys. 32, 297 (1976).
[14] D. L. Huestis and D. C. Lorents, Stanford Research Institute (*private communication*).
[15] B. A. Huber, T. M. Miller, H. D. Zeman, R. L. Leon, P. C. Cosby, J. T. Moseley, and J. R. Peterson, "A Laser-Ion Coaxial Beams Spectrometer," Rev. Sci. Instrum. (in press).
[16] G. Lange, B. Huber, and K. Wiesemann, J. Phys. E 9, 734 (1976).
[17] H. D. Zeman, Rev. Sci. Inst. (in press).
[18] J.-B. Ozenne, J. Durup, R. W. Odom, C. Pernot, A. Tabché-Fouhaillé, and M. Tadjeddine, Chem. Phys. 18, 75 (1976) and references therein.
[19] N. P. F. B. van Asselt, J. G. Maas, and J. Los, Chem. Phys. 11, 253 (1975) and references therein.
[20] A. Tabché-Fouhaillé, J. Durup, T. J. Moseley, J.-B. Ozenne, C. Pernot, and M. Tadjeddine, Chem. Phys. 17, 81 (1976).
[21] R. N. Zare and D. R. Herschbach, Proc. IEEE 51, 173 (1963); R. N. Zare, Ph.D. Thesis, Harvard University (1964).
[22] C. Y. Ng, D. J. Trevor, B. H. Mahan, and Y. T. Lee, J. Chem. Phys. 66, 446 (1977).
[23] B. A. Huber, R. Abouaf, P. C. Cosby, R. P. Saxon, and J. T. Moseley, "Photofragment Spectroscopy and Potential Curves of Kr_2^+" (to be published).
[24] These calculations are a part of the thesis to be presented by M. Tadjeddine at the Universite de Paris-Sud, Orsay, France; a summary is available in M. Tadjeddine and J. T. Moseley, "Angular Distribution and Rotational Effects in Photofragment Spectroscopy," report on SRI Project 6400, Stanford Research Institute, Menlo Park, California (1977).
[25] For the analogous bound–bound case, formulas are given in M. Yoshimine, D. McLean, and B. Liu, J. Chem. Phys. 58, 4412 (1973).
[26] J. Cohen and B. Schneider, J. Chem. Phys. 61, 3230 (1974).
[27] E. U. Condon and G. H. Shortley, *The Theory of Atomic Spectra* (Cambridge University, Cambridge, 1963).

Photofragment spectroscopy and potential curves of Kr_2^+ [a]

R. Abouaf,[b] B. A. Huber,[c] P. C. Cosby, R. P. Saxon, and J. T. Moseley

Molecular Physics Center, SRI International, Menlo Park, California 94025
(Received 21 November 1977)

Photofragment energy distributions have been measured for the process $Kr_2^+[1(1/2)_u]+h\nu \rightarrow Kr^+ + Kr$ using a 3 keV ion beam and CW lasers, both coaxial and crossed with the ion beam, at 11 wavelengths between 4680 and 7993 Å. Transitions to the dissociative states $1(1/2)_g$ and $2(1/2)_g$ are observed. The experimental results are used to adjust recent theoretical calculations to provide potential curves for the Kr_2^+ states $1(1/2)_u$, $1(1/2)_g$, and $2(1/2)_g$ with an uncertainty of ±20 meV at internuclear distances near the ground state potential minimum.

I. INTRODUCTION

In contrast to the other rare gas dimer ions, Kr_2^+ has been relatively ignored, both experimentally and theoretically. Apparently, only two differential scattering[1,2] measurements have been made on $Kr^+ + Kr$. The first[1] yielded no direct information on the potential curves. In the second,[2] primary rainbow maxima were observed, yielding a ground state well depth of 1.21 ± 0.1 eV for Kr_2^+, but satisfactory potential curves were not obtained. Barr, Dee, and Gilmore[3] have constructed potential curves for Kr_2^+, following the example of Mulliken[4] for Xe_2^+, but there have apparently been no detailed calculations on Kr_2^+ prior to very recent work[5] by W. R. Wadt. Somewhat more information does exist on the well depth. Electron impact appearance potentials[6] have yielded a lower limit of about 1.0 eV. Photoionization threshold measurements have yielded lower limits of 0.995[7] and 1.13 eV,[8] and a value of 1.15 ± 0.02 eV[9] for the well depth. Using those values (except for the more recent values of Refs. 2 and 9), Mulliken[4] estimated a "true value" of 1.2 eV.

The lack of accurate potential curves for this molecule thus provides a motivation for the work reported here. In addition, the most promising candidate for an efficient high power ultraviolet laser is a laser based on KrF. In this laser, absorption by Kr_2^+ is believed[10] to be an important loss mechanism, and the present effort to optimize this laser requires a better understanding of the Kr_2^+ potential curves and transitions.

We report here the measurement of photofragment energy distributions for the reaction

$$Kr_2^+(1(\tfrac{1}{2})_u) + h\nu \rightarrow Kr^+ + Kr. \qquad (1)$$

The experimental results are used along with recent calculations[5] to provide accurate Kr_2^+ potential curves and absorption spectra in the visible and ultraviolet. Both the experiments and the interpretation parallel that recently reported[11] for Ar_2^+.

II. EXPERIMENTAL PROCEDURES

The measurements reported here were made using ion photofragment spectrometer which has been described in detail elsewhere.[12] Basically, with this apparatus photons from a laser can be directed either coaxially or crossed with an ion beam having a typical energy of 3 keV. Photofragments produced in the laser-ion interaction region which are ejected into a 2 mrad angle along the ion beam direction pass into an energy analyzer where their energy distribution can be measured. The energy resolution is typically 20 meV in the molecular ion center-of-mass frame. In the crossed beams configuration, angular distributions of the photofragments can be measured by rotating the laser polarization. However, for the work reported here, the laser polarization for crossed beams was always parallel to the ion beam direction. In the coaxial beams configuration the laser polarization is necessarily always perpendicular to the ion beam direction.

A typical experimental photofragment kinetic energy spectrum, obtained at 6471 Å for parallel laser polarization, is shown in Fig. 1. The spectrum is nearly symmetric since fragments ejected with kinetic energy either forward or backward along the beam direction are detected with nearly equal efficiency. The center of the spectrum, corresponding to separation energy W equal to zero, is at 1500 eV, as expected for the photo-

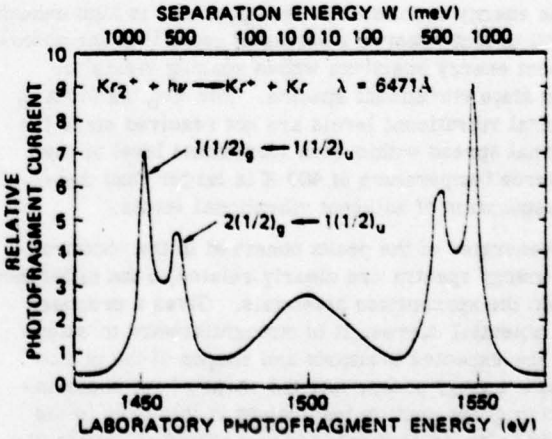

FIG. 1. Photofragment kinetic energy spectrum for Kr_2^+ photodissociation at 6471 Å. The broad peak centered at 1500 eV ($W = 0$) is due to collision-induced dissociation.

[a] Supported by the U. S. Air Force Office of Scientific Research, and the National Science Foundation under Grant No. CHE77-0428.

[b] Permanent address: Laboratoire des Collisions Electroniques, Université de Paris-Sud, 91405 Orsay, France.

[c] Permanent address: Ruhruniversität, Institüt für Experimental Physik II, Bochum, West Germany.

 0021-9606/78/6805-2408$01.00

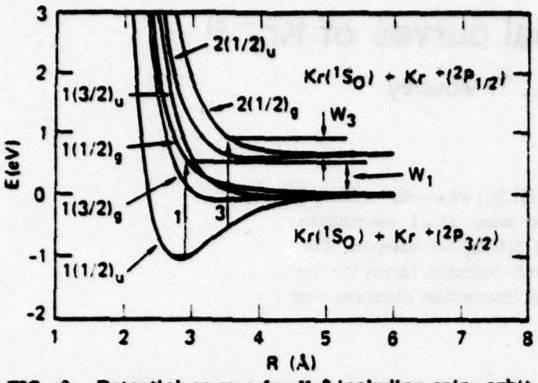

FIG. 2. Potential curves for Kr_2^+ including spin–orbit coupling as calculated by Wadt (Ref. 5). The arrows and separation energies correspond to two of the three optically allowed transitions involving the ground $1(\frac{1}{2})_u$ state.

dissociation of a homonuclear diatomic of energy 3000 eV. A photofragment from a homonuclear diatomic will appear at 0° or 180° in the laboratory frame with a kinetic energy T given by[12,14]

$$T = \tfrac{1}{2} T_0 \pm (WT_0)^{1/2} + \tfrac{1}{2} W , \qquad (2)$$

where T_0 is the parent ion kinetic energy and W is the total kinetic energy of separation in the center-of-mass frame. The separation energy scale at the top of Fig. 1 is calculated using Eq. (2).

The procedure for interpreting such experimental data in terms of the potential curves has been discussed in detail in our recent paper[11] on Ar_2^+. It can be summarized with reference to the computed[5] Kr_2^+ potential curves shown in Fig. 2. At a given photon energy, one can expect transitions to occur to the $1(\frac{1}{2})_g$ state (arrow 1), resulting in photofragments of total separation energy near W_1, to the $1(\frac{3}{2})_g$ state, resulting in photofragments of total separation energy near W_2 (not indicated in the figure), and to the $2(\frac{1}{2})_g$ state (arrow 3), resulting in photofragments of energy near W_3, assuming appropriate vibrational levels of the ground $1(\frac{1}{2})_u$ state are populated in each case. Transitions to the ungerade states are not expected since they are dipole forbidden. If the ground state vibrational levels are sufficiently spaced, and the energy resolution of the apparatus is high enough one will in fact observe a series of peaks[15] in the photofragment energy spectrum whose spacing yields the ground state vibrational spacing. For Kr_2^+, as for Ar_2^+, individual vibrational levels are not resolved since the rotational spread within each vibrational level at the ion source temperature of 400 K is larger than the energy separation of adjacent vibrational levels.

The energies of the peaks observed in the photofragment energy spectra are clearly related to the difference between the appropriate potentials. Given a proposed set of potential curves, it is straightforward to calculate[11] the expected locations and shapes of the photofragment energy peaks, and the shape of the photodissociation cross section (equivalent in this case to the absorption cross section), for any specified degree of excitation of the ground state. Direct inversion of the experimental data to determine potential curves is, of course, much more difficult and not unique.

The procedure we follow, which is discussed in detail in our earlier paper,[11] is to adjust the best available calculated potential curves so that they reproduce the experimental photofragment energy spectra and photodissociation cross section. This procedure locates the curves very accurately with respect to one another in energy, but does not give information on the internuclear separation.

Experimental photofragment energy spectra, such as the one shown in Fig. 1, are obtained over a wide wavelength range, including that necessary to photodissociate the $v=0$ level of the ground state. The wavelengths which do photodissociate $v=0$ can be identified from the progression of $(h\nu - W)$ values as a function of wavelength, since they will yield the maximum value of this quantity. This maximum value of $(h\nu - W)$, when corrected by the average rotational energy of the ions, yields the bond energy, $D_0(Kr_2^+)$. The calculated ground state potential curve can now be adjusted to agree with the experimentally determined bond energy.

If the photodissociation cross section for ions primarily in $v=0$ is available, it can be used to adjust the appropriate dissociative potential. In this case, such a cross section was available[16] for the $1(\frac{1}{2})_g - 1(\frac{1}{2})_u$ transition, and it was used to locate the $1(\frac{1}{2})_g$. Using these potential curves, photofragment energy spectra can be calculated and compared with experiment. If necessary, iterative adjustment of the potentials can be made until curves are obtained which reproduce both photodissociation and photofragment energy experimental data.

If the appropriate photodissociation cross section is not available, or if the observed transitions are not occurring near the equilibrium internuclear separation, the observed separation energies as a function of transition energy can be used[11] to locate points on the dissociative curves relative to the ground state. Again, iterative adjustment can be made until an acceptable agreement with the experimental data is obtained. This procedure was used for $2(\frac{1}{2})_g - 1(\frac{1}{2})_u$ transition.

III. EXPERIMENTAL RESULTS

Photofragment energy spectra such as the one illustrated in Fig. 1 were obtained at 11 wavelengths between 4680 and 7993 Å. At most of these wavelengths spectra were obtained for laser polarizations both parallel and perpendicular to the ion beam direction. Both peaks in the spectra were always better resolved, peaked at slightly lower W values, and relatively more intense for parallel laser polarization, showing[11] that the two transitions observed were parallel ones. Because of the large spin-orbit splitting in Kr_2^+, and the fact that the $2(\frac{1}{2})_g$ curve correlates with the higher $Kr^+(^2P_{1/2})$ limit (see Fig. 2) it is clear that the lower energy peak corresponds to the $2(\frac{1}{2})_g - 1(\frac{1}{2})_u$ transition and the higher energy peak to $1(\frac{1}{2})_g - 1(\frac{1}{2})_u$. The fact that the magnitude of the higher energy peak relative to the lower is the same for both parallel and perpendicular laser polarizations shows that $1(\frac{1}{2})_g - 1(\frac{1}{2})_u$ transition is

TABLE I. Summary of results for the transition $1(\frac{1}{2})_g - 1(\frac{1}{2})_u$. All experimental results are for crossed beams (parallel polarization).

λ Å	W_{exp} (eV)	$h\nu - W_{exp}$ (eV)	W_{calc} (eV)	v level at peak
7993	0.450	1.101	0.449	3
7525	0.530	1.118	0.520	2
6764	0.674	1.159	0.674	0
6471	0.777	1.139	0.768	1

negligible relative to the $1(\frac{1}{2})_g - 1(\frac{1}{2})_u$. This is in contrast to the case for Ar_2^*.[11] There the effects of the transition to the $1(\frac{1}{2})_g$ could be clearly seen when the laser polarization was perpendicular to the ion beam direction, even though the cross section for this transition was only about 5% of that for the transition to the $1(\frac{1}{2})_g$.

Table I summarizes the results of measurements on the higher energy peak at four wavelengths using crossed beams. The maximum in the quantity $(h\nu - W_{exp})$ at 6764 Å indicates this quantity corresponds to the bond energy $D_0(Kr_2^*)$. To this value must be added the average rotational energy of Kr_2^* at the assumed source temperature of 400 K, which is 17 meV. Thus we determine $D_0(Kr_2^*) = 1.176 \pm 0.020$ meV, where the uncertainty takes into account the uncertainties in both the photofragment kinetic energy measurement and the ion source temperature. This value is in agreement with the previously reported,[2-7] but less precise values, and with the recent value of 1.15 ± 0.02 meV reported by Ng, Trevor, Mahan, and Lee.[8] If our value, with its quoted uncertainty, and that of Ng *et al.* are correct, they, together, imply a bond energy of Kr_2^* in the range 1.156 to 1.170 eV.

At the other available wavelengths no clear features were observed which could be attributed to this $1(\frac{1}{2})_g - 1(\frac{1}{2})_u$ transition. The reason for this is clear from the potential curves shown in Fig. 2. Since the repulsive walls of the $1(\frac{1}{2})_u$ and $1(\frac{1}{2})_g$ curves have nearly the same R dependence, it is necessary to go to very high vibrational levels (approximately $v = 40$) before the transition at the next available wavelength, 5682 Å, is energetically accessible.

The $1(\frac{1}{2})_u$ and $1(\frac{1}{2})_g$ potential curves of Wadt[5] were adjusted as previously discussed, yielding the W_{calc} values shown in Table I. In order to obtain agreement with the Kr_2^* bond energy it was necessary to lower the calculated $1(\frac{1}{2})_u$ curve by 0.138 eV. It was then made to correlate with the appropriate $Kr^*(^2P_{3/2}) + Kr$ limit by exponentially decreasing the size of this translation with R, for $R > 4$ Å. Then to obtain agreement with the photodissociation cross section[16] and the photofragment energy spectrum it was necessary to lower the calculated $1(\frac{1}{2})_g$ curve by 0.036 eV, again decreasing the translation at large R.

The correspondence between the two sets of W values is excellent, supporting the validity of the adjusted curves. Note also that the $(h\nu - W)$ values show a spacing relative to the one corresponding to $v = 0$ (6764 Å) of about (n times 20 meV) where $n = 1$ for 6471 Å, 2 for 7525 Å, and 3 for 7993 Å. This value of 20 meV is approximately the predicted vibrational spacing of the lower vibrational levels, and in fact the calculation predicts that the vibrational level contributing most heavily at 6471 Å is $v = 1$, at 7525 Å is $v = 2$, and at 7993 Å is $v = 3$, as shown in the last column of Table I.

Table II provides a similar summary of the results for the $2(\frac{1}{2})_g - 1(\frac{1}{2})_u$ transition. For this transition, $h\nu - W_{exp}$ is the binding energy of the initial state plus 0.666 eV, the difference between $Kr_{3/2}^*$ and $Kr_{1/2}^*$. The calculated values of W and the principal vibrational levels contributing, were determined using the adjusted $1(\frac{1}{2})_u$ potential discussed above, and the $2(\frac{1}{2})_g$ potential curve as calculated by Wadt. Agreement in the W values was obtained by raising the calculated potential curve by only 10 meV.

As a further check on the potential curves determined here, photodissociation cross sections were calculated for the two observed transitions, for ions in thermal equilibrium at 300 K. The $1(\frac{1}{2})_g - 1(\frac{1}{2})_u$ transition can then be compared with the measurements of Lee, Smith, Miller, and Cosby,[16] and the $2(\frac{1}{2})_g - 1(\frac{1}{2})_u$ to the measured[17] absorption in an electron-beam excited Ar/Kr gas mixture, which was attributed to this transition. In order to make this comparison, the calculations and experimental measurements must be normalized. For the $1(\frac{1}{2})_g - 1(\frac{1}{2})_u$ transition, the calculations were normalized to the experiment, since absolute values of the cross sections were determined.[16] This required multiplying the calculated values by 0.59, or in other words, the calculated transition moment[18] is larger than that implied by the experiment by about 25%. However, this difference is within the combined uncertainties of the calculation and the experiment. For the $2(\frac{1}{2})_g - 1(\frac{1}{2})_u$ transition, the experimental measurements[17] were of the relative absorption. Thus they were normalized to the calculated cross sections. The results are shown in Fig. 3. The fact that the experimental absorption

TABLE II. Summary of results for the transition $2(\frac{1}{2})_g - 1(\frac{1}{2})_u$. All experimental results are for crossed beams (parallel polarization).

λ Å	W_{exp} (eV)	$h\nu - W_{exp}$ (eV)	W_{calc} (eV)	v level at peak
7993	0.233	1.298	0.27	28–29
7525	0.316	1.331	0.32	26
6764	0.428	1.405	0.42	21
6471	0.493	1.423	0.47	19
5682	0.652	1.530	0.65	13
5309	0.754	1.581	0.742	11
5145	0.806	1.604	0.792	9–10
4880	0.894	1.647	0.896	8–9
4765	0.946	1.656	0.942	8
4680	0.971	1.678	0.970	7

TABLE III. Kr_2^+ potential curves used in this work in eV. The values not in parentheses represent the parts of the curves investigated in this work.

R(Å)	$1(\frac{1}{2})_u$	$1(\frac{1}{2})_g$	$2(\frac{1}{2})_g$
2.0	(4.7058)	(9.9949)	(14.6320)
2.1	(2.6631)	(7.2417)	(11.6173)
2.2	(1.0251)	(4.9684)	(9.0377)
2.3	(−0.0535)	(3.3582)	(7.0603)
2.4	(−0.6128)	(2.3706)	(5.6607)
2.5	(−0.8824)	(1.7461)	(4.6287)
2.6	(−1.0661)	(1.2538)	(3.7753)
2.7	−1.1689	0.8833	(3.0845)
2.8	−1.1862	0.6354	(2.5492)
2.9	−1.1592	0.4612	(2.1242)
3.0	−1.1015	(0.3422)	1.7896
3.1	−1.0256	(0.2520)	1.5265
3.2	−0.9410	(0.2075)	1.3200
3.3	−0.8536	(0.1698)	1.1591
3.4	−0.7681	(0.1428)	1.0346
3.5	−0.6872	(0.1218)	0.9395
3.6	−0.6124	(0.1043)	0.8675
3.7	−0.5446	(0.0885)	0.8134
3.8	(−0.4855)	(0.0736)	(0.7730)
3.9	(−0.4344)	(0.0597)	(0.7436)
4.0	(−0.3897)	(0.0465)	(0.7227)

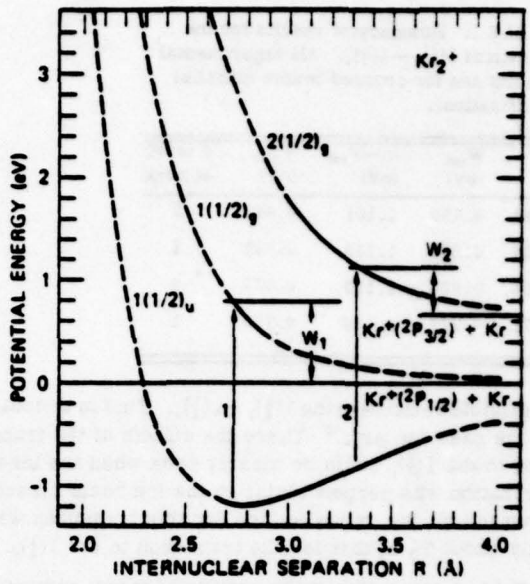

FIG. 4. Potential curves for Kr_2^+ determined in this work. The solid portions of the curves were studied here; the dashed portions come from the calculations of Wadt (Ref. 5) adjusted as discussed in the text. The arrows and separation energies correspond to the two observed transitions at 6764 Å.

for the $2(\frac{1}{2})_g$ transition is broader than the calculation is not surprising, since the ions in this case may well not be in equilibrium at 300 K, and other absorbers may also be present.

Figure 4 shows the potential curves determined in this work. Table III gives numerical values for these potentials. The values not in parentheses are for the parts of the curves actually probed in the work reported here; the values in parentheses come directly from the calculations of Wadt, adjusted as previously described. Similarly, the solid line portions of the curves of Fig. 4 were studied in the work reported here. The bond energy of the ground state and the location of the two dissociative potentials in energy relative to the ground state should be accurate to within ±20 meV. As previously stated, no direct information is obtained on the internuclear separation; this scale is set by the calculation.[5]

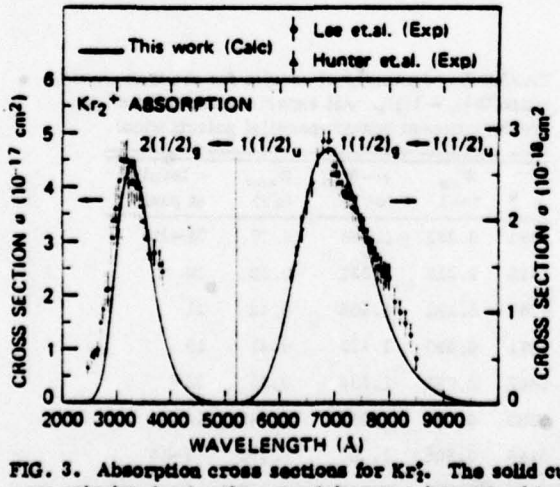

FIG. 3. Absorption cross sections for Kr_2^+. The solid curves were calculated using the potential curves determined in this work. The experimental points for the $2(\frac{1}{2})_g - 1(\frac{1}{2})_u$ transition are from the absorption measurements of Hunter *et al.* (Ref. 17); those for the $1(\frac{1}{2})_g - 1(\frac{1}{2})_u$ are from the photodissociation measurements of Lee *et al.* (Ref. 16).

ACKNOWLEDGMENTS

The authors gratefully acknowledge private communication of the calculations of W. R. Wadt prior to their publication. R. Abouaf acknowledges support by the Centre National de la Recherche Scientifique and a NATO travel grant; B. A. Huber acknowledges partial support by the Deutsche Forschungsgemeinschaft.

[1] M. Barat, J. Baudon, M. Abignoli and J. C. Houver, J. Phys. B 3, 230 (1970).
[2] H.-U. Mittmann and H.-P. Weise, Z. Naturforsch. Teil A 29, 400 (1974).
[3] T. L. Barr, D. Dee, and F. R. Gilmore, J. Quant. Spectrosc. Radiat. Transfer 15, 625 (1975).
[4] R. S. Mulliken, J. Chem. Phys. 52, 5170 (1970).
[5] W. R. Wadt, J. Chem. Phys. 67, 3068 (1977).
[6] M. S. Munson, J. L. Franklin, and F. H. Field, J. Phys. Chem. 67, 1542 (1963); C. E. Melton and W. H. Hammill, *ibid.* 41, 1469 (1964).
[7] R. E. Huffman and D. H. Katayama, J. Chem. Phys. 45, 138 (1966).
[8] J. A. R. Samson and R. B. Carins, J. Opt. Soc. Am. 56, 1140 (1966).
[9] C. Y Ng, D. J. Trevor, B. H. Mahan, and Y. T. Lee, J. Chem. Phys. 66, 446 (1977).
[10] D. L. Huestis and E. Zamir, Quarterly Report No. 1, ERDA Contract No. E(04-3)-115, Stanford Research Institute,

Menlo Park, CA (1976); R. O. Hunter, C. Howton, and J. Oldenettel, AIAA 15th Aerospace Sciences Meeting, Paper #77-26, Los Angeles, CA (1977).
[11]J. T. Moseley, R. P. Saxon, B. A. Huber, P. C. Cosby, R. Abouaf, and M. Tadjeddine, J. Chem. Phys. 67, 1659 (1977).
[12]B. A. Huber, T. M. Miller, H. D. Zeman, R. L. Leon, P. C. Cosby, J. T. Moseley, and J. R. Peterson, Rev. Sci. Instrum. 48, 1306 (1977).
[13]J.-B. Ozenne, J. Durup, R. W. Odom, C. Pernot, A. Tabche-Fouhaille, and M. Tadjeddine, Chem. Phys. 16, 75 (1976) and references therein.
[14]N. P. F. B. van Asselt, J. G. Maas, and J. Los, Chem. Phys. 11, 253 (1975) and references therein.
[15]A. Tabche-Fouhaille, J. Durup, J. T. Moseley, J.-B. Ozenne, C. Pernot, and M. Tadjeddine, Chem. Phys. 17, 81 (1976).
[16]L. C. Lee, G. P. Smith, T. M. Miller, and P. C. Cosby, Phys. Rev. A (in press).
[17]R. O. Hunter, J. Oldenettel, C. Howton, and M. V. McGusker, Chem. Phys. Lett. (to be published).
[18]W. R. Wadt, private communication.

PHOTODISSOCIATION CROSS SECTIONS OF Ne_2^+, Ar_2^+, Kr_2^+, AND Xe_2^+ FROM 3500 TO 5400 Å

L. C. Lee and G. P. Smith
Molecular Physics Laboratory
SRI International, Menlo Park, CA 94025

ABSTRACT

The photodissociation (photoabsorption) cross sections of Ne_2^+, Ar_2^+, Kr_2^+, and Xe_2^+ have been measured from 3500 to 5400 Å. The rare gas dimer ions were produced in a drift tube mass spectrometer, and the Kr^+ and Ar^+ ion laser lines were used as the photon source. The cross sections decrease monotonically with increasing photon wavelength from 3500 to 5000 Å, and then increase with photon wavelength. The cross sections have values of 1.93, 13.3, 24.8, and 29.6 x 10^{-18} cm^2 at (3569 and 3507) Å for Ne_2^+, Ar_2^+, Kr_2^+, and Xe_2^+, respectively. The current measurements are compared with various theoretical calculations. The dependence of the Ne_2^+ and Ar_2^+ cross sections on the effective kinetic temperature was investigated by increasing the ion drift velocity, and was attributed to vibrational excitation of the ions.

MP 78-66R

Physical Review A
(In press)

I Introduction

The photoabsorption cross sections of rare gas dimer ions, Ne_2^+, Ar_2^+, Kr_2^+, and Xe_2^+, have recently been extensively investigated, because these processes are important for detailed characterization and optimization of the rare gas excimer and rare gas-halogen lasers.[1] The photoabsorption of rare gas dimer ions occurs by transitions[2,3] from the bound ground electronic state, $1(\frac{1}{2})u$, to repulsive states, which results in dissociation. Several measurements have been made[4,5] on the photodissociation cross sections of the $1(\frac{1}{2})g - 1(\frac{1}{2})u$ transition in the visible region. The experimental data for this transition are reasonably consistent with theoretical calculations.[2-6] On the other hand, absolute photodissociation cross section measurements on the $2(\frac{1}{2})g - 1(\frac{1}{2})u$ transition in the ultraviolet region have only been made by Vanderhoff[7] for Ar_2^+, Kr_2^+, and Xe_2^+ at 3.0 and 3.5 eV, and relative photoabsorption cross section measurements attributed to Ar_2^+ and Kr_2^+ have been made by Hunter et al.[8] Theoretical calculations on this photoabsorption band are very extensive.[2,6,9,10] Since this ultraviolet absorption band is important in various laser applications involving the rare gases, additional experimental study of this band is of interest. We report here absolute photodissociation cross section measurements on all four of these ions in the 3500-5400 Å region.

II Experimental

The measurements reported here were made using a drift tube mass spectrometer which has been described in detail in a previous paper.[11] Basically, the apparatus consists of an ion source, drift region, mass analyzer, and ion detector. The source and drift regions were filled with the gas of interest at a pressure of 0.4 torr. Ions produced in an electron impact source move along the drift tube under the influence of a weak uniform electric field toward a 1-mm diameter exit aperture. For the photodissociation cross section measurements, the ratio of the applied electric field to the gas number density, E/N, was limited to 10 and 20 Townsend (1 Td = 10^{-17} V-cm^2). The dependence of the apparent photodissociation cross section on the applied electric field was also studied by varying E/N from 10 to 170 Td.

The drifting ions intersect a laser beam of diameter ~ 1.5 mm in front of the exit aperture. Various visible lines of Ar^+ and Kr^+ ion lasers, tuned by a prism, were used as the photon source. The ions were inside the laser cavity. At the uv lines of the Kr^+ ion laser, which consists of 25% 3569 Å and 75% 3507 Å, the ions were outside the laser cavity. The photodissociation cross sections at these photon wavelengths are large, so the laser power was reduced to avoid the diffusion effect caused by a high percentage of ion destruction.[12] The laser was mechanically chopped at 100 Hz. The ions of interest were selected by a quadrupole mass spectrometer and detected by a channeltron electron multiplier. The number of ions were

counted for equal periods during which the laser was on and off. The cross sections were placed on an absolute scale by normalization to the O^- and O_2^- photodetachment cross sections.[13,14] The reduced ion mobilities used for such normalization were obtained from the recent literature.[15,16]

At each wavelength the number of ion counts were accumulated until the statistical uncertainty in the photodestruction signal was less than 10%. The relative intracavity photon intensity is determined by measurement of the laser output power, with an uncertainty of less than 5% for every wavelength measured. The ion mobility is known to within 5% of its true value. Including the uncertainty in the O^- and O_2^- photodetachment cross sections used for normalization, the experimental uncertainty for the absolute photodissociation cross sections is estimated to be $\pm$ 20%.

III Photodissociation Cross Sections at Low E/N

The photodissociation cross sections of molecular ions are dependent[2,9] on the rotational and vibrational populations of the ions. Thus, data on photodissociation cross sections are meaningful only if the populations of the ions are reasonably well defined. The populations of dimer ions can be affected by the applied electric field (see Section IV) and by the processes[5] that form the ions. The dimer ions are mainly formed by a three-body reaction[5] that may produce the ions in vibrationally excited states. However, at low values of E/N (less than about 20 Td), the ion kinetic energies acquired from the field are much less than from thermal collisions at room temperature, and these ions will be well relaxed by collisions in the drift region. They are essentially in thermal equilibrium[5] at near room temperature (300 K). The photodissociation cross sections

of Ne_2^+, Ar_2^+, Kr_2^+, and Xe_2^+ at various photon wavelengths are listed in Table I, where Ne_2^+ and Ar_2^+ were measured at 10 Td, and Kr_2^+ and Xe_2^+ at 20 Td. The reduced ion mobilities used to calculate their drift velocities are 6.26, 1.83, 0.995, and 0.617 $cm^2/V \cdot sec$ for Ne_2^+,[15] Ar_2^+,[15], Kr_2^+,[16] and Xe_2^+,[16] respectively, in their parent gases.

The photoabsorption bands reported here result from the $2(\frac{1}{2})g \leftarrow 1(\frac{1}{2})u$ transition. $1(\frac{1}{2})u$ is the ground electronic state, which is bound. $2(\frac{1}{2})g$ is a repulsive state dissociating into $Rg^+(^2P_{\frac{1}{2}}) + Rg$, where Rg = Ne, Ar, Kr, or Xe. These potential curves are described in detail in the literature.[2,3,9,10]

The present results are compared with other experimental measurements[7] and theoretical calculations[2,3,6,9,10] in Figures 1-3. The present measurements agree very well with the experimental data given by Vanderhoff[7] at 3.0 and 3.5 eV for the Ar_2^+ and Kr_2^+ ions, but to a lesser degree for Xe_2^+. For Xe_2^+, the present data are lower than the values of Vanderhoff,[7] but are consistent within the experimental uncertainties. The theoretical calculations agree qualitatively with the present measurements, but quantitatively the theoretical calculations require adjustment. For Ar_2^+, the present data agree best with the ab initio calculations of Stevens et al.[2] In these calculations[2] a basis set of Slater-type functions has been used to construct the single-configuration wavefunctions for the four Ar_2^+ electronic states, $^2\Sigma_u^+$, $^2\Sigma_g^+$, $^2\Pi_g$, and $^2\Pi_u$. A large basis set has been used in anticipation that the transition moment would be sensitive to any deficiencies. As shown in Fig. 1, their calculations[2] agree very well with

the measurements. The calculations of Moseley et al.[10] for Ar_2^+ and Abouaf et al.[6] for Kr_2^+ are semiempirical. In these calculations the potential curves and the transition moments were adopted from the ab initio calculation,[2,3] but the potential curves were adjusted in accord with the observations of photofragment spectroscopy.[6,10] As shown in Fig. 2, these semiempirical calculations for Kr_2^+ agree quite well with the cross section measurements. The band shapes for the ab initio calculations of Wadt et al.[9] also agree quite well with the measurements, as shown in Figs. 1-3. However, their peak positions require a shift toward shorter wavelengths. This shift has been pointed out by Wadt et al.[9] in comparing their calculations with the photoabsorption measurements of Hunter et al.[8] Nevertheless, this shift of the peak positions requires an adjustment in the potential curves of less than 0.1 eV. This adjustment is within the possible error of 0.1-0.2 eV in the potential curves as indicated by Wadt et al.[9] From these investigations, the photodissociation cross sections of the Ar_2^+ and Kr_2^+ dimer ions in the ultraviolet band seem well established. For Xe_2^+, however, the discrepancy between the theoretical calculations and experimental measurements is large, indicating the need for substantial adjustment in the potential curves.

The relative cross sections measured by Hunter et al.[8] are consistent with the calculation of Stevens et al.[2] for Ar_2^+, and with Abouaf et al.[6] for Kr_2^+. When the relative absorption data of Hunter et al.[8] are normalized to the present measurements, both sets of data agree. This

suggests that the absorptions measured by Hunter et al.[8] may be properly attributable to Ar_2^+ and to Kr_2^+.

IV Photodissociation Cross Sections at High E/N

An attempt to investigate qualitatively the relationship between E/N and vibrational excitation was made. When an ion drifts under the influence of an electric field, it acquires kinetic energy in addition to its thermal energy. This additional kinetic energy may result in excitation of the dimer ions into higher rotational or vibrational states. Since each state has its own transition probability, the apparent photodissociation cross sections of the dimer ions can depend strongly on their initial excitations.[2,9] The cross sections can thus be affected by the acquired kinetic energy. In order to study this effect, the photodissociation cross sections were measured at a drift distance of 20 cm and a gas pressure of 0.4 torr for various E/N values from 10 to 170 Td. The results for photodissociation of Ne_2^+ at (3569 and 3507) Å and of Ar_2^+ at 4131 Å are shown in Table II, in which the ion kinetic energy and the effective translational temperature are also listed. The ion kinetic energy, E_K, is calculated from the ion drift velocity, v_d, as given by[15,17,18]

$$E_K = \tfrac{1}{2} m v_d^2 + \tfrac{1}{2} M v_d^2 + \tfrac{3}{2} dkT ,$$

and the effective kinetic "temperature" is defined as

$$T^* = \tfrac{3}{2} E_K/k$$

where m and M are the masses of ion and parent molecule, respectively, T is

the gas temperature, and k is the Boltzmann constant. The ion drift velocity is calculated from the product of the reduced ion mobility,[15,16] E/N, and the Loschmidt number (2.69×10^{19} molecules/cm^3). The effective kinetic temperature is not a true temperature. The translational, rotational, and vibrational populations at an effective kinetic temperature are not expected to have Boltzmann distributions.

As shown in Table II, the apparent cross section of Ar_2^+ is less affected by the applied electric field than for Ne_2^+. This is because Ar_2^+ has a lower reduced mobility than Ne_2^+, and therefore its kinetic energy and resulting vibrational excitation are less sensitive to the applied electric field. Since Kr_2^+ and Xe_2^+ have even lower reduced mobilities, their photodissociation cross sections will be less sensitive to E/N than Ar_2^+.

Translational to rotational energy transfer is expected to be a fast process, largely because the energy gap between rotational quantum states is small for the heavier diatomics. The effective rotational temperature of the ions at any E/N should therefore be close to the effective translational temperature. Furthermore, Stevens et al.[2] have shown theoretically that rotational excitation does not affect the Ar_2^+ photodissociation cross section. Thus only vibrational excitation is likely to be responsible for any E/N variation in the cross section. The amount of vibrational excitation is determined by two competing processes: translational to vibrational energy transfer from the kinetically hot Ar_2^+ (excitation), and vibrational

to translational energy transfer from Ar_2^+ collisions with the 300 K Ar gas (deexcitation). Such V-T processes are generally slow, but in this case they will be augmented by the switching reaction $Ar_2^+ + Ar \rightarrow Ar + Ar_2^+$. The rates for the excitation and the deexcitation processes may depend on the kinetic energy of the Ar_2^+ ions acquired. Currently, little quantitative information is available on these important energy transfer rates.

At 4131 Å, the dependence of the Ar_2^+ photodissociation cross sections on the vibrational and the effective kinetic temperatures is shown in Fig. 4. The cross sections for the vibrational temperature, where the rotational and vibrational populations are in a Boltzmann distribution, were obtained from the theoretical calculations of Stevens et al.[2] For a suitable comparison, the cross section given by Stevens et al.[2] at 300K was normalized to the present measurement. The calculated cross sections of Stevens et al.[2] are larger than the experimental measurements, but their relative values for various vibrational temperatures are probably correct, because their calculations are very consistent with the experimental measurements for both the visible[5] and the ultraviolet bands (see Fig. 1). As shown in Fig. 4, at low effective kinetic temperature, T^*, the apparent photodissociation cross section is equal to the value at the same vibrational temperature. This temperature equivalence indicates that the excitation process determines the vibrational excitation. At high effective kinetic temperature, the cross section at each T^* is smaller than the value at the same vibrational temperature. The deexcitation of Ar_2^+ by collision with

the surrounding 300 K gas becomes dominent, and a maximum vibrational excitation is approached.

The apparent cross sections at the various applied electric fields are not dependent on the ion drift distance. This indicates that a steady state is quickly established at each E/N. The vibrational excitation in the steady state may depend on the gas pressure and composition. From such dependence, quantitative data, such as vibrational excitation and relaxation rates, may be obtained. Further investigations on this subject are planned.

V. Concluding Remarks

Including the results reported in a previous paper,[5] the measurements for the rare gas dimer ions now cover the photon wavelength region from 3500 to 8600 Å. Combining these experimental measurements with the extensive theoretical investigations,[2,3,6,9,10] the photodissociation cross sections for the transitions, $2(\frac{1}{2})g - 1(\frac{1}{2})u$ and $1(\frac{1}{2})g - 1(\frac{1}{2})u$, are very well established.

The photodissociation cross sections monotonically decrease with increasing photon wavelength from 3500 to 5000 Å. At longer photon wavelengths the photodissociation cross sections increase again. This increase is caused by the photoabsorption of the $1(\frac{1}{2})g - 1(\frac{1}{2})u$ transition, which has been investigated previously.[4,5]

The ultraviolet absorption bands of rare gas dimer ions reported here are red shifted with increasing atomic number as predicted by theoretical calculations.[9] At the uv lines (3569 and 3507 Å) Ne_2^+ is just starting to absorb, while Xe_2^+ is apparently near the absorption maximum. The oscillator strengths for this ultraviolet absorption band are of the same magnitude[3] for all the rare gas dimer ions reported here, in contrast to the visible band, where the absorption oscillator strengths[3,5] increase from Ne_2^+ to Ar_2^+ to Kr_2^+ to Xe_2^+. The ultraviolet band has a large transition moment, and the electronic states involved are similar for all rare gas dimer ions. In contrast, the transition moment responsible for the visible band is very small,[2,3] and its transition strength depends strongly on the spin-orbit coupling[2-6] which increases as the atomic number of the rare gas increases. Because of the weak spin-orbit coupling, the absorption cross section of Ne_2^+ in the visible region was too small to be measured.

Acknowledgement

We are indebted to Dr. J. T. Moseley for suggesting this work and helpful discussions. We also wish to thank Dr. J. R. Peterson and Dr. P. C. Cosby for helpful comments. The authors gratefully acknowledge the use of a laboratory computer system obtained under an equipment grant from the National Science Foundation. This work was supported by the U.S. Army Research Office and the U.S. Air Force Office of Scientific Research.

REFERENCES

1. J. J. Ewing and C. A. Brau, Appl. Phys. Lett. 27, 350 (1975); E. R. Ault, R. S. Bradford, Jr. and M. L. Bhaumik, Appl. Phys. Lett. 27, 413 (1975); C. A. Brau and J. J. Ewing, Appl. Phys. Lett. 27, 435 (1975); J. A. Mangano and J. H. Jacob, Appl. Phys. Lett. 27, 495 (1975); J. M. Hoffman, A. K. Hays, and G. C. Tisone, Appl. Phys. Lett. 28, 538 (1976); J. R. Murray and H. T. Powell, Appl. Phys. Lett. 29, 252 (1976).
2. W. J. Stevens, M. Gardner, A. Karo, and P. Julienne, J. Chem. Phys. 67, 2860 (1977).
3. W. R. Wadt, J. Chem. Phys. 68, 402 (1978).
4. T. M. Miller, J. H. Ling, R. P. Saxon, and J. T. Moseley, Phys. Rev. A 13, 2171 (1976).
5. L. C. Lee, G. P. Smith, T. M. Miller, and P. C. Cosby, Phys. Rev. 17, 2005 (1978).
6. R. Abouaf, B. A. Huber, P. C. Cosby, R. P. Saxon, and J. T. Moseley, J. Chem. Phys. 68, 2406 (1978).
7. J. A. Vanderhoff, J. Chem. Phys. 68, 3311 (1978).
8. R. O. Hunter, J. Oldenettel, C. Howton, and M. V. McCusker, "UV Absorptions of Rare Gas Ions in E-Beam Pumped Rare Gases," to be published.
9. W. R. Wadt, D. C. Cartwright, and J. S. Cohen, Appl. Phys. Lett. 31, 672 (1977).

10. J. T. Moseley, R. P. Saxon, B. A. Huber, P. C. Cosby, R. Abouaf, and M. Tadjeddine, J. Chem. Phys. 67, 1659 (1977).

11. J. T. Moseley, P. C. Cosby, R. A. Bennett, and J. R. Peterson, J. Chem. Phys. 62, 4826 (1975).

12. G. P. Smith, P. C. Cosby, and J. T. Moseley, J. Chem. Phys. 67 3818 (1977).

13. L. M. Branscomb, S. J. Smith, and G. Tisone, J. Chem. Phys. 43, 2906 (1965).

14. L. C. Lee and G. P. Smith, "Photodissociation and Photodetachment Cross Sections of Atmospheric Negative Ions. VI. Ions in $O_2/CH_4/H_2O$ Mixtures from 4000 to 8600 Å", to be published.

15. E. W. McDaniel and E. A. Mason, The Mobility and Diffusion of Ions in Gases (Wiley, New York, 1973); also, H. W. Ellis, R. Y. Pai, E. W. McDaniel, E. A. Mason, and L. A. Viehland, Atom. Data. Nucl. Data Tables 17, 177 (1976).

16. H. Helm, J. Phys. B: Atom. Molec. Phys. 9, 2931 (1976).

17. G. H. Wannier, Phys. Rev. 83, 281 (1951); 87, 795 (1952); Bell Syst. Tech. J. 32, 170 (1953).

18. M. McFarland, D. L. Albritton, F. C. Fehsenfeld, E. E. Ferguson, and A. L. Schmeltekopf, J. Chem. Phys. 59, 6620 (1973).

Table I

Photodissociation cross sections (10^{-18} cm^2) of dimer ions at various photon wavelengths, λ. Ne_2^+ and Ar_2^+ were measured at 10 Td, and Kr_2^+ and Xe_2^+ at 20 Td

λ (Å)	Ne_2^+	Ar_2^+	Kr_2^+	Xe_2^+
5309		< 0.012	0.033 ± 0.004	0.028 ± 0.005
5208		< 0.028	0.026 ± 0.006	0.022 ± 0.004
4825		0.024 ± 0.012	0.100 ± 0.014	0.102 ± 0.011
4762	< 0.11	0.035 ± 0.016	0.122 ± 0.013	0.147 ± 0.016
4680		0.082 ± 0.022	0.203 ± 0.022	0.244 ± 0.024
4579		0.130 ± 0.012	0.39 ± 0.03	0.64 ± 0.03
4131	< 0.09	1.05 ± 0.10	3.18 ± 0.28	5.50 ± 0.55
4067		1.60 ± 0.17	3.63 ± 0.37	7.32 ± 1.33
3569 3507	1.93 ± 0.20	13.3 ± 1.1	24.8 ± 1.9	29.6 ± 2.0

Table II

Apparent photodissociation cross section $\sigma(10^{-18}\ cm^2)$, average ion kinetic energy E_K (meV), and effective kinetic temperature $T^*(K)$ at various E/N (10^{-17} V·cm^2). Ne_2^+ was photodissociated by photons of wavelengths (3569 + 3507) Å and Ar_2^+ by 4131 Å.

E/N	Ne_2^+			Ar_2^+		
	E_K	T^*	σ	E_K	T^*	σ
0	39	300		39	300	
10	48	368	1.93 ± 0.20	40	312	1.05 ± 0.10
20	78	602	2.96 ± 0.19	45	349	1.45 ± 0.10
30				53	406	1.69 ± 0.18
40	208	1604	3.97 ± 0.35	65	502	1.75 ± 0.20
50				78	602	2.00 ± 0.23
60				96	744	2.88 ± 0.15
70				119	917	3.11 ± 0.35
80				145	1118	3.88 ± 0.26
100				208	1604	4.89 ± 0.32
120				281	2173	6.25 ± 0.36
140				359	2775	7.00 ± 0.42
160				440	3398	7.35 ± 0.74
170				462	3571	8.17 ± 0.82

Figure Captions

Figure 1 Photodissociation cross sections for Ar_2^+. The data given by Vanderhoff (Ref. 7) and the theoretical results given by Stevens et al. (Ref. 2), Wadt et al. (Ref. 9), and Moseley et al. (Ref. 10) are shown.

Figure 2 Photodissociation cross sections for Kr_2^+. The data given by Vanderhoff (Ref. 7) and the theoretical results given by Abouaf et al. (Ref. 6) and Wadt et al. (Ref. 9) are shown.

Figure 3 Photodissociation cross sections for Xe_2^+. The data given by Vanderhoff (Ref. 7) and the theoretical results given by Wadt et al. (Ref. 9) are shown.

Figure 4 The dependence of the Ar_2^+ photodissociation cross sections on the vibrational and the effective kinetic temperatures. Ar_2^+ was photodissociated at 4131 Å. The vibrational temperature dependence was adopted from the calculations of Stevens et al. (Ref. 2) and normalized to the present measurement at 300 K.

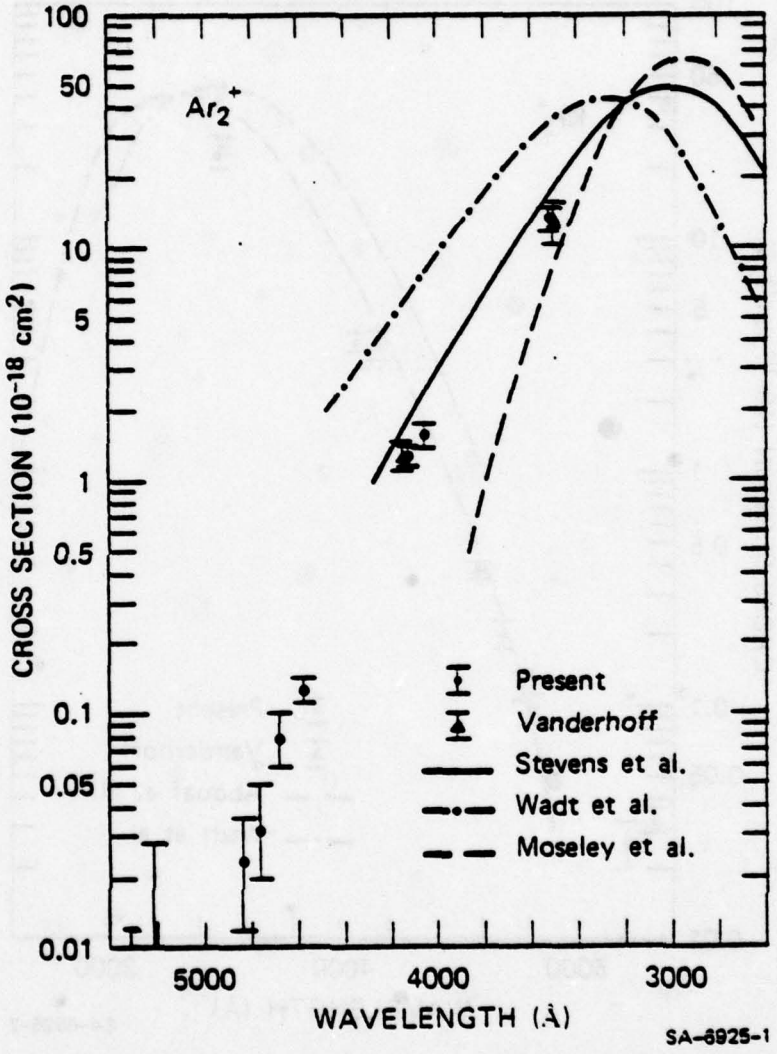
100
50
10
5
1
0.5
0.1
0.05
0.01
Ar_2^+
CROSS SECTION (10^{-18} cm^2)
Present
Vanderhoff
Stevens et al.
Wadt et al.
Moseley et al.
5000
4000
3000
WAVELENGTH (Å)
SA-6925-1

FIGURE 1

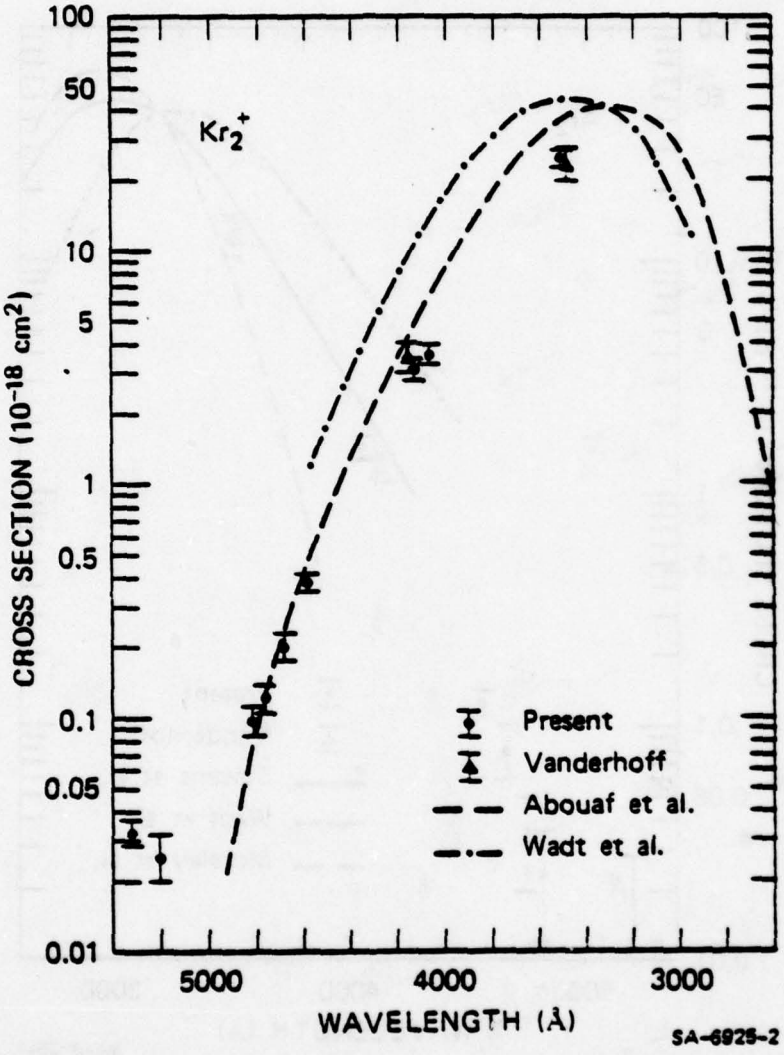
100
50
10
5
1
0.5
0.1
0.05
0.01
Kr_2^+
CROSS SECTION (10^{-18} cm^2)
Present
Vanderhoff
Abouaf et al.
Wadt et al.
5000
4000
3000
WAVELENGTH (Å)
SA-6925-2

FIGURE 2

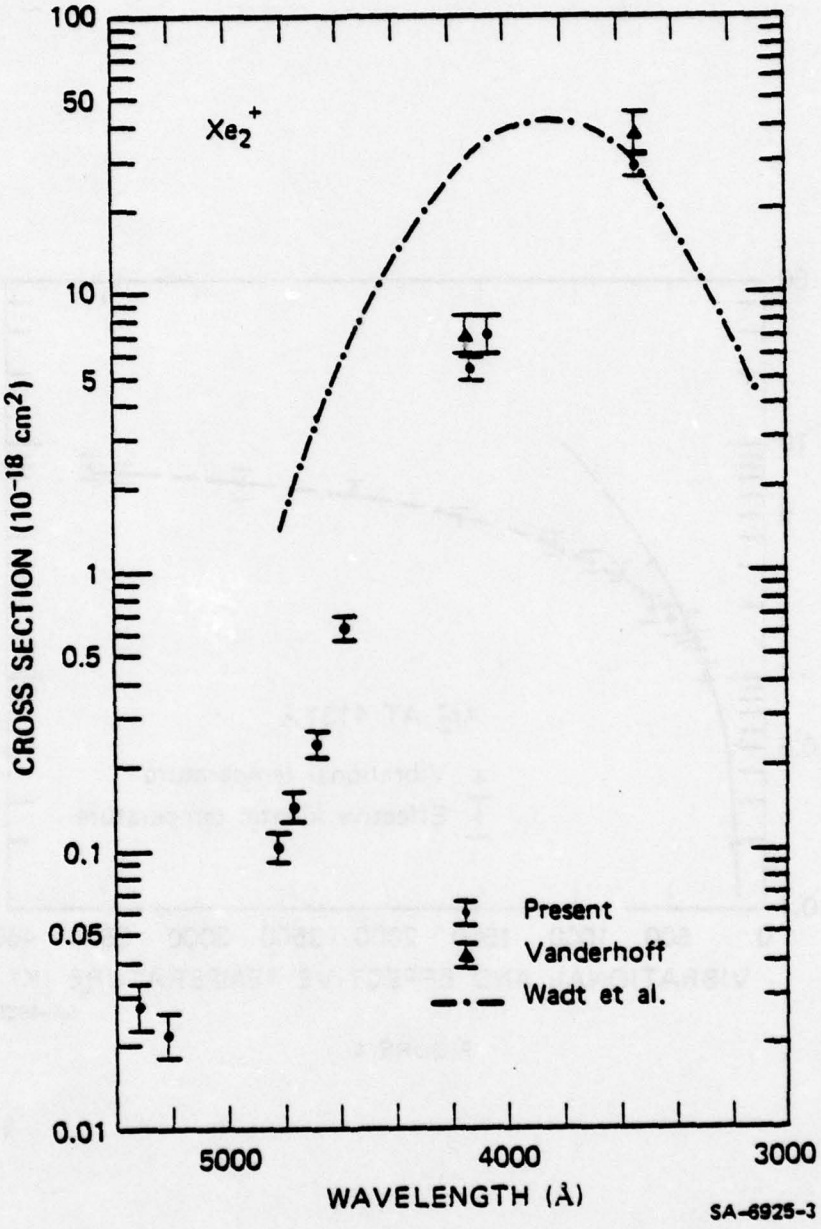
100
50
10
5
1
0.5
0.1
0.05
0.01
Xe_2^+
CROSS SECTION (10^{-18} cm^2)
Present
Vanderhoff
Wadt et al.
5000
4000
3000
WAVELENGTH (Å)
SA-6925-3

FIGURE 3

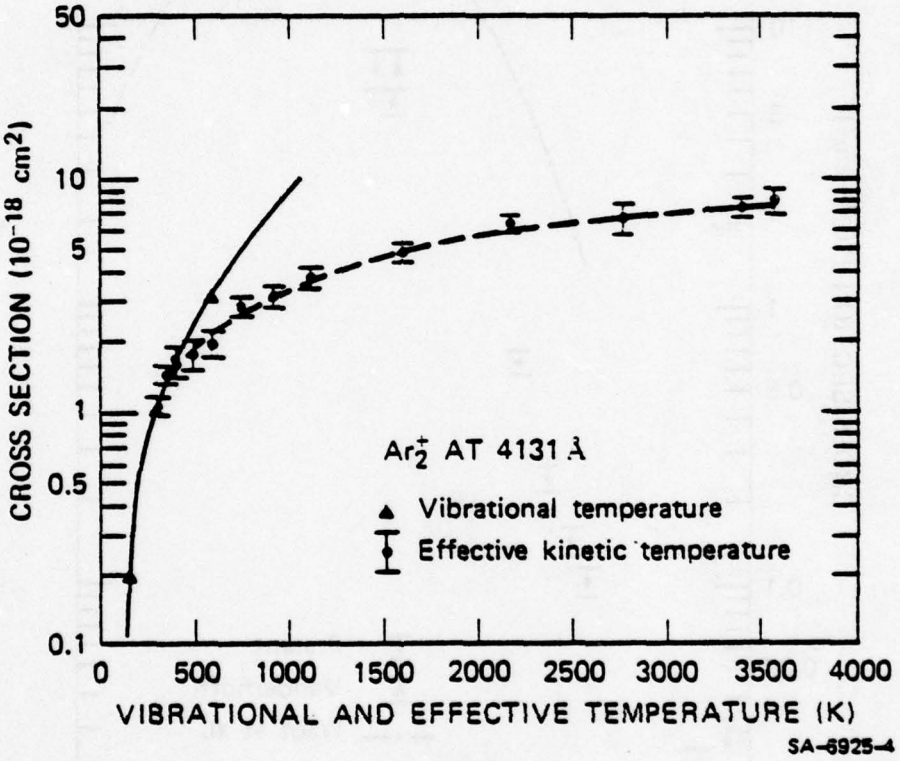
50
10
5
1
0.5
0.1
CROSS SECTION (10^{-18} cm^2)
Ar_2^+ AT 4131 Å
Vibrational temperature
Effective kinetic temperature
0
500
1000
1500
2000
2500
3000
3500
4000
VIBRATIONAL AND EFFECTIVE TEMPERATURE (K)
SA-6925-4

FIGURE 4

Photodissociation spectroscopy of O_3^- [a)]

P. C. Cosby, J. T. Moseley, J. R. Peterson, and J. H. Ling

Molecular Physics Laboratory, SRI International, Menlo Park, California 94025
(Received 17 February 1978)

The photodissociation cross section of gas-phase O_3^- has been measured using a tunable dye laser over a wavelength range of 6400–5080 Å. The cross section exhibits considerable structure which is consistent with dissociation from vibrational levels of a quasibound excited electronic state. Analysis of the structure indicates progressions in two vibrational modes of the excited state. Photodissociation spectra of ions prepared in both excited and ground vibrational levels also yields two vibrational frequencies for the ground $X\,^2B_1$ state and an apparent rate coefficient for vibrational relaxation in O_2. The molecular constants determined here for the two O_3^- electronic states are compared with those obtained from absorption spectra of the ion in other media. Identification of the dissociating state is discussed.

I. INTRODUCTION

The O_3^- ion is an important intermediate in current *D*-region negative ion reaction schemes of the ionosphere.[1] This ion also represents a relatively simple triatomic system for which detailed calculations[2–5] of its electronic structure are becoming feasible. The O_3^- ion has been studied in ozonide[6] and chlorate[7,8] crystals, in liquid ammonia solution,[6,9,10] and isolated in rare gas matrices.[11–15] From these resonance Raman, infrared, and visible absorption spectra a number of molecular constants have been measured for the ion in these environments.

The formation and reactions of O_3^- in the gas phase have been studied by a number of investigators using drift tube,[16,17] flowing afterglow,[18,19] and beam[20–23] techniques. The photodetachment cross section of this ion has been measured[24] and the electron affinity of O_3 obtained both from these data and from ion–molecule reaction[19,21–23] studies. We have previously reported[25,26] the total photodestruction cross section of O_3^- between 6400 and 4579 Å and have observed photodissociation of the ion in this wavelength region. It was suggested there that the structure in the cross section reflected absorption into levels of an excited electronic state of O_3^- which is predissociated. The purpose of the present paper is to present an analysis of the O_3^- photodestruction cross section and to attempt to characterize the states of O_3^- relevant to the dissociation process.

II. EXPERIMENTAL

The experiments were performed using a drift tube mass spectrometer–tunable dye laser apparatus which has been previously[27] described. O^- ions are produced in the ion source by dissociative electron attachment[28] of O_2. These ions enter the drift region which contains O_2 at a pressure of 0.3–0.4 torr and move down the drift tube under the influence of a weak applied electric field. The ratio of the electric field strength to O_2 gas density (E/N) was maintained at 5 Td (1 Td = 10^{-17} V cm^2) so that the directed drift velocity was less than one-tenth the mean thermal speed of the ions and molecules at 300 °K. While drifting, the O^- ions produce O_3^- via the three-body reaction[16,17]:

$$O^- + 2O_2 \rightarrow O_3^- + O_2. \qquad (1)$$

The drift region is terminated by an end plate containing a 1-mm diameter extraction aperture. Ions passing through this aperture enter a high vacuum region where they are mass selected by a quadrupole mass spectrometer and detected indivudually by an electron multiplier.

Just prior to entering the extraction aperture the ion swarm intersects the cavity of the tunable dye laser. The photon beam has a diameter of approximately 2 mm and its axis is positioned within 2 mm of the extraction aperture. The total photodestruction cross section of an ion is measured by chopping the laser at 100 Hz, tuning the mass spectrometer to the appropriate mass, and counting the number of ions arriving at the detector during the alternate periods which the laser is on and off. Photofragment ions resulting from a photodissociation can also be identified.

The distance from the ion source to the laser interaction region can be varied over a range of 2.5–50.8 cm. Thus both the ratio of O_3^-/O^- ions arriving at the laser and the number of "thermalizing" collisions the ions undergo prior to photon interaction can be varied over a wide range.

The dye laser used in this experiment is a commercial "jet-stream" model pumped by a 16 W argon ion laser. The laser had a linewidth of approximately 0.4 Å (FWHM) and its wavelength was set relative to a calibrated monochromator to a precision of 0.5 Å and an absolute accuracy of ±1 Å.

All reported cross sections were measured relative to the O^- photodetachment data of Branscomb, Smith, and Tisone.[29] However, photodissociation of O_3^- to produce O^- occurs[26] in the wavelength range reported here. In order to avoid the error[25] introduced into the apparent O^- photodetachment cross section by the photofragment O^- ions, the O_3^- cross section is measured relative to the O_3^- photodetachment cross section. The cross section for O_3^- has been measured[26] at lower pressures, in the absence of O_3^-, relative to that of O^-. At photon energies less than approximately 2.1 eV, the production of photofragment O^- becomes immeasurably small and

a)This research supported by the U. S. Army Ballistic Research Laboratory through the U. S. Army Research Office, and by the U. S. Air Force Office of Scientific Research.

 0021-9606/78/6906-2771$01.00

identical O_3^- photodestruction cross sections are obtained relative to either the O^- or O_2^- cross sections.

III. PHOTODISSOCIATION SPECTRUM

The total photodestruction cross section of O_3^- is shown in Fig. 1 as a function of photon energy. These data were obtained at a drift distance of 30.5 cm in 0.3 torr of O_2 gas. The absolute error in the cross section scale is ± 12% which includes the uncertainties in the O^- and O_2^- cross sections and in the relative mobilities[30] of O_2^- and O_3^-. The error bars in this figure are the statistical (counting) errors for O_2^- and O_3^- at each photon energy. An additional source[31] of error must be considered for the data at photon energies less than ~2.08 eV. Since a small quantity of unreacted O^- ions are present in the laser interaction region, the destruction of a fraction of these ions by photodetachment will produce an identical loss of these O_3^- ions, which would have been produced in this region via Reaction (1) had the O^- ions not been photodetached. The effect of this small loss becomes increasingly significant as the O_3^- photodestruction cross section decreases. At the lowest photon energy shown, this O^- loss is equivalent to an apparent O_3^- photodestruction cross section of 1.6×10^{-20} cm^2. The photodestruction cross section has been corrected for this effect and the error bars in Fig. 1 reflect the uncertainties in the correction procedure.

The O_3^- photodestruction cross section was measured at a number of laser powers ranging from 10 to 150 W. In this range, the data of Fig. 1 were independent of photon flux, thus establishing that the photodestruction process occurs via single photon absorptions. Two photodestruction processes are energetically possible for ground state O_3^- ions at photon energies above 1.9 eV:

$$O_3^- + h\nu \rightarrow O^- + O_2, \tag{2}$$

and

$$O_3^- + h\nu \rightarrow O_3 + e^-. \tag{3}$$

We observe photofragment O^- ions in sufficient quantities to account for 85 ± 15% of the O_3^- photodestruction at photon energies above 2.1 eV. Thus Reaction (2) dominates the photodestruction spectrum at photon energies greater than this value. Below 2.1 eV the total photodestruction cross section becomes sufficiently small that the detection of photofragment O^- is difficult because changes in the O^- current are dominated by either the loss of source produced O^- through photodetachment, or by the production of photofragment O^- from trace quantities of CO_3^- ions. However, Wong, Vorburger, and Woo[24] have reported a cross section for Reaction (3) which varies smoothly from $3.1\pm3.2\times10^{-19}$ cm^2 to $5.3\pm2.6\times10^{-19}$ cm^2 at photon energies between 2.0 and 2.4 eV. Consequently, the contribution of Reaction (3) to the total destruction in this region is negligible and the data shown in Fig. 1 can be considered the O_3^- photodissociation spectrum.

The photodissociation cross section in Fig. 1 consists of a series of broad maxima, each of which contains three or more narrower components. In order to identify that structure due to absorptions into the dissociating state of O_3^-, and that due to the effects of vibrationally excited levels of the O_3^- ground electronic state, which may be populated in newly formed ions, the cross section was measured at various drift distances ranging from 5 to 45.7 cm. At the shortest drift distance, most O_3^- ions have undergone only a few collisions prior to the photon interaction and, in fact, almost 4% of the photodissociated O_3^- ions are produced via Reaction (1) within the laser interaction region. At the longest drift distance, the O_3^- ions have undergone an average of several thousand collisions and essentially no nascent ions are present in the laser interaction region. The O_3^- photo-

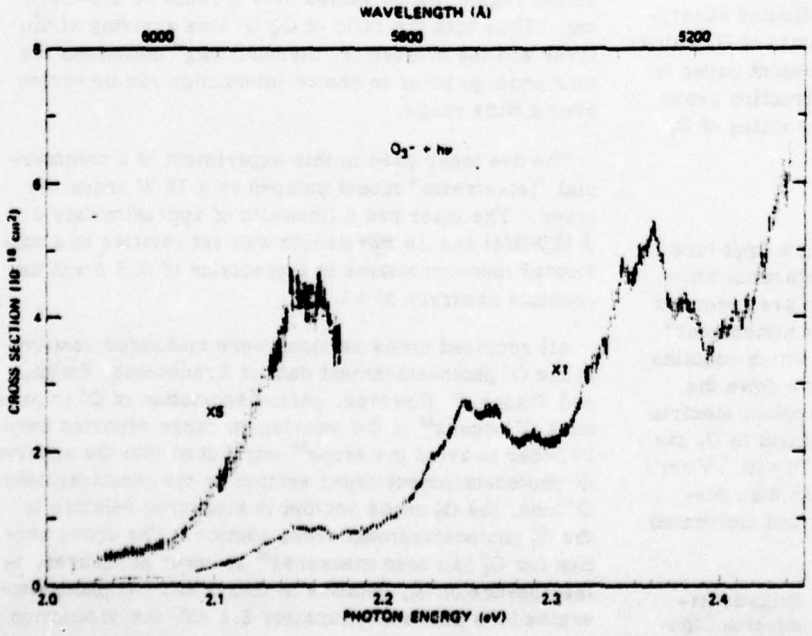

FIG. 1. Total photodestruction cross section of O_3^- as a function of photon energy. The predominant process observed is photodissociation into $O^- + O_2$. The ordinate has been expanded by a factor of five for the data in the wavelength range of 6200–5700 Å.

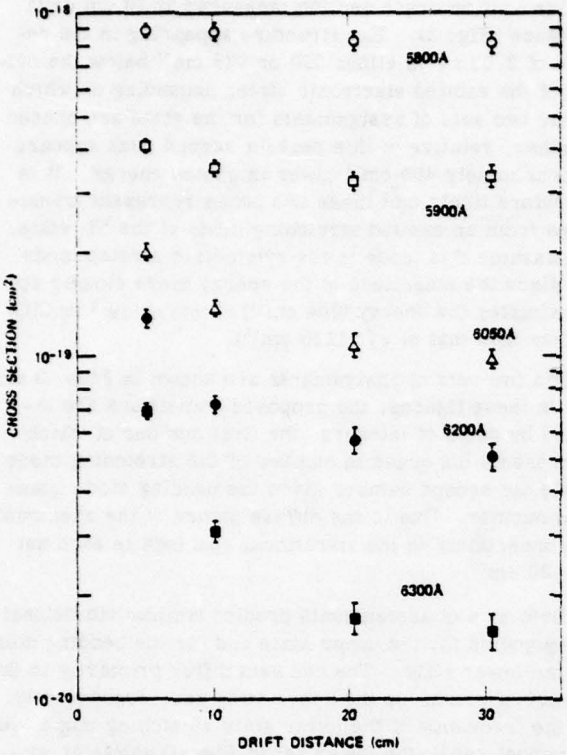

FIG. 2. Drift distance dependence of the O_3^- photodestruction cross section at five wavelengths.

destruction cross section was found to be independent of drift distance for photon energies greater than 2.15 eV. At lower photon energies, however, a drift distance dependence was observed. Figure 2 presents these drift distance results at five wavelengths. As can be seen from this figure, the cross section becomes increasingly dependent on drift distance as the photon energy is decreased. The cross section is largest at short drift distances, where the fraction of nascent O_3^- in the photon interaction region is expected to be greatest, and decreases in an exponential manner as the number of thermalizing collisions is increased. By subtracting the asymptotic value of the cross section at each wavelength, an approximate binary "relaxation rate"[32] for the reaction

$$O_3^{-\prime} + O_2 - O_3^- + O_2$$

is found to be 10^{-14} cm^3 sec^{-1}.

This behavior suggests that the O_3^- ions are produced in Reaction (1) with a significant amount of internal energy. An analogous case for the O_3 molecule has been reported. In observing infrared emission from nascent O_3 formed by the reaction

$$O + 2O_2 - O_3 + O_2,$$

von Rosenberg and Trainor[33] found 30%–50% of the 1.05 eV exothermicity of this reaction [c.f. ~1.6 eV for Reaction (1)] goes into vibrational modes of the O_3 molecule. Further, these modes are relaxed by O_2 with a rate coefficient[33–35] of approximately 2×10^{-14} cm^3 sec^{-1}.

The wavelength dependence of the O_3^- photodestruction cross section in the region of 2 eV is given by the upper and lower curves in Fig. 3 for drift distances of 10.3 and 30.5 cm, respectively. It is seen that the cross section for the less relaxed O_3^- ions is larger and exhibits structure not apparent in the cross section for ions having undergone more thermalizing collisions. We therefore conclude that, in general, features at photon energies less than approximately 2.15 eV in the photodestruction spectrum of Fig. 1 are attributable to excited levels of the O_3^- ground electronic state whereas structure appearing at higher photon energies characterizes an excited electronic state of O_3^- which dissociates.

IV. VIBRATIONAL ASSIGNMENTS

Recent configuration interaction calculations[2,4,5] of O_3^- predict a $^2B_1$ ground state of C_{2v} symmetry with a bond distance of 1.27–1.41 Å and bond angle of 115–116.8°. Three excited states[4,5] are found within 4 eV of the ground state. However, dipole transitions from $X\,^2B_1$ are allowed only to two of these states, the $^2A_1$ and $^2A_2$. Both the $^2A_1$ and $^2A_2$ are predicted[5] to have somewhat larger equilibrium bond distances than $X\,^2B_1$ and the equilibrium bond angles differ from that of the ground state by approximately $+10°$ and $-10°$. Thus, optical absorptions to either of these states from the ground state would be expected to produce progressions in both the symmetric stretch and bending modes of the upper state. Transitions to the asymmetric stretch would be expected to be weak, but might be observable.

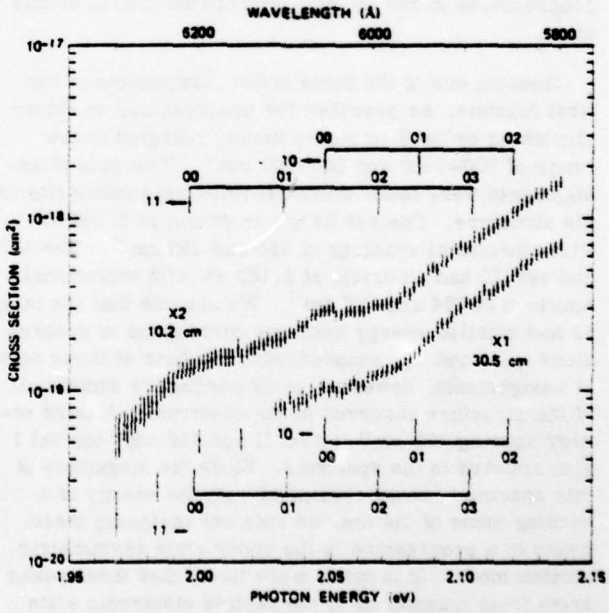

FIG. 3. Total photodestruction cross section of O_3^- as a function of photon energy. The upper and lower sets of data were obtained at drift distances of 10.2 and 30.5 cm, respectively. For clarity, the upper data have been displaced along the ordinate by a factor of 2. Transitions $(10 - 0v'_2)$ and $11 - 0v'_2)$ arising from excited stretching modes of the $X\,^2B_1$ state which are expected from assignments I and II are given by the lines in the upper and lower halves of the figure. Qualifications regarding these assignments are given in the text.

The visible absorption spectrum of O_3^- has been measured for various alkali metal ozonides dissolved in liquid ammonia[9,10] or isolated in rare gas matrices.[12,13] It has also been measured in irradiated single crystals of alkali metal chlorates.[8] In each case a series of partially resolved maxima are observed extending from 2.2 to 3.5 eV which are separated by 800–900 cm^{-1}. These spectra have been interpreted as absorptions from the ground electronic state of O_3^- to vibrational levels of an excited O_3^- electronic state. The energy of the transition between the lowest levels of the ground and excited electronic states was dependent on the environments in which the measurements were made, but lie within the range of 2.15–2.25 eV.

The widths of the maxima and their energy spacings are comparable for both the absorption spectra and the photodissociation spectrum. Also, the thresholds for these spectra occur in roughly the same photon energy regions. It therefore appears reasonable that both spectra represent transitions from the $^2B_1$ ground of O_3^- to vibrational levels in either the $^2A_1$ or $^2A_2$ excited states.

The broad maxima in the photodissociation spectrum are spaced by roughly 800 cm^{-1}, which is comparable to the energy of vibrational stretching modes of other triatomics. The smaller components of these maxima, however, are spaced at irregular intervals of order 150 cm^{-1}, which is unusually small. The bending mode in the $^2A_2$ state[36] of the isoelectronic molecule ClO_2, for example, is 296.3 cm^{-1}. Thus, in order to assign the structure in the photodissociation spectrum to specific levels of the excited electronic state, we search for progressions in two or more vibrational modes of this state.

Choosing one of the three major components of the first maxima, we searched for progressions in either stretching or bending modes having energies in the range of 700–1400 and 200–600 cm^{-1}. Two sets of assignments were found which provided reasonable fits to the structure. One set (I) had an origin at 2.146 eV with vibrational spacings of 855 and 290 cm^{-1}. The second set (II) had an origin at 2.163 eV with vibrational spacings of 794 and 282 cm^{-1}. We assume that the larger and smaller energy spacings correspond to progressions in ω_1' and ω_2', respectively. Neither of these sets of assignments, however, could adequately explain all of the structure observed in the spectrum. A third energy spacing 403 cm^{-1} for set II and 419 cm^{-1} for set I also appears in the spectrum. Since the magnitude of this spacing is more consistent with the energy of a bending mode of the ion, we rule out assigning these peaks to a progression in the upper state asymmetric stretch mode. It is much more likely that these peaks arise from transitions to the excited electronic state from the excited bending mode (ω_2'') of the $O_3^-(X\,^2B_1)$ ground state. In Boltzmann equilibrium at 300 °K, approximately 12% of the molecules will be in the first excited ν_2 mode of the ground electronic state. Thus, absorptions arising from this mode contribute to the observed structure.

An additional assignment may be made from the photodissociation cross section measured at 10 cm drift distance (Fig. 3). The structure appearing in the region of 2.05 eV is either 790 or 928 cm^{-1} below the origin of the excited electronic state, depending on which of the two sets of assignments for the state are chosen. Further, relative to this peak, a second peak appears approximately 400 cm^{-1} lower in photon energy. It is therefore likely that these two peaks represent transitions from an excited stretching mode of the $^2B_1$ state. We assume this mode is the symmetric stretch mode ω_1'' since the magnitude of the energy more closely approximates the energy (964 cm^{-1}) of this mode[36] in ClO_2 rather than that of ω_3'' (1133 cm^{-1}).

The two sets of assignments are shown in Figs. 3 and 4. In these figures, the proposed transitions are labeled by pairs of integers, the first number of which represents the quantum number of the stretching mode while the second number gives the bending mode quantum number. Due to the diffuse nature of the spectrum, the uncertainty in the vibrational spacings in each set is ±20 cm^{-1}.

Both sets of assignments predict similar vibrational frequencies for the upper state and for the bending mode of the lower state. The two sets differ primarily in the choice of origin for the upper state and, consequently, in the frequency of the lower state stretching mode. Assignment set II (the lower set in Fig. 4) shows an extended progression in the upper state stretching mode for which little or no anharmonicity is observed. This is consistent with the large difference in stretching frequencies found for the two electronic states and with the small anharmonicity observed[13] in the matrix absorption spectra. Transitions originating from the first excited level of the ground state bending mode comprise a significant protion of the spectrum at low quantum numbers, but their intensities appear to decrease with increasing photon energy. Such a behavior is important if the room tempeature photodissociation spectrum is truly comparable to matrix absorption spectra obtained at temperatures of less than 22 °K.

The primary disadvantage of assignment set II is that it fails to account for the two small humps at 2.096 and 2.130 eV which occur on the low energy side of the first peak in Fig. 4. Although it is possible these features could arise from transitions out of an excited stretching mode of the ground state (Fig. 3), the population of such a level would be relatively small at 300 °K and the strength of these features does not appear to change with drift tube conditions. Assignment set I fully accounts for these features as transitions from the first excited bending mode of the lower state. Further, set I assigns the most prominent feature in the region of 2.15 eV to the origin of the upper state. This set of assignments, however, requires an anharmonicity of approximately 15 cm^{-1} in the upper state stretching frequency to obtain a fit of the observed structure. Moreover, the intensities of transitions originating from the excited lower state bending mode appear to increase with increasing photon energy. In contrast to set II, neither of these characteristics of set I would appear to be consistent with the matrix absorption spectra.

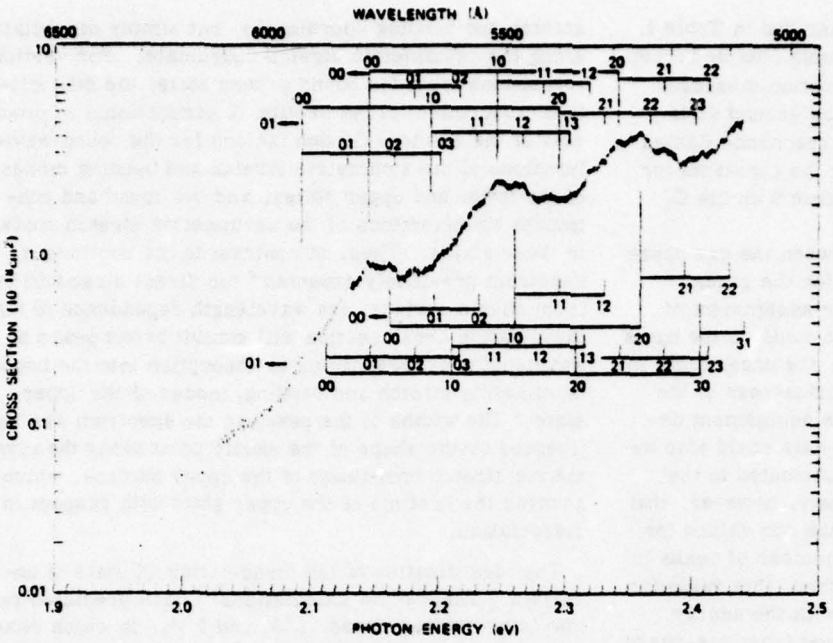

FIG. 4. Photodestruction cross section of O_3^- as a function of photon energy showing the assignment of transitions to two vibrational modes of the dissociating electronic state. Transitions arise from both the ground vibrational levels $(00 - v_1'' v_3'')$ and from the first excited bending mode $(01 - v_1'' v_3'')$ of the $X\,^2B_1$ state. Assignments made from frequency set I are shown in the upper part of the figure while those from set II are in the lower part. Qualifications regarding these assignments are given in the text.

The broad widths of the peaks and the limited energy range over which the photodissociation spectrum has been measured with the dye laser do not presently allow a clear distinction between the two assignment sets, nor is it certain that either of these assignments is precisely correct. It seems certain, however, that excited state vibrational frequencies near 800 and 300 cm^{-1} are required to explain the observed structure. The low quantum numbers for the transitions also limit the usefulness of isotopic substitution in verifying the assignments. The photodissociation spectrum of $^{18}O_3^-$ (18-18-18) was briefly measured over the energy range of 2.10-2.34 eV. General shifts of the broad maxima in the regions of 2.15 and 2.25 eV by 0 ± 15 cm^{-1} and -32 ± 15 cm^{-1} were observed and are consistent with either set of assignments. Unfortunately, the quantity of $^{18}O_2$ gas available was insufficient to measure the cross sections to the precision required for detecting the small shifts expected for the individual transitions in this region. Thus, in order to better determine the vibrational assignments, extension of the dye laser measurements to 2.6 eV are planned.

The two sets of values for the vibrational energies of the O_3^- ground and excited states and for the origin of the excited state which were determined from the

TABLE I. Summary of O_3^- molecular constants.

	Ground state $X\,^2B_1$			Excited state ($^2A_1$, $^2A_2$)			
Source	ω_1''	ω_2''	ω_3''	ω_1'	ω_2'	ω_3'	T_0(eV)
This work[a](I)	790 ± 50	419 ± 20		855 ± 20	290 ± 20		2.146
(II)	928 ± 50	403 ± 20		794 ± 20	282 ± 20		2.163
Matrix[b]				934–908	~300		2.183–2.254
Matrix[c]			802.0	818			
Matrix[d]	1012–1026						
Matrix[e]		553.6–618.6	786.7–814.3				
Crystal[f]	1016–1029			857			
Liquid ammonia[g]				~820	~400		~2.19
ClO_3[h]	963.5	451.7	1133.0	722.4	296.3	780.1	2.6057

[a]Qualifications regarding the choice of assignments I and II are discussed in the text.
[b]Reference 15.
[c]References 11 and 12.
[d]Reference 14.
[e]Reference 13.
[f]References 7 and 8.
[g]Reference 10.
[h]Reference 36.

photodissociation spectrum are summarized in Table I. The values for the excited state constants obtained from the previously mentioned visible absorption measurements are also listed, together with the ground state constants reported from infrared and resonance Raman spectra. Also shown in this table are the constants for the ClO_2 molecule, which is isoelectronic with the O_3^- ion.

The most serious disagreement between the gas phase data and those of other media occurs for the ground state energy levels. It is possible our assignment of ω_1'' could be in error, since it was not made on the basis of an extended progression. Further, the uncertainty in this spacing is ± 50 cm^{-1}, due to the diffuseness of the single peak near 2.05 eV on which this assignment depends. The agreement between these data could also be improved if the gas phase data were attributed to the asymmetric stretch mode. It is unlikely, however, that our value for ω_2'' is more uncertain than our values for ω_1' and ω_2', since it is supported by a number of peaks in the photodissociation spectrum. Further, this value for the bending mode is more consistent with the energy levels of ClO_2, which were also obtained from gas-phase spectra. Undoubtedly the greatest cause for disagreement among the various spectra arises from the weak bonding[13,15] between O_3^- and the cation in rare gas matrices as well as interaction with the atoms of the matrix. Such perturbations of O_3^- can be even more serious in a crystal environment.

V. IDENTIFICATION OF THE EXCITED STATE

One important characteristic of the O_3^- photodissociation spectrum is that dissociation of the upper electronic state takes place from the lowest energy levels of that state and continues to occur over a photon energy range of at least 0.55 eV. Secondly, the degree of diffuseness in the spectral features does not noticeably vary with the vibrational level of the upper state. This also appears to be true of the absorption spectrum[15] over a photon energy range of 1.3 eV. A third characteristic is that no evidence is found for absorption into the asymmetric stretch mode of the upper state. Finally, it appears that nearly every absorption into the excited state results in a dissociation. For example, a molar extinction coefficient of 2050 $l.M^{-1}$ cm^{-1} at 4579 Å has been reported[10] for KO_3 dissolved in liquid NH_3. This coefficient, which is equivalent to an absorption cross section of 3.4×10^{-18} cm^2, compares favorably to the O_3^- photodissociation cross section[25] of 4.9×10^{-18} cm^2 at this wavelength. In fact, agreement between these measurements is likely to be much closer when one considers the absorption and photodissociation cross sections are rapidly varying functions of wavelength in this region and that the NH_3 solution absorption spectrum is shifted ~ 100 Å to the blue of the gas phase photodissociation spectrum.

All of these characteristics are consistent with a direct dissociation process, such as that recently proposed by Pack,[37] occurring in the upper electronic state. In Pack's treatment, the potential surface of the dissociating state is considered bound along its symmetric stretch and bending coordinates, but simply dissociative along the asymmetric stretch coordinate. For vertical transitions from the bound ground state, the dissociation (absorption) cross section is proportional to products of the Franck–Condon factors for the bound wavefunctions of the symmetric stretch and bending modes of the lower and upper states, and the bound and continuum wavefunctions of the asymmetric stretch modes in these states. Thus, in contrast to the continuous spectrum previously expected[38] for direct dissociation from such a surface, the wavelength dependence of the dissociation cross section will exhibit broad peaks at wavelengths corresponding to absorption into the bound (symmetric stretch and bending) modes of the upper state. The widths of the peaks in the spectrum are influenced by the shape of the saddle point along the asymmetric stretch coordinate of the upper surface, which governs the lifetime of the upper state with respect to dissociation.

The identification of the dissociating O_3^- state is uncertain. Theoretical calculations[4,5] have predicted two low-lying excited states, $1\,^2A_1$ and $1\,^2A_2$, to which dipole-allowed transitions are possible from the ground $X\,^2B_1$ state. The $1\,^2A_1 - X\,^2B_1$ transition occurs at the lower photon energy, but previous investigations[12,15] have attributed the visible absorption band to $1\,^2A_2 - X\,^2B_1$. The basis for this assignment has been that the $1\,^2A_2 - X\,^2B_1$ transition has been ovserved[36] in ClO_2 with a threshold at 2.606 eV. Such an analogy has limitations, however, since the spectrum of the $1\,^2A_2 - X\,^2B_1$ transition in ClO_2 is not diffuse,[39] even though the entire spectrum appears at photon energies above the dissociation energy[36] of the ground state (2.50 eV).

An unambiguous assignment of the dissociating state could be obtained from a measurement of the angular distribution of O^- photofragments. For the case of $^2A_1 - {}^2B_1$, the O^- distribution would be isotropic in the plane perpendicular to the direction of laser polarization, whereas the distribution of fragments from $^2A_2 - {}^2B_1$ would have more parallel character. An angular distribution measurement would also provide a check on the direct dissociation model by probing the lifetime of the dissociating state.[40] In contrast to the case[41] of CO_3^-, such a distribution cannot be obtained for O_3^- in the drift tube apparatus. The numerous collisions, caused by the much higher neutral gas densities required for O_3^- formation, would randomize the initial angular distribution of O^- photofragments prior to their detection. Consequently, this question must be investigated in the future using a beam[42] apparatus.

VI. BOND ENERGY

Since photodissociation is observed from the lowest level of the O_3^- excited state, the thresholds of 2.146 or 2.163 eV reported here provide only an upper limit to the dissociation energy $D_0(O_2\text{–}O^-)$ of the $O_3^-(X\,^2B_1)$ state. The actual dissociation energy could, in principle, be obtained from a measurement of the kinetic energy of the O^- photofragments and a knowledge of the internal energy of the corresponding O_2 product. In the absence of these more direct data, $D_0(O_2\text{–}O^-)$ can be related to

the dissociation energy of O_3 and the electron affinities of O and O_3 by the equation:

$$D_0(O_2-O^-) = EA(O_3) + D_0(O_2-O) - EA(O). \quad (4)$$

The threshold for O_3^- photodetachment has been measured[24] to be 1.99 ± 0.1 eV. This value represents an upper limit to $EA(O_3)$ since the Franck–Condon factors for the $O_3(X\,^1A_1) - O_3^-(X\,^2B_1)$ transition are not sufficiently well known to insure the product neutral is not produced with internal energy at the photodetachment threshold. The electron affinity has also been deduced from the kinetic energy thresholds for O_3^- formation in reactions of various species with O_3. The reactants used in these studies were (I^-),[21] ≥ 1.96 eV; (Cs),[22] 2.14 ± 0.15 eV; (F^-, Br^-, Cl^-, I^-, CO_3^-),[23] 2.15 ± 0.15 eV; and (OH^-),[19] ≥ 1.8234 eV. Provided the O_3 molecule does not have significant internal energy at the time of reaction, these measurements represent lower limits to $EA(O_3)$, since the product O_3^- ion may be formed with internal energy. Combining the photodetachment and reaction values, the electron affinity of O_3 is determined to be 2.06 ± 0.06 eV. This value is also consistent with those obtained by a theoretical calculation[2] and crystallographic studies.[43]

Using the above value for $EA(O_3)$ and the recommended values for $EA(O)$[44] and $D(O_2-O)$[45] of $1.462^{+.003}_{-.007}$ eV and 1.05 ± 0.02 eV, respectively, the dissociation energy of the $O_3^-(X\,^2B_1)$ state is found from Eq. (4) to be 1.65 ± 0.06 eV.

It has been pointed out[19] that if the above values are all correct within their stated uncertainties, a significant discrepancy exists regarding either the dissociation energy of CO_3^-, $D(CO_2-O^-)$, or of O_3^-. From reaction rate studies, the difference in the dissociation energies of CO_3^- and O_3^- was determined[19] to be *at least* 0.58 eV, while the photodissociation of CO_3^- led[42] to an *upper limit* of 1.9 eV for the dissociation energy of CO_3^-. These two values place an *upper limit* on the dissociation energy of O_3^- of 1.32 eV, in clear disagreement with the value of 1.65 eV obtained above. It is not yet known whether one of the numbers quoted above is significantly in error, or several of them are slightly in error in such a way as to account for the 0.3 eV discrepancy.

VII. SUMMARY

The O_3^- photodestruction cross section has been measured over a wavelength range of 6400–5080 Å. The ion photodissociates in this region to form $O^- + O_2$ with a cross section that exhibits structure consistent with dissociation from vibrational levels of an excited electronic state. Progressions in the symmetric stretch and bending modes of the excited state are identified and transitions originating from these modes in the $X\,^2B_1$ state are observed. It is found that the structure in the cross section can be explained by either of two sets of vibrational frequencies for these states. The assignments, given in Table I, fix the origin of the excited state at *either 2.146 or 2.163 eV above the* $X\,^2B_1$ *state*. The identity of the dissociating state is not experimentally established; however, recent calculations indicate it is either the $1\,^2A_1$ or $1\,^2A_2$.

Evidence is found for the formation of vibrationally excited O_3^- in the reaction $O^- + 2O_2 - O_3^- + O_2$. Relaxation of the excited ion in O_2 is observed with an apparent rate coefficient of 10^{-14} cm^3 sec^{-1}.

Note added in proof: S. E. Novick, P. C. Engelking, P. L. Jones, J. H. Futrell, and W. C. Lineberger (private communication) have recently determined frequencies of 982 ± 28 cm^{-1} for ω_1'' and 551 ± 36 cm^{-1} for ω_2''. Their value for ω_1'' argues for the selection of set II in this work. However, their value for ω_2'' is substantially different from either possibility reported here. This difference is not presently understood.

ACKNOWLEDGMENT

The authors gratefully acknowledge helpful conversations with Dr. David L. Huestis during this investigation.

[1] L. Thomas, Radio Sci. 9, 121 (1974); F. E. Niles and M. G. Heaps, Third General Scientific Assembly of the International Association of Geomagnetism and Aeronomy: Abstracts of Papers (Seattle, 1977), p. 58.
[2] M. M. Heaton, A. Pipano, and J. J. Kaufman, *Int. J. Quantum Chem.* 6, 181 (1972).
[3] J. M. Sichel, Can. J. Chem. 51, 2124 (1973).
[4] D. G. Hopper, W. B. England, P. J. Fortune, B. J. Rosenberg, P. Benioff, G. Das, and A. C. Wahl, 30th Symposium on Molecular Structure and Spectroscopy: Abstracts of Papers (Ohio State U., Columbus, Ohio, 1975), p. 84; A. C. Wahl, W. B. England, B. J. Rosenberg, D. G. Hopper, and P. J. Fortune, "Theoretical Studies of the Atmospheric Triatomic Molecules H_2O, N_2O, NO_2, CO_2, O_3, and Their Ions," Argonne National Lab. Rep. ANL-77-3 (Argonne National Lab, Argonne, IL, 1977).
[5] T. H. Dunning and P. J. Hay, 31st Symposium on Molecular Structure and Spectroscopy; Abstracts of Papers (Ohio State U., Columbus, Ohio, 1976), p. 118; T. H. Dunning (private communication, 1975).
[6] A. D. McLachlan, M. C. R. Symons, and M. G. Townsend, J. Chem. Soc. London 1959, 952.
[7] J. B. Bates, *Chem. Phys. Lett.* 28, 75 (1974).
[8] J. B. Bates and J. C. Pigg, J. Chem. Phys. 62, 4227 (1975).
[9] I. J. Solomon, A. J. Kacmarek, J. M. McDonough, and K. Hattori, J. Am. Chem. Soc. 82, 5640 (1960).
[10] P. A. Giguere and K. Herman, Can. J. Chem. 52, 3941 (1974).
[11] M. E. Jacox and D. E. Milligan, Chem. Phys. Lett. 14, 518 (1972).
[12] M. E. Jacox and D. E. Milligan, J. Mol. Spectrosc. 43, 148 (1972).
[13] R. C. Spiker and L. Andrews, J. Chem. Phys. 59, 1851 (1973).
[14] L. Andrews and R. C. Spiker, J. Chem. Phys. 59, 1863 (1973).
[15] L. Andrews, J. Chem. Phys. 63, 4465 (1975).
[16] L. G. McKnight, Phys. Rev. A 2, 762 (1970).
[17] R. M. Snuggs, D. J. Volz, I. R. Gatland, J. H. Schummers, D. W. Martin, and E. W. McDaniel, Phys. Rev. A 3, 487 (1971).

[18]F. C. Fehsenfeld and E. E. Ferguson, J. Chem. Phys. 61, 3181 (1974).
[19]I. Dotan, J. A. Davidson, G. E. Streit, D. L. Albritton, and F. C. Fehsenfeld, J. Chem. Phys. 67, 2874 (1977).
[20]R. K. Curran, J. Chem. Phys. 35, 1849 (1961).
[21]J. Berkowitz, W. A. Chupka, and D. Gutman, J. Chem. Phys. 55, 2733 (1971).
[22]E. W. Rothe, S. Y. Tang, and G. P. Reck, J. Chem. Phys. 62, 3829 (1975).
[23]C. Lifshitz, R. L. C. Wu, T. O. Tiernan, and D. T. Terwilliger, J. Chem. Phys. 68, 247 (1978).
[24]S. F. Wong, T. V. Vorburger, and S. B. Woo, Phys. Rev. A 5, 2598 (1972).
[25]P. C. Cosby, R. A. Bennett, J. R. Peterson, and J. T. Moseley, J. Chem. Phys. 63, 1612 (1975).
[26]P. C. Cosby, J. H. Ling, J. R. Peterson, and J. T. Moseley, J. Chem. Phys. 65, 5267 (1976).
[27]J. T. Moseley, P. C. Cosby, R. A. Bennett, and J. R. Peterson, J. Chem. Phys. 62, 4826 (1975).
[28]L. M. Chanin, A. V. Phelps, and M. A. Biondi, Phys. Rev. 128, 219 (1962).
[29]L. M. Branscomb, S. J. Smith, and G. Tisone, J. Chem. Phys. 43, 2906 (1965).
[30]R. M. Snuggs, D. J. Volz, J. H. Schummers, D. W. Martin, and E. W. McDaniel, Phys. Rev. A 3, 477 (1971).
[31]J. A. Vanderhoff, J. Chem. Phys. 67, 2332 (1977).
[32]B. A. Huber, P. C. Cosby, J. R. Peterson, and J. T. Moseley, J. Chem. Phys. 66, 4520 (1977).
[33]C. W. von Rosenberg and D. W. Trainor, J. Chem. Phys. 61, 2442 (1974); *ibid.* 63, 5348 (1975).
[34]D. I. Rosen and T. A. Cool, J. Chem. Phys. 62, 466 (1975).
[35]K. K. Hui, D. I. Rosen, and T. A. Cool, Chem. Phys. Lett. 32, 141 (1975).
[36]A. W. Richardson, R. W. Redding, and J. C. D. Brand, J. Mol. Spectrosc. 29, 93 (1969).
[37]R. T Pack, J. Chem. Phys. 65, 4765 (1976).
[38]G. Herzberg, *Molecular Spectra and Molecular Structure. III. Electronic Spectra and Electronic Structure of Polyatomic Molecules* (Van Nostrand Reinhold, New York, 1966).
[39]J. B. Coon, J. Chem. Phys. 14, 665 (1946).
[40]R. N. Zare and D. R. Herschbach, Proc. IEEE 51, 173 (1963).
[41]J. T. Moseley, P. C. Cosby, and J. R. Peterson, J. Chem. Phys. 65, 2512 (1976).
[42]B. A. Huber, T. M. Miller, P. C. Cosby, H. D. Zeman, R. L. Leon, J. T. Moseley, and J. R. Peterson, Rev. Sci. Instrum. 48, 1306 (1977).
[43]R. H. Wood and L. A. D'Orazio, J. Chem. Phys. 69, 2562 (1965).
[44]H. Hotop and W. C. Lineberger, J. Phys. Chem. Ref. Data 4, 539 (1975).
[45]J. L. Gole and R. N. Zare, J. Chem. Phys. 57, 5331 (1972).

JOURNAL OF MOLECULAR SPECTROSCOPY 70, 326–329 (1978)

The Dissociation Energy of $O_2(X^3\Sigma_g^-)$

The currently-accepted value for the dissociation energy of the ground state of diatomic oxygen is $D(O_2X^3\Sigma_g^-) = 41\,260 \pm 15\ cm^{-1}$. This is a "best value" established experimentally by Brix and Herzberg (*1*) from the convergence limits of two absorption band systems: the $B^3\Sigma_u^-(v') \leftarrow X^3\Sigma_g^-(v'' = 0)$ Schumann-Runge bands and the $A^3\Sigma_u^+(v') \leftarrow X^3\Sigma_g^-(v'' = 0)$ Herzberg *I* bands, as shown in the lower part (dashed vertical lines) of Fig. 1. The $\pm 15\ cm^{-1}$ uncertainty arises from two sources. First, it reflects the energy spread between the *uppermost* observed nonpredissociating rotational level and the *lowermost* observed predissociating rotational level between which the dissociation limit must lie. Secondly, it includes the inability to rule out possible potential maxima of a few cm^{-1}. In this Note, we show that, with the advent of laser photofragment spectroscopy, the dissociation energy of oxygen can now be obtained with at least comparable uncertainty from a completely independent spectroscopic "cycle" and that the resulting value is in remarkable agreement with Brix and Herzberg's value.

The solid vertical lines in Fig. 1 show that $D(O_2X^3\Sigma_g^-)$ is part of a cycle that involves the $b^4\Sigma_g^-$ state of O_2^+:

$$E(O_2^+b) + T(v = 4, N = 9) = D(O_2X) + E(O^+{}^4S^\circ_{\frac{3}{2}}) + W(N = 9, {}^2P_{\frac{3}{2}}). \qquad (1)$$

The two ionization potentials, $E(O_2^+b)$ and $E(O^+{}^4S^\circ_{\frac{3}{2}})$, have been known for several years. The novel feature of the new cycle specified by Eq. (1) is that the *kinetic* energies, $W(N, {}^2P_J)$, of the $O^+ + O$ fragments from predissociating $b^4\Sigma_g^-$-state rotational levels that lie above the $O^+({}^4S^\circ_{\frac{3}{2}}) + O({}^3P_J)$ dissociation limits can now be measured to approximately "spectroscopic" accuracy. Since the potential energies of these rotational levels, $T(v = 4, N \geqslant 9)$, are now also known accurately, the energies W and T can be combined with the previously-known ionization potentials in Eq. (1) to define a value for $D(O_2X)$. Each of these four measurements and their uncertainties are discussed below.

$E(O_2^+b)$. The ionization potential to the $O_2^+b^4\Sigma_g^-(v = 0)$ state was determined by Yoshino and Tanaka (*2*) from members of a Rydberg series from the $O_2X^3\Sigma_g^-(v = 0)$ state converging on the first five vibrational levels of the $O_2^+b^4\Sigma_g^-$ state. The convergence limits of the measured band heads were converted to band-origin limits in the standard way (*3*) (head-origin difference $\leqslant 12\ cm^{-1}$) using the rotational constants B_e'' and B_e' from high-resolution studies of the $O_2X^3\Sigma_g^-$ (*4*) and $O_2^+b^4\Sigma_g^-$ (*5*) states available at the time. The differences between the band-origin limits of the five members of the series agreed typically within $\pm 1.5\ cm^{-1}$ with the vibrational quanta $\Delta G'_{v+\frac{1}{2}}$ of the $b^4\Sigma_g^-$ state established by the high-resolution study (*5*). The value $E(O_2^+b) = 146\,556 \pm 2\ cm^{-1}$ quoted by Yoshino and Tanaka is the band origin of the (0,0) band limit. The $\Delta G'_{v+\frac{1}{2}}$ comparisons show that it has good support from the other four series members, which were measured less well.

We have checked this value by fitting Yoshino and Tanaka's (0,0) data to the standard Rydberg form using nonlinear least squares. The various test fits, which were done using different portions of the converging progression, gave limits that were all well within $\pm 2\ cm^{-1}$ of the value above. Furthermore, we have verified that the current-best B_e values (*6*, *7*) yield the same head-to-origin conversion that was used by Yoshino and Tanaka. Such a conversion should be a very accurate one in the present case since both the upper and lower states involved in this Rydberg series are Σ states, whose structure therefore closely resembles that of the $^1\Sigma$ states on which the conversion is based (*3*). All of these checks support Yoshino and Tanaka's $\pm 2\ cm^{-1}$ estimate of their possible measurement and (short) extrapolation errors.

0022-2852/78/0702-0326$02.00/0

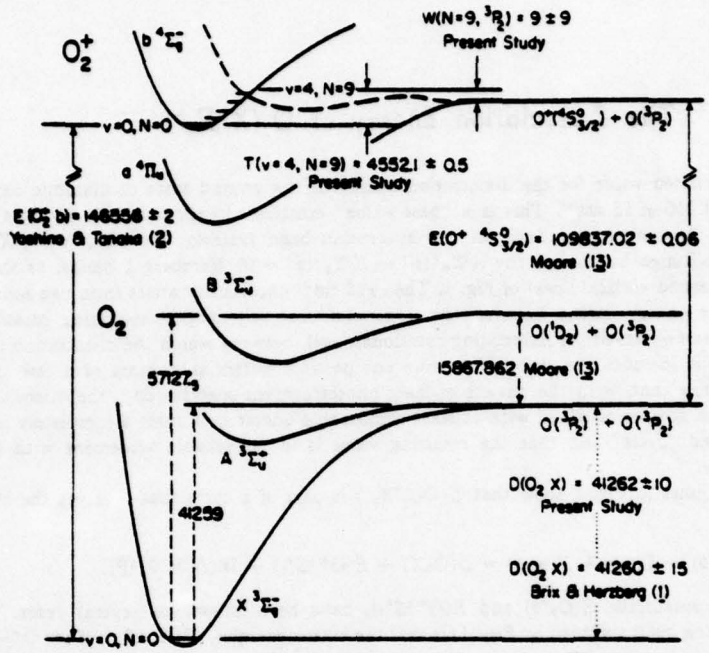

FIG. 1. Cyclic determinations of the dissociation energy of ground state diatomic oxygen. The energies are expressed in reciprocal centimeters and are not all to scale. The underlined numbers in parentheses refer to the references.

$T(v = 4, N = 9)$. The energy levels of the $b^4\Sigma_g^-$ state are known from a recent analysis (*7*) of high-resolution grating-spectrometer measurements of the wavelengths of the $O_2^+ b^4\Sigma_g^- - a^4\Pi_u$ First Negative band system. The $G(v)$-Dunham coefficients of Table IX, Ref. (*7*) provide the energy separation between the rotationless ($N = 0$) vibrational levels $v = 4$ and $v = 0$. The energies of the rotational levels within the $v = 4$ level are given by a diagonalization of the $^4\Sigma$ Hamiltonian containing the $v = 4$ rotational constants from Table IX, Ref. (*7*). The sum of these vibrational and rotational energies for $N = 9$ yields $T(v = 4, N = 9) = 4552.1 \pm 0.5$ cm^{-1}, i.e., the energy separation between the $v = 4$, $N = 9$ and $v = 0$, $N = 0$ levels.

Each rotational level of the $b^4\Sigma_g^-$ state is actually a closely spaced set of four multiplets (*7*). For example, the separation of the extreme multiplet levels is 0.48 cm^{-1} for $v = 4$, $N = 9$. The above $T(v = 4, N = 9)$ value corresponds to the median of the quartet components, since such small splittings are much smaller than the limiting measurement error in the present study.

The ±0.5 cm^{-1} uncertainty stated above incorporates three sources of error: (a) the statistical precision (~0.05 cm^{-1}, one standard error) predicted from propagation of error using the variance-covariance matrix (*8*) associated with the $b^4\Sigma_g^-$-state molecular constants, (b) a very conservative estimate of how much the predictive properties of the low-order Dunham model, which was fitted to data for $0 \leq b^4\Sigma_g^-(v) \leq 3$, could deteriorate in extrapolating one vibrational level to $v = 4$, and (*c*) the above-mentioned multiplet splittings.

$W(N = 9, {}^3P_2)$. The kinetic energy of the $O^+ + O$ fragments from the predissociating levels $v = 4$, $N \geq 9$ of the $O_2^+ b^4\Sigma_g^-$ state is determined (*9*) with a newly constructed laser photofragment apparatus (*10*). In brief, a mass-selected beam of long-lived metastable $O_2^+ a^4\Pi_u$ ions in a distribution of vibrational levels passes colinearly with the beam of a tunable dye laser. The dye-laser wavelength can be varied to correspond to selected lines of the (4,4) $O_2^+ b^4\Sigma_g^- - a^4\Pi_u$ band, thereby pumping the population of the rotational levels of the $b^4\Sigma_g^-(v = 4)$ state (*11*). The rotational levels $N \geq 9$ are predissociated (*12*), producing $O^+ + O$ fragments, the kinetic energies of which increase with

increasing rotational quantum number. The photofragment O^+ ions are energy-analyzed and detected. A detailed discussion of the photofragment spectroscopy of the O_2^+ quartet states is given in Ref. (*9*).

Photofragments were observed from the rotational levels $N = 9$, 13, 15, and 17 predissociating in various combinations to the three dissociation limits $O^+(^4S^\circ_{\frac{3}{2}}) + O(^3P_2, ^3P_1, ^3P_0)$ (the O^+ state is not split). Since the energy separations between the N levels and those between the $O(^3P_J)$ multiplets are both known (*7*, *13*), the measured energies $W(N, ^3P_J)$ can be uniquely matched to the N and ^3P_J levels. Thus, the first level above the lowest-energy multiplet limit, $O^+(^4S^\circ_{\frac{3}{2}}) + O(^3P_2)$, can be unequivocally established as $N = 9$ and the kinetic energy measurements yield $W(N = 9, ^3P_2) = 9 \pm 9$ cm^{-1}. This was the smallest of the $W(N, ^3P_2)$ values measured, and since the energy resolution of the apparatus is best near $W = 0$ (*9*, *10*), this value has the smallest uncertainty. (The fact that the $N = 9$ level lies just slightly above the dissociation limit was very fortuitous for the present enterprise!) The other $T(v = 4, N)$, $O(^3P_J)$, and $W(N, ^3P_J)$ energies, although the latter are less accurate, are quite consistent with the above $W(N = 4, ^3P_2)$ value.

It is worth noting that $W(N, ^3P_J)$, since it is the infinite-separation kinetic energy, is insensitive to the height of a successfully-penetrated or surmounted potential maximum. Thus, the spectroscopic cycle in Eq. (1) is not plagued by the uncertainty of such a maximum, as cycles involving a band-convergence dissociation limit sometimes are (*14*).

The ± 9 cm^{-1} uncertainty is the halfwidth at half-maximum (HWHM) of the photofragment peak scanned as a function of kinetic energy. The above value for $W(N = 9, ^3P_2)$ is the average of thirteen measurements of the kinetic energies of $N = 9$ fragments that had originated from different $a^4\Pi_u$ ($v = 4$) rotational levels. The standard error of the mean was 0.9 cm^{-1}. Since this indicator of precision is much smaller than the HWHM quoted above and the absolute accuracy of the energy scale is even much less than this, it is clear that the error given here is quite conservative. The -9 cm^{-1} side of the uncertainty actually represents a *very firm* lower limit, since observation of an O^+ photofragment signal requires $W \geq 0$.

$E(O^+ ^4S^\circ_{\frac{3}{2}})$. From atomic spectroscopy, the energy required to ionize the ground-state oxygen atom $O(^3P_2)$ into the ground-state oxygen ion $O^+(^4S^\circ_{\frac{3}{2}})$ is $E(O^+ ^4S^\circ_{\frac{3}{2}}) = 109\,837.02 \pm 0.06$ cm^{-1} (*13*), a value that is essentially "exact" on the scale of the present study.

The values given above (and summarized in Fig. 1) for the energies in the cycle defined by Eq. (1) yield $D(O_2X) = 41262 \pm 10$ cm^{-1}. (This value can straightforwardly yield, to the same uncertainty, dissociation energies for the $O_2^+ b^4\Sigma_g^-$ and $a^4\Pi_u$ states.) The individual errors in the cycle given by Eq. (1) are 9, 2, 0.5, and 0.06 cm^{-1}. The above ± 10 cm^{-1} uncertainty of $D(O_2X)$ makes the very reasonable assumption that the errors in the kinetic energy and wavelength measurements are largely independent (*8*).

The present value for the dissociation energy, $41\,262 \pm 10$ cm^{-1}, agrees almost exactly with the value determined by Brix and Herzberg (*1*): $41\,260 \pm 15$ cm^{-1}, the difference being considerably smaller than either of the uncertainties. Figure 1 shows that the cycles used to determine the two values have *no* measurements in common. The various wavelength measurements were even in very different parts of the spectrum. Such excellent agreement between two independent measurements of the same quantity using substantially different methods is the strongest type of "proof" that experiment can offer.

ACKNOWLEDGMENT

This work was supported in part by the National Science Foundation under Grant No. CHE 77-00428, the Air Force Office of Scientific Research, and the Defense Nuclear Agency.

REFERENCES

1. P. Brix and G. Herzberg, *Can. J. Phys.* **32**, 110–135 (1954).
2. K. Yoshino and Y. Tanaka, *J. Chem. Phys.* **48**, 4859–4867 (1968).
3. G. Herzberg, "Spectra of Diatomic Molecules," 2nd ed., p. 171, Van Nostrand, New York, 1950.
4. H. D. Babcock and L. Herzberg, *Astrophys. J.* **108**, 167–190 (1948).
5. T. E. Nevin, *Phil. Trans. Roy. Soc.* (*London*) **A237**, 471–507 (1938); *Proc. Roy. Soc.* (*London*) **A174**, 371–378 (1940); and T. E. Nevin and T. Murphy, *Proc. Roy. Irish Acad.* **A46**, 169–181 (1941).

6. J. W. C. JOHNS AND D. W. LEPARD, *J. Mol. Spectrosc.* 55, 374–406 (1975).
7. D. L. ALBRITTON, A. L. SCHMELTEKOPF, W. J. HARROP, R. N. ZARE, AND J. CZARNY, *J. Mol. Spectrosc.* 67, 157–184 (1977).
8. D. L. ALBRITTON, A. L. SCHMELTEKOPF, AND R. N. ZARE, *in* "Molecular Spectroscopy: Modern Research" (K. Narahari Rao, Ed.), Vol. II, pp. 55–57, Academic Press, New York, 1976.
9. M. TADJEDDINE, R. ABOUAF, P. C. COSBY, B. A. HUBER, AND J. T. MOSELEY, *J. Chem. Phys.* (submitted).
10. B. A. HUBER, T. M. MILLER, P. C. COSBY, H. D. ZEMAN, R. L. LEON, J. T. MOSELEY, AND J. R. PETERSON, *Rev. Sci. Instrum.* 48, 1306–1313 (1977).
11. J. T. MOSELEY, M. TADJEDDINE, J. DURUP, J.-B. OZENNE, C. PERNOT, AND A. TABCHE-FOUHAILLE, *Phys. Rev. Lett.* 37, 891–895 (1976).
12. A. CARRINGTON, P. G. ROBERTS, AND P. J. SABRE, *Mol. Phys.* 34, 291–295 (1977).
13. C. E. MOORE, "Selected Tables of Atomic Spectra, Atomic Energy Levels and Multiplet Tables, OI," NSRDS-NBS 3, Sec. 7, U.S. Government Printing Office, Washington, D.C., 1976.
14. A. G. GAYDON, "Dissociation Energies," 3rd ed., pp. 80–81, Chapman and Hall, London, 1968

D. L. ALBRITTON

Aeronomy Laboratory, NOAA Environmental Research Laboratories
Boulder, Colorado 80302

J. T. MOSELEY AND P. C. COSBY

Molecular Physics Center, SRI International
Menlo Park, California 94025

M. TADJEDDINE

Laboratoire des Collisions Ioniques
Université de Paris-Sud, 91405 Orsay, France.

APPENDIX G

High-Resolution Photofragment Spectroscopy of the O_2^+ $b^4\Sigma_g^-$ ($v' = 3,4,5$) $\leftarrow$ $a^4\Pi_u$ ($v'' = 3,4,5$) First Negative System Using Coaxial Dye-Laser and Velocity-Tuned Ion Beams

P. C. Cosby, J.-B. Ozenne,[1] and J. T. Moseley
Molecular Physics Laboratory, SRI International
Menlo Park, California 94025

and

D. L. Albritton
Aeronomy Laboratory, NOAA Environmental
Research Laboratories, Boulder, Colorado 80303

manuscript pages	57
Figures	8
Tables	6

Journal of
Molecular
Spectroscopy
(in press)

MP 79-02
1/5/79

ABSTRACT

A new photofragment spectrometer employing coaxial tunable single-mode laser and velocity-tuned fast-ion beams has been used to measure transition energies in the $O_2^+ b^4\Sigma_g^- \leftarrow a^4\Pi_u$ First Negative system to an accuracy and precision that are an order of magnitude better than was previously possible in Doppler-limited emission spectroscopy. The technique consists of velocity-tuning a beam of metastable $O_2^+ a^4\Pi_u$ ions such that a set of First Negative rotational transitions can be sequentially brought into resonance with the laser wavelength. The subsequent absorption transitions promote the ions to predissociating levels of the $b^4\Sigma_g^-$ state and observation of the O^+ photofragments is the signal that denotes that each absorption transition has occurred. Repetition of the velocity tuning at different dye-laser frequencies provides a scan of the First Negative spectrum for predissociating upper-state vibrational levels, which are inaccessible to emission spectroscopy. The O^+ photofragment ions have a kinetic energy that depends on the height of the predissociating rotational level above the separated-atom limit. The present apparatus incorporates a photofragment energy analyzer that can often be used to separately record the wavenumbers of transitions to different upper-state rotational levels, but whose wavenumbers could not otherwise be resolved. A set of 359 wavenumbers involving the (4,4), (4,5), (5,5), and (3,3) bands were recorded with an estimated accuracy of $\pm$ 0.0032 cm^{-1} and a precision of 0.0028 cm^{-1}, the latter being estimated precisely with a statistical technique. These data were fitted to $^4\Sigma$ and $^4\Pi$ Hamiltonians

used in recent studies of the First Negative emission spectrum to determine molecular constants for the $v' = 4,5$ and $v'' = 4,5$ levels. The former represent an extension of the $b^4\Sigma_g^-$ state to new levels and the latter represent substantial improvements over the constants that were available from previous moderate-resolution emission studies. These photofragment molecular constants were merged with those from the previous emission studies to yield a new consistent set of molecular constants and Dunham coefficients for the O_2^+ $b^4\Sigma_g^-$ and $a^4\Pi_u$ states. In the fit to the photofragment bands, it was found that the Hamiltonians, which were sufficient for the emission data, are inadequate to describe these states within the precision of the present measurements.

APPENDIX H

OBSERVATION OF PREDISSOCIATED LEVELS OF CH^+

P. C. Cosby, H. Helm* and J. T. Moseley
Molecular Physics Laboratory, SRI International
Menlo Park, California 94025

ABSTRACT

The predissociation of CH^+ has been studied by observation of the appearance of C^+ photofragments as a function of excitation wavelength, near 3500 Å. The dissociation energy of the C^+ fragments was also measured. Thirty-seven discrete transitions were observed to lead to dissociation within 350 cm^{-1} of the dissociation limit. The most reasonable attribution of these observations is to predissociation of the $A^1\Pi$ and $a^3\Pi$ states. If this is correct, then the number of quasi-bound levels which could contribute to the radiative association $C^+(^2P) + H(^2S)$ is much larger than previously expected.

*Max Kade Foundation Fellow at SRI International, 1979-80

MP 79-29
5/21/79

The Astrophysical
Journal
(in press)

I. INTRODUCTION

Knowledge of the $C^+(^2P) + H(^2S)$ radiative recombination rate is crucial to an understanding of the formation of CH^+, which is a basic building block in interstellar molecular processes (see, for example, Dalgarno and Black, 1976), but direct measurement of this rate is outside the scope of present experimental techniques. Recent calculations by Uzer and Dalgarno (1979) and Abgrall, Guisti-Suzor, and Roueff (1976), show that quasi-bound levels of the $A^1\Pi$ state near the dissociation limit exist, which enhance the radiative association rate. However, the increase calculated by Abgrall et al. using the potentials of Green, Hornstein, and Bender (1973) is insufficient to remove the discrepancy between the observed and calculated abundances of CH^+ in diffuse interstellar clouds. We present here the first experimental observation of near threshold quasi-bound levels of CH^+. The density of levels near the dissociation limit is found to be substantially greater than predicted. Other transitions were observed which appear to be between the $\underline{a}^3\Pi$ and $\underline{b}^3\Sigma^-$ states, with the $\underline{b}$ state predissociated by the $\underline{c}^3\Sigma^+$ state.

II. APPARATUS AND EXPERIMENTAL PROCEDURE

The apparatus, a laser-ion coaxial beams spectrometer has been described in detail previously, as has its application to spectroscopic studies of O_2^+ similar to those reported here for CH^+ (see, for example, Huber et al. 1977, Moseley et al. 1979, and Cosby et al. 1979). For this work CH^+ was produced by dissociative electron impact ionization of C_2H_2 or CH_4, accelerated to a specified energy between 2 and 4 keV, selected from other source-produced ions by a magnetic analyzer, collimated to 2 mrad and deflected into the laser interaction region. In this region, a laser beam was made coaxial with the ion beam over a distance of 50 cm. The Kr and Ar ion lasers used in this work provided five prism selected wavelengths between 3507 and 3638 Å. Transitions in the CH^+ ions were velocity-tuned into resonance with the fixed laser frequency by varying the velocity of the CH^+ beam in the interaction region. By directing the laser beam both parallel and antiparallel to the ion beam, a total of ten spectral regions, each approximately 7 to 10 cm^{-1} in width were investigated. The C^+ fragments formed by photodissociation are deflected into an energy analyzer, and the energy-selected ions are detected by an electron multiplier. The appearance of C^+ fragments at a particular wavelength is thus evidence that an absorption leading to dissociation has taken place; the energy of the C^+ fragments can be used straightforwardly to determine the energy of the dissociated level above the appropriate dissociation limit, called the separation energy W.

Thus, the data obtained are of two types. Wavelength scans are made for several energy analyzer settings by scanning the ion beam velocity. Peaks in the observed C^+ production can then be examined (at fixed absorption wavelength) with the energy analyzer to determine the separation energy W.

Figure 1 shows a typical wavelength scan for $W \approx 0$, covering the range from 28483.7 to 28485.8 cm^{-1}, obtained using the single mode output of a krypton ion laser at 28502.745 cm^{-1}. The transition energies were calibrated as described in Cosby et al. (1977), with an uncertainty of less than 0.01 cm^{-1}. On this narrow energy range of 2.1 cm^{-1}, four peaks are clearly distinguishable. The continuum background in Figure 1, is due to a direct dissociation, most likely from the $X^1\Sigma^+$ state to the repulsive part of the $A^1\Pi$, as calculated by Uzer and Dalgarno (1978). Collisional dissociation was shown to account for only about 1% of the total signal.

The separation energy corresponding to transitions such as those shown in Figure 1 can be obtained by fixing the wavelength on one of the transitions and scanning the energy analyzer (Huber et al. 1977). The W values obtained here have a larger uncertainty than the highly precise values obtained for O_2^+ levels by Pernot et al. (1979), because of the necessity to correct the measured spectra by subtracting the contribution due to direct dissociation, which has a W of about 300 cm^{-1}. For this work the uncertainty for the strong transitions is $\pm$ 25 cm^{-1} for W values less than 150 cm^{-1}.

III. RESULTS

Table I gives the results obtained using the five laser lines near 3500 Å, for transitions which produced photofragments with separation energies less than 350 cm^{-1} (43 meV). A similar number of transitions were observed leading to separation energies in the range of 1 to 2 eV. These transitions are not relevant to the astrophysical problem under consideration here, and thus will not be discussed in detail. No transitions were observed leading to separation energies intermediate to these two regions. A number of transitions were also observed at visible wavelengths between 4000 and 6500 Å. These transitions have not yet been analyzed and will not be discussed in detail here. Table I also lists the regions covered around each laser line by velocity tuning. Most transition energies were measured to an accuracy of $\pm$ 0.2 cm^{-1}; those in the second, sixth and seventh regions that are given to three decimal places were measured to $\pm$ 0.008 cm^{-1}, and all those in the third region were measured to $\pm$ 0.024 cm^{-1}. All line widths given are the observed full-width at half-maximum. They have not been corrected for apparatus-induced broadening, which is necessary before lifetimes can be determined . (Moseley et al.(1979)).

Several observations can be made with reference to Table I. In the region studied, the transitions lie very close together, with an average spacing of less than 0.5 cm^{-1} in parts of the spectrum. The energy of the upper level with respect to the dissociation limit is very low. Out of 22 transitions for which W was determined, 14 have separation

energies less than 100 cm^{-1}. Finally, the widths of the observed peaks vary substantially, from 200 to 1560 MHz, indicating a substantial variation in the lifetimes of the predissociated levels.

IV. DISCUSSION

The major question to be answered is that of the origin of the quasi-bound levels. A number of possible processes can be discussed with reference to the potential curves of Figure 2. Although quasi-bound levels have been predicted in the $A^1\Pi$ state near the $C^+(^2P) + H(^2S)$ dissociation limit, the predicted levels cannot account, even qualitatively, for the large number of observed transitions. We thus examined other possible explanations for the observations. Each of the possibilities considered will be discussed in turn.

Any splitting of the X or A states would have to be in the range of 0.3 to 1 cm^{-1} in order to assist in explaining the large number of observed transitions. If any such splitting existed for the lower vibrational levels of the X or A states, it would have been observed in the emission spectra obtained by Douglas and Herzberg (1942) and Douglas and Morton (1969). We cannot propose any mechanism to split the X state levels by this amount. Nuclear hyperfine interaction, for example, would lead to splittings of less than 10^{-4} cm^{-1} for either of these singlet states.

The metastable $\underline{a}^3\Pi$ state may be appreciably populated in our experiment. The observation of C^+ photofragments with W in the range of 1 to 2 eV is most easily explained by transitions between the $\underline{a}^3\Pi$ and $\underline{b}^3\Sigma^-$ state, followed by predissociation of the $\underline{b}$ state by $\underline{c}^3\Sigma^+$, as predicted by Lorquet et al. (1971). Dissociation of metastable CH^+ by this mechamism has been previously invoked by Newton and Sciamanna (1972) to explain C^+ fragments from CH^+ formed by electron impact on a number of molecules. However, given the

potentials of Figure 2, it is difficult to propose an effective mechanism for the production of near threshold C^+ photofragments from any of the triplet states. Conceivably, b state levels excited by the laser could radiatively decay into quasi-bound levels of the a state just above the threshold, which could dissociate. However, Franck-Condon factors for such transitions would be extremely poor.

Processes in which a higher lying metastable state is the origin for the transitions also seem unlikely to be responsible for the observed transitions. Above the a state, and below 10 eV, only the lowest $^5\Sigma^-$ and $^3\Delta$ states are possibly long-lived enough to reach the laser interaction region. However, both of these states are expected by Lorquet et al. (1971) to be predissociated, the $^3\Delta$ by six different curve crossings. Further, the $^5\Sigma^-$ state that they predict would have to be lowered by over 2 eV to make it possible to yield near threshold C^+ photofragments. Finally, for neither the $^5\Sigma^-$ nor the $^3\Delta$ are appropriate upper states predicted to which 3500 Å transitions to predissociated levels would be expected.

The possibility of two-photon processes was considered. Using the calculated potentials of Lorquet et al. (1971) and of Kirby, Saxon and Liu (1979), we could find no possible two-photon processes using 3500 Å radiation that would lead to near-threshold C^+. If one of the triplet potential curves from the $C^+(^4P) + H(^2S)$ limit is bound, then a two-photon process near 3500 Å might be possible, but a similar process would not be possible in the visible.

Collisional dissociation of CH^+ excited by the laser to bound levels near the dissociation limit could yield apparent predissociations. Several peaks were explicitly checked for this possibility by increasing the pressure in the interaction region by over two orders of magnitude. No increase in the peak height was observed, demonstrating that collisional dissociation is not responsible for these peaks. Further, the line width for a peak caused by collisional dissociation would be apparatus-limited, since the appropriate lifetime is that of the excited bound level. Thus, only the peaks with linewidths of about 200 MHz could possibly be due to this mechanism. Collisional dissociation of laser-excited bound levels might be responsible for a few of the observed peaks, and thus this mechanism will be further investigated. However, the majority of the peaks observed here (and perhaps all of them) must be due to a true predissociation.

Since none of the possible explanations listed above appear attractive, we reconsidered the predicted mechanism of quasi-bound levels of the $A^1\Pi$ state. In fact, as can be seen from Figure 3, which was obtained from the calculations of Bazet et al. (1975), predissociation of rotationally quasi-bound levels of the $A^1\Pi$ state is not the only possible predissociation mechanism. Figure 3 illustrates that the $C^+(^2P) + H(^2S)$ limit is split by 64 cm^{-1} due to the spin-orbit interaction in $C^+(^2P)$. The $^1\Pi_1$ state, which correlates to the upper limit, $^2P_{\frac{1}{2}}$, is spin-orbit coupled to the $^3\Pi_1$ state, which correlates to the lower limit, $^2P_{\frac{3}{2}}$. Thus, bound levels of $^1\Pi_1$ which lie above the $^2P_{\frac{1}{2}}$ limit could be predissociated by $^3\Pi_1$ to this limit.

Further, for levels close to the dissociation limits, the coupling will be intermediate to Hunds cases (a) and (c), and thus optical transitions will become allowed from the ground $^1\Sigma_o^+$ state to the $^3\Pi_o+$ and $^3\Pi_1$ states, as well as to the $^1\Pi_1$ state. Each of these states may have rotationally quasi-bound levels, with the $^1\Pi_1$ and $^3\Pi_o+$ dissociating to the $^2P_{\frac{3}{2}}$ limit, and the $^3\Pi_1$ to $^2P_{\frac{1}{2}}$ limit. In addition, bound levels of the $^3\Pi_o$ state can be predissociated by rotational coupling to the $^3\Pi_1$ state.

The possibilities discussed above, which have apparently not been previously considered in the predissociation of CH^+, could certainly increase the number of transitions from the $^1\Sigma^+$ ground state to predissociated levels, and might explain the high density of peaks that we observe. The predissociation of bound levels of $^1\Pi_1$ and $^3\Pi_o+$ to the $^2P_{\frac{1}{2}}$ limit could explain the preponderance of peaks which correspond to separation energies of less than 100 cm^{-1}, since the density of $^1\Pi_1$ and $^3\Pi_o+$ levels is likely to be high just above the $^2P_{\frac{1}{2}}$ dissociation limit.

Clearly, a substantial amount of work remains to be done on these CH^+ transitions. Most crucial is to definitively identify the predissociated levels and to assign the transitions involved. Double-resonance experiments are currently being set up which should allow such assignments. In order to assess the importance of these levels in the $C^+ + H$ radiative association, the levels must be identified and their lifetimes and transition strengths to the ground state determined. The high density of quasi-bound levels near the dissociation limit indicated by the results presented here could

lead to an increase in the expected radiative association rate, as well as to an improved understanding of the long-range interactions of two atoms approaching to form a molecule and of the near-threshold dissociation processes of simple molecules.

V. ACKNOWLEDGEMENTS

The authors wish to thank Drs. Roberta Saxon and David Huestis for many helpful discussions. This research was supported by the National Science Foundation under Grant No. CHE-77-00428, and the United States Air Force Office of Scientific Research.

REFERENCES

Abgrall, H., Guisti-Suzor, A., and Roueff, E. 1976, Ap. J. 207, L69.

Bazet, J. F., Harel, C., McCarroll, R., and Riera, A. 1975, Astron. and Astrophys 43, 223.

Cosby, P. C., Ozenne, J.-B., Moseley, J. T., and Albritton, D. L. 1979, J. Mol. Spec. (in press).

Dalgarno, A. and Black, J. H. 1976, Rep. Prog. Phys. 39, 573.

Douglas, A. E. and Herzberg, G. 1942, Can. J. Res. 20, 71.

Douglas, A. E. and Morton, J. R. 1960, Ap. J. 131, 1.

Green, S., Bagus, P. S., Liu, B., McLean, A. D., and Yoshimine, M. 1972, Phys. Rev. A 5, 1614.

Huber, B. A., Miller, T. M., Cosby, P. C., Zeman, H. D., Leon, R. L., Moseley, J. T., and Peterson, J. R. 1977, Rev. Sci. Instr. 48, 1306.

Kirby, K., Saxon, R. P., and Liu, B. 1979, private communication, to be published.

Lorquet, A. J., Lorquet, J. C., Wankenne, H., Momigny, J., and Lefebvre-Brion, H. 1971, J. Chem. Phys. 55, 4053.

Moseley, J. T., Cosby, P. C., Ozenne, J.-B., and Durup, J. 1979, J. Chem. Phys. 70, 1474 (1979).

Newton, A. S., and Sciamanna, A. F. 1973 J. Chem. Phys. 58, 1292.

Pernot, C., Durup, J., Ozene, J.-B., Beswich, J. A., Cosby, P. C., and Moseley, J. T. 1979, J. Chem. Phys. (in press).

Uzer, T. and Dalgarno, A. 1978, Chem. Phys. 32, 301.

Uzer, T. and Dalgarno, A. 1979, Chem. Phys. submitted.

TABLE I

Observed predissociation transitions of CH^+ leading to C^+ fragments with separation energies less than 350 cm^{-1}.

TRANSITION ENERGY (cm^{-1})	W (cm^{-1})	LINEWIDTH (MHz)
(Region covered: 28523.1 to 28518.6 cm^{-1} and 28068.8 to 28064.3 cm^{-1})[a]		
28522.53	<30	
28521.97	b	
28521.64		
28521.44		
28520.80	40[c]	
28520.23		
28519.83		
28519.45		
(Region covered: 28493.9 to 28480.3 cm^{-1})		
28488.499		
28487.925		
28487.222	110	430
28486.888		520
28485.583	50	430
28485.153	65	530
28484.391	70	370
28484.344	34	1300
(Region covered: 28468.9 to 28461.7 cm^{-1})		
28466.37		
28464.86		
28463.977	95	230
28463.897	28	200
28463.884	28	200
(Region covered: 28457.3 to 28447.6 cm^{-1})		
28455.01	50	300
28454.54		750
28454.17	225	750
28453.86		750
28453.14		
28453.43		
28451.34	140	
28450.80	50	
28448.22	80	
28447.87	60	
(Region covered: 28432.5 to 28422.9 cm^{-1})		
28431.13	100	750
(Region covered: 28036.1 to 28028.8 cm^{-1})		
28034.463	320	610
28033.47	< 250	750
28033.068	< 160	750
28032.810	< 160	750
(Region covered: 27501.2 to 27494.1 cm^{-1})		
27498.921	74	1560

(Regions covered with no observed transitions: 28068.4 to 28064.0 cm^{-1} and 27465.5 to 27459.9 cm^{-1})

a. Both 3507 Å and 3564 Å lines of Kr ion laser were present in the interaction region. Transition energies calculated assuming 3507 Å line was responsible for all dissociations.

b. If no value for W is given, it was not explicitly determined but is less than 350 cm^{-1}.

c. The uncertainty in W is $\pm$ 25 cm^{-1} wherever a precise value is stated.

d. This transition energy may be smaller by about 25 cm^{-1}.

FIGURE CAPTIONS

Figure 1. Spectrum of near threshold C^+ photofragments versus absorption energy obtained by using the single mode output of a krypton ion laser at 28502.745 cm^{-1}. The absorption energy scale is given by the Doppler shift away from the laser wavenumber.

Figure 2. Lower potential curves of CH^+, following the calculations of Green, et al. (1972), Lorquet et al. (1971) and Kirby et al. (1979).

Figure 3. The region of the CH^+ potential curves near the $C^+(^2P_{\frac{1}{2},\frac{3}{2}}) + H(^2S)$ dissociation limits, following the calculations of Bazet et al. (1975).

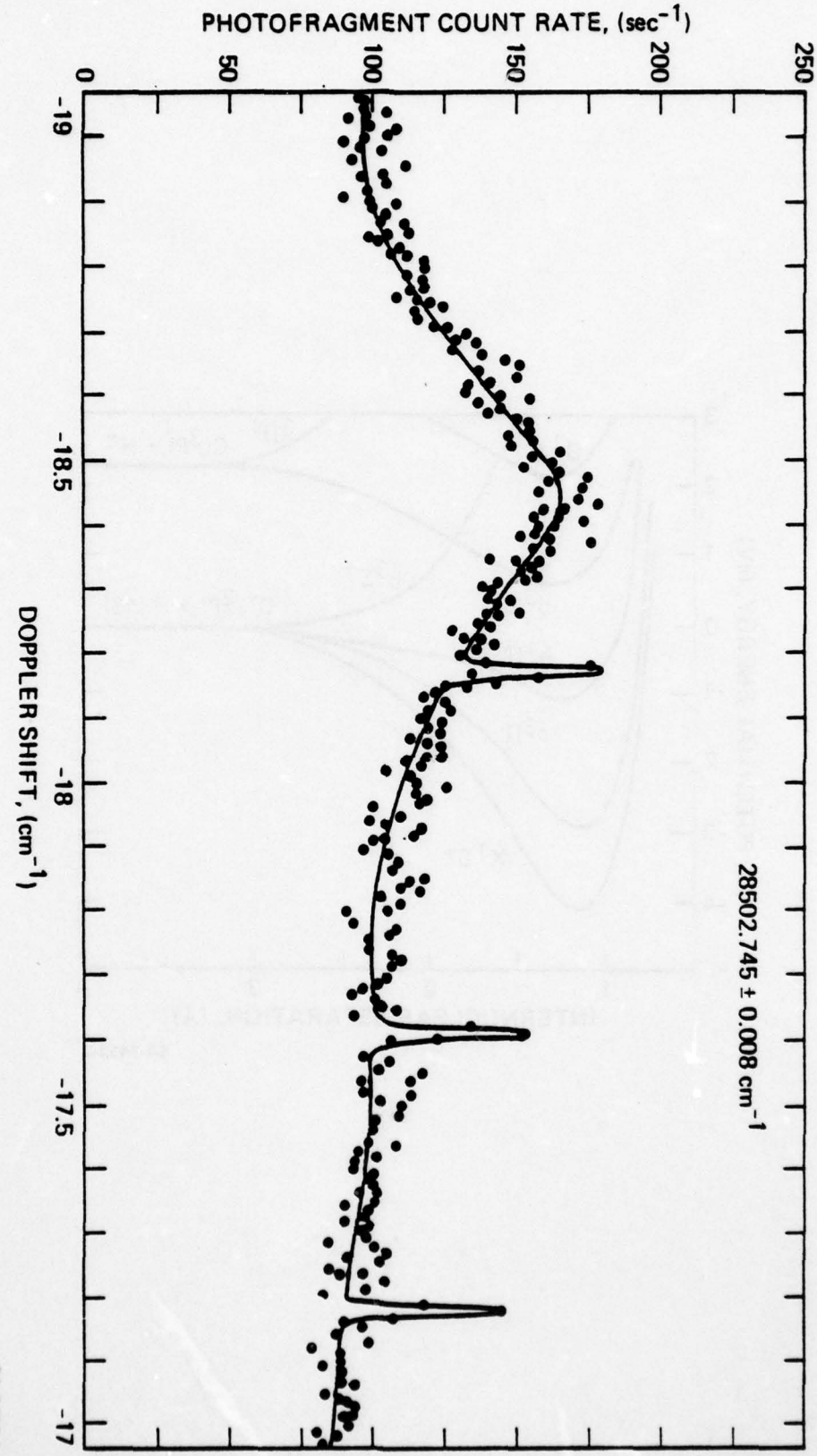

Ap. J. Lett.
Cosby, Helm &
Moseley
Figure 1

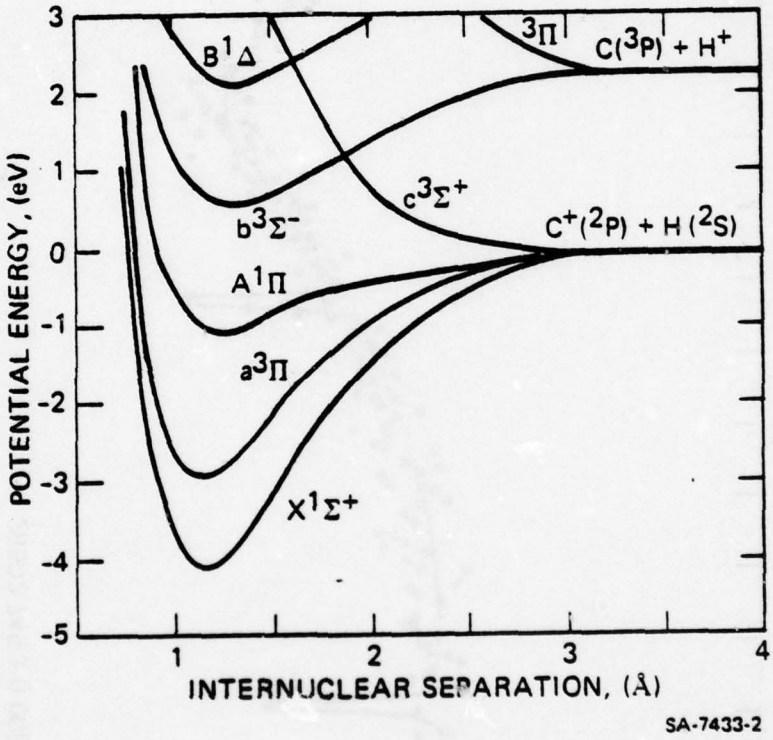

Ap. J. Lett.
Cosby, Helm &
Moseley
Figure 2

AD-A073 000 SRI INTERNATIONAL MENLO PARK CA MOLECULAR PHYSICS LAB F/G 7/4
ION PHOTOFRAGMENT SPECTROSCOPY--POTENTIAL SURFACES OF MOLECULAR--ETC(U)
JUL 79 J T MOSELEY, P C COSBY, J R PETERSON F44620-76-C-0095
UNCLASSIFIED SRI-MP-79-49 AFOSR-TR-79-0943 NL

2 OF 2
AD
A073000

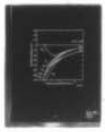

END
DATE
FILMED
9 79
DDC

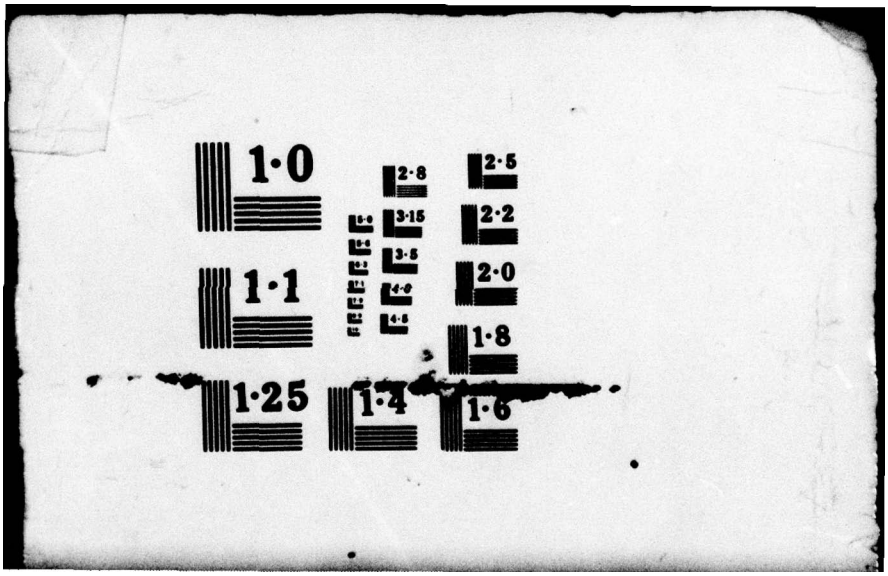
1·0
1·1
1·25
1·4
1·6
1·8
2·0
2·2
2·5
2·8
3·15
3·5
4·0

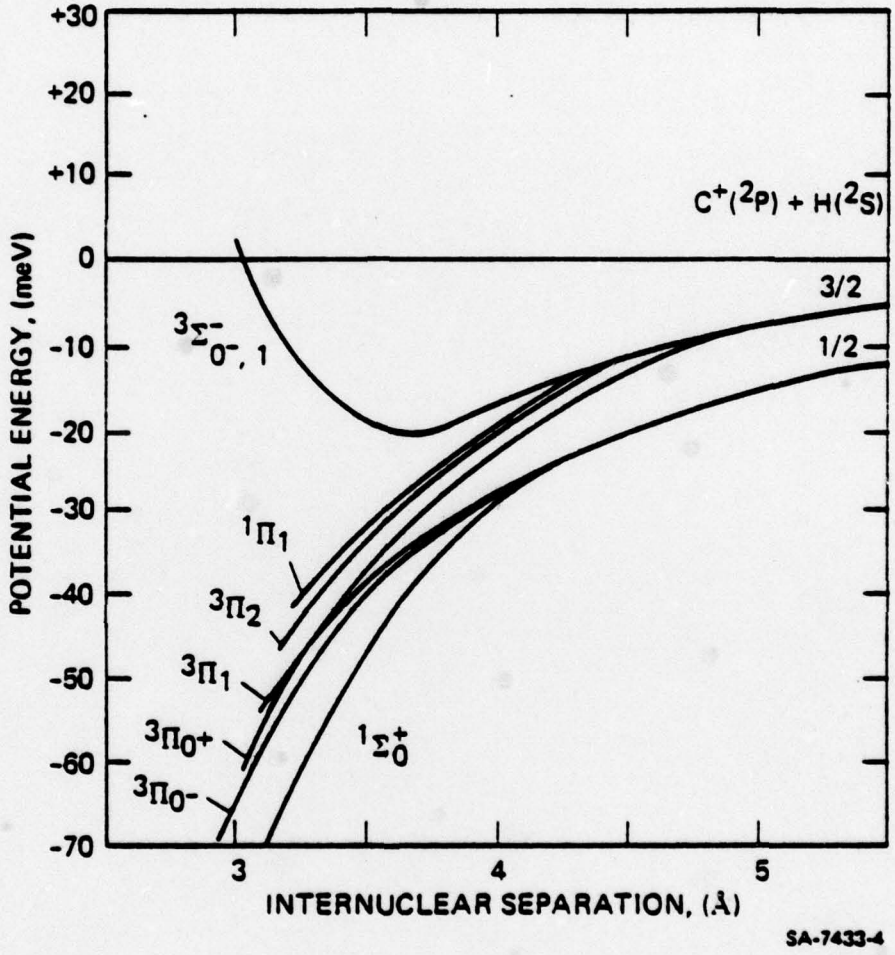

Ap. J. Lett.
Cosby, Helm &
Moseley
Figure 3